UNIVERSITY OF CALIFORNIA,
IRVINE

Hygroscopicity of Mixed Inorganic/ Surfactant Ultrafine Aerosol Particles

DISSERTATION

submitted in partial satisfaction of the requirements
for the degree of

DOCTOR OF PHILOSOPHY

in Chemistry

by

Ahmad Alshawa

Dissertation Committee:
Professor Sergey A. Nizkorodov, Chair
Professor John C. Hemminger
Professor Donald R. Blake

2008

The dissertation of Ahmad Alshawa
is approved and is acceptable in quality and form for
publication on microfilm and in digital formats:

_____

_____

_____
Committee Chair

University of California, Irvine
2008

DEDICATION

My parents, my wife Marwa and my daughters Susana and Nadeen, and friends

in recognition of their worth

TABLE OF CONTENTS

LIST OF FIGURES

LIST OF TABLES

ACKNOWLEDGEMENTS

I would like to express my sincere appreciation to my committee chair, Professor Sergey Nizkorodov, who continually and convincingly conveyed a spirit of adventure to research, and for his insightful discussions and comments, without his guidance and persistent help this dissertation would not have been possible.

I also would like to thank Dr. Joelle Underwood whose experimental design of electrospray system made the current investigation possible; Prof. Otto Dopfer for his participation in UFP characterization experiments; I also would like to thank all AirUCI collaborators, especially Dr. Ron Grimm for his insightful discussions and comments; Dr. Teresa M. McIntire for her tremendous help in TEM imaging. I also would like to thank all the members of the Nizkorodov group, in particular Chris Harmon for his friendship and for his innovative ideas for upgrading different parts of the experimental design. I would like to thank Dr. James Pitts Jr. for many stimulating discussions and suggestions during air purifiers' investigation of hazardous ozone emission.

CURRICULUM VITAE

Ahmad Alshawa

EDUCATION

Ph.D.,Physical Chemistry, anticipated Jan. 2008
University of California Irvine, CA
Dissertation: Hygroscopicity of Mixed Inorganic/Surfactant Ultrafine Aerosol Particles
Advisor: Prof. Sergey Nizkorodov

B.S. Chemistry, Summa Cum Laude, 2000
Minor in Mathematics and Physics
Montclair State University, Montclair, NJ

PUBLICATIONS

- A. Alshawa, Sergey Nizkorodov, Joelle Underwood and Enosh Cohen "Hygroscopicity of Mixed Inorganic/Surfactant Ultrafine Aerosol Particles , in preparation (2007)
- A. Alshawa, A. R. Russell, and S.A. Nizkorodov "Kinetic analysis of competition between aerosol particle removal and generation by ionization air purifiers" Env. Sci. Tech. 41 (2007) 2498-2504.
- N. Britigan, A. Alshawa, S.A. Nizkorodov "Quantification of ozone levels in indoor environments generated by ionization and ozonolysis air-purifiers", JAWMA 56 (2006) 601-610.

WORKING EXPERIECNE

Upper division labs Head TA, *University of California Irvine, Department of Chemistry, 2007-present.* Maintained, troubleshooted, repaired and calibrated GC/MS, AA, ICP, UV/VIS for Chem. 151L. Replaced instruments' components. Ordered spare parts. Instructed TA's and undergraduates in the proper usage of instruments. Prepared writing instructions for equipment use and safety.

Teaching Experience, Cypress College, Department of Chemistry, 2007-present. Lectured and supervised General Chemistry for undergraduates including laboratories. Developed course syllabus, lectures PowerPoints.

Teaching Assistant*, University of California Irvine, Department of Chemistry, 2002-present*

Instructed and supervised different levels of undergraduate laboratories in:

- Physical Chemistry, Chem153, 2003, 2004, 2005, 2006
- Advanced Instrumental Analysis, Chem152, 2004
- Analytical Cchemistry, Chem151, 2004
- General Chemistry LC, 2004
- Graduate ChaMP summer program, 2003

- General chemistry LB, 2002

Assisted in development of two new experiments for physical chemistry in 2006. Developed and maintained a website for physical chemistry in 2006.

CONFERENCES

- AirUCI Seminar, UCI, Irvine, CA.92697. Nov. 2006. Ahmad Alshawa, Joelle Underwood, Steven Ng. Enosh Cohen, Sergey Nizkorodov, " Generation and Hygroscopicity of Ultrafine Aerosol Particles"
- ACS 232 National meeting, San Francisco, Sep, 2006. Ahmad Alshawa, Joelle Underwood, Sergey Nizkorodov, and Steven Ng. UCI, Irvine, CA 92697 "Hygroscopicity of ultrafine organic aerosol particles: The role of chemical composition and structure".
- 23rd Informal Symposium on "Kinetics and Photochemical Processes in the Atmosphere" (February 15, 2006). Ahmad Alshawa, Joelle Underwood, Steven Ng. Sergey Nizkorodov." Aerosolized inverted micelles as model systems for probing atmospheric reactions of ultrafine organic particles"

ABSTRACT OF THE DISSERTATION

Hygroscopicity of Mixed Inorganic/ Surfactant Ultrafine Aerosol Particles

by

Ahmad Alshawa

Doctor of Philosophy in Chemistry

University of California, Irvine, 2008

Professor Sergey A. Nizkorodov, Chair

Ultrafine organic aerosol particles UFP (defined as particles with aerodynamic diameters < 100nm) are ubiquitous in the atmosphere. They are characterized by having an enhanced Kelvin effect and a greater surface energy contribution to the overall energy. The combination of their small size and chemical composition can drastically alter their hygroscopic behavior compared to fine particles. While a significant fraction of these particles were found to comprise organic surfactants, their hygroscopic effect is not well characterized.

Phase transitions in binary systems are usually described assuming ideal behavior. However, mixtures of inorganic salts and surface active agents may or may not be ideal, and therefore experimental measurements presented here are needed in order to assess the deviations from the ideal behavior. The main goal of this work is to understand the effects of surface active agents on hygroscopicity of binary system of inorganic/

surfactants in ultrafine particles and the relationship between the structure and hygroscopicity in such systems.

Hygroscopic growth measurements were preformed on internally mixed particles (7-20nm) of Sodium Chloride and anionic surfactants Dioctyl Sodium Sulfosuccinate (AOT) and Sodium Dodecyl Sulfate (SDS) at different weight fractions. The deliquescence relative humidities were measured using a novel Tandem Nano Differential Mobility Analyzer (Tandem-NDMA). Hygroscopicity of mixtures of NaCl and AOT were reported in terms of hygroscopic growth factors. The growth factors of internally mixed 17.0 nm aerosol particles of NaCl and AOT or SDS surfactants were investigated at different total conditioning residence times. Initial results for 25% w/w AOT with NaCl and 25 % w/w SDS with NaCl showed a growth factor depression as well as a shift in the deliquescence relative humidity to lower values compared to the pure NaCl particles. Such a behavior was theoretically attributed to differences between the rates of spreading of each surfactant at the particle interface compared to rate of surface area increase of the deliquescing droplets. The experimental results presented here suggest that a small amount of surfactant is sufficient to cause a significant change in the water uptake by the inorganic soluble core.

The rate of deliquescence of ultrafine ambient aerosol particles can substantially alter both its potential role as cloud condensation Nuclei (CCN) and its deposition rate in human respiratory system. There is one important concern in investigating hygroscopicity of ultrafine particles (UFP) as to whether or not particles have actually attained final equilibrium during the measurement time. In this work, the effects of mass transfer and size on deliquescence of aerosol particles were also addressed. It was shown that unless

the deliquescence relative humidity is at equilibrium, hygroscopicity measurements can be potentially compromised by mass transfer effects.

Chapter 5 of this dissertation describes how organic ultrafine particles can be generated indoors by ionization air purifiers in the presence of certain VOCs. It was shown that the operation of an ozone-generating air-purifier in a closed indoor environment results in an increase in the steady-state ozone concentration that is directly proportional to the air-purifier's ozone emission rate. Chapter 6 addresses the kinetic analysis of competition between aerosol particle removal and generation by ionization air purifiers. It was shown that air purifiers may increase the respirable PM mass concentration instead of reducing it as advertised by the manufacturer.

Chapter 1

1. Ultrafine Particles

1.1. Introduction

Ultrafine aerosol particles UFP (defined as particles with aerodynamic diameters < 100nm)[1] are ubiquitous in the atmosphere. They are frequently observed in the troposphere during nucleation events when their molecular precursors condense into new particles through various condensation processes [2].

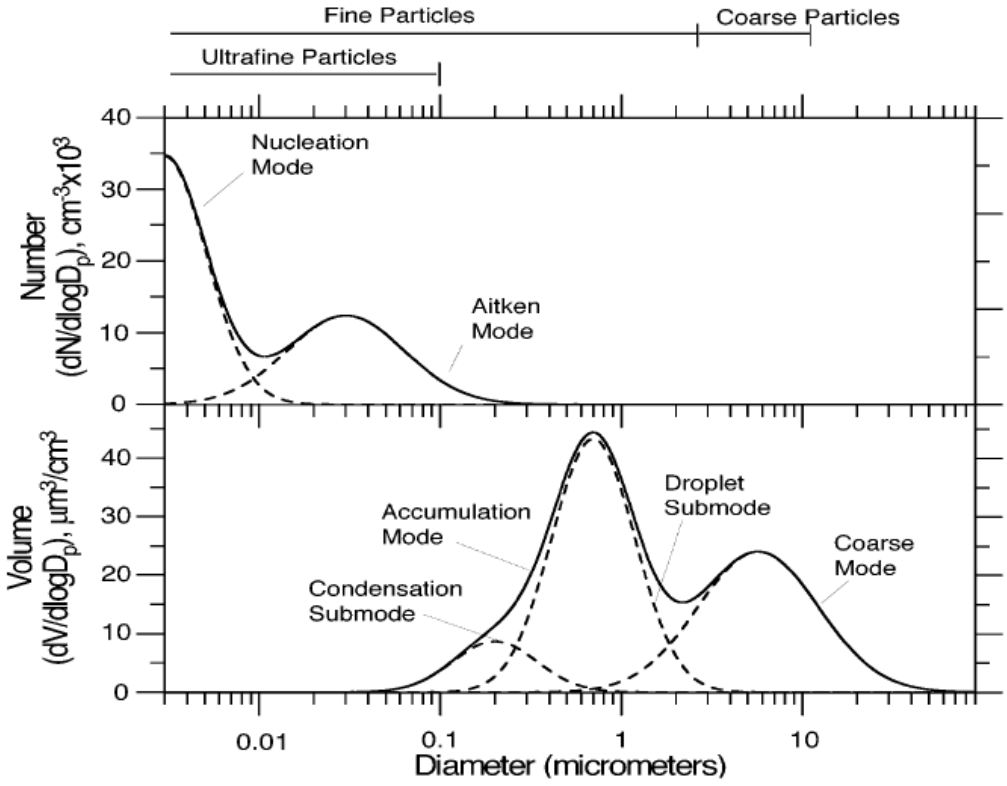

Figure 1.1: Nucleation, accumulation and coarse modes of ambient particles (Courtesy of Constantinos Sioutas, Ultrafine Particles Conference, Los Angeles 2006)

As a result of their very low inertia, UFP are highly mobile in the atmosphere, and depending on the conditions, they have a life time ranging from fraction of a second up to several hours or days with respect to deposition [3]. Furthermore, UFP efficiently coagulate to form accumulation or coarse modes as shown in Fig.1.1. UFP are also known as transient mode particles due to their rapid losses to deposition and coagulation. Nevertheless, UFP are the most abundant of all particles, dominating the number distribution and making a significant contribution to the surface area of atmospheric particulate matter.

To illustrate this point, let us consider an aerosol characterized by mass concentration of 10 $\mu g/m^3$ and containing monodisperse particles. This mass concentration translates into one particle per cm^3 for 2.5 μm particles, compared to $2.0x10^6$ cm^{-3} particles of 20 nm in size. In addition, the combined surface area for such collection of 20 nm particles is two orders of magnitude higher than that for 2.5 μm particles. Therefore their surface to volume ratio is dramatically increased for an aerosol dominated by UFP[4].

As shown in table 1, a single 10 μm particle has the same mass as 10^9 particles of 10 nm diameter. As the particle size gets smaller, and its surface-to-volume ratio increases, its physicochemical properties may become uniquely different from corresponding properties of a larger particle. As the number of molecules in UFP is small, a high proportion of them reside at the surface. For example, a 20 nm size particle has 12% of its molecules at the surface. This fraction increases to 25% for a 10 nm particle [5].

Table 1.1 Comparison of number, area and size for different particles having the same weight concentration [3]

Particle diameter (μm)	Relative particle number	Relative surface area
10	1	1
1	10^3	10^2
0.1	10^6	10^4
0.01	10^9	10^6

1.2. Sources of Ambient Ultrafine Particles

Atmospheric UFP mostly originate from combustion processes and from heterogeneous and homogeneous nucleation of non-volatile products of photochemical processes involving organic species. These sources can be categorized into primary and secondary. The primary source emits particles in the atmosphere directly (for example combustion processes) [6, 7], whereas the secondary source emits molecular precursors, which then undergo various gas to particle conversion processes [8]. According to the California Air Resources Board (CARB), the main sources of emission of UFP in California South Coast Air Basin in 1996 are on-road motor vehicles (43%), stationary source fuel combustion (32%), diesel engines (10%), and other industrial processes (15%). Kim et al have studied UFP sources and formation, and found that urban sources are dominated by nearby freeways, while inland sources of emissions are mostly photochemical formation of SOA [9]. The number concentration of these particles is highly dynamic, and their diurnal variations can be highly dependent on the presence of lager particles. UFP have an average ambient background levels of 1-4x10^4 cm^{-3} , but their mass concentration is normally is not greater than 2 μg m^{-3} [10].

1.3. Chemical Composition of Atmospheric UFP

Numerous field experiments have been conducted to characterize the size distribution and the chemical composition of UFP. They found that UFP composition included 32-67% organic compounds, 3.5-17.5% elemental carbon, 1-18 % sulfate, 0-19% nitrate, 0-9% ammonium ions, 0-2% sodium, 0-2% chloride, 1-26% trace metal oxides, of which Fe, Ti, Cr, Zn were the most abundant trace elements.

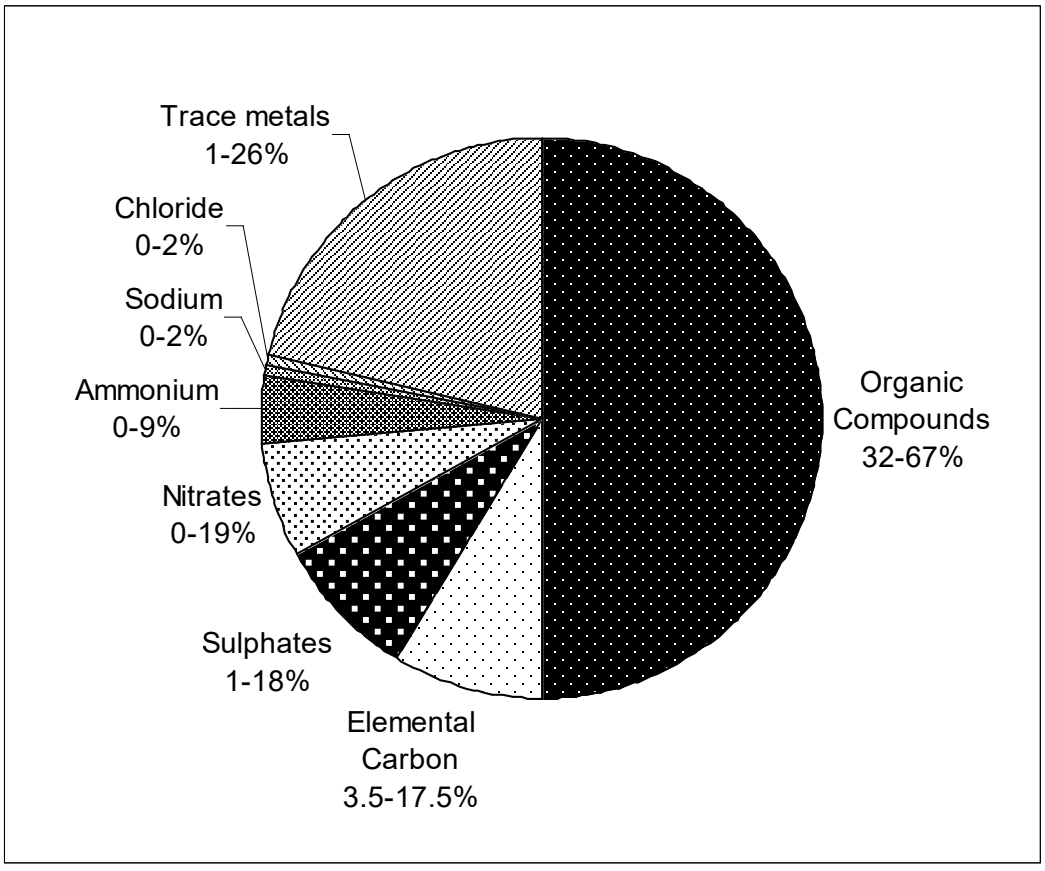

Figure 1.2: Composition of ultrafine aerosol particles in Los Angeles atmosphere [7]

UFP mass concentration was found to be in the range of 0.5-1.5 $\mu g/m^3$ [11-15]. UFP composition is location dependent, and there are strong differences between urban and rural locations [16].

Compositional analysis of individual UFP utilizing mass spectrometry has found that organics may vary from 10-70% by mass [17-19]. Other studies have also found that the composition of atmospheric ultrafine particles comprise significant amount of organics compared to larger particles that comprise mostly inorganics.[20-23]. In addition, a significant fraction of the organic material in particles has been shown to have surfactant properties [24-26].

1.4. Health Effects of UFP

In light of the increasing amount of epidemiological and toxicological evidence, ultrafine particles are now recognized as a potential cause for the adverse health effects of air pollution. Per unit mass, UFP are more potent than fine particles for causing inflammatory response. Their enhanced surface-to-volume ratio and large number density relative to other particles, makes it possible for UFP to efficiently transport toxic substances into various tissues [27]. There is a growing concern about the exact role these particles may play in the observed increase in respiratory and cardiovascular premature deaths [28, 29]. According to Hughes, approximately 10^{11} particles are deposited daily inside different parts of the respiratory system of an average adult [8]. Figure 1.3 shows fraction deposition model of inhaled particles according to the International Commission on Radiological Protection ICRP (1994). In that model, larger particles are more likely to be deposited in the upper airways of nasal cavity, nasopharyngeal/ laryngeal and the tracheobronchi, whereas UFP have higher deposition probabilities in the alveoli region.

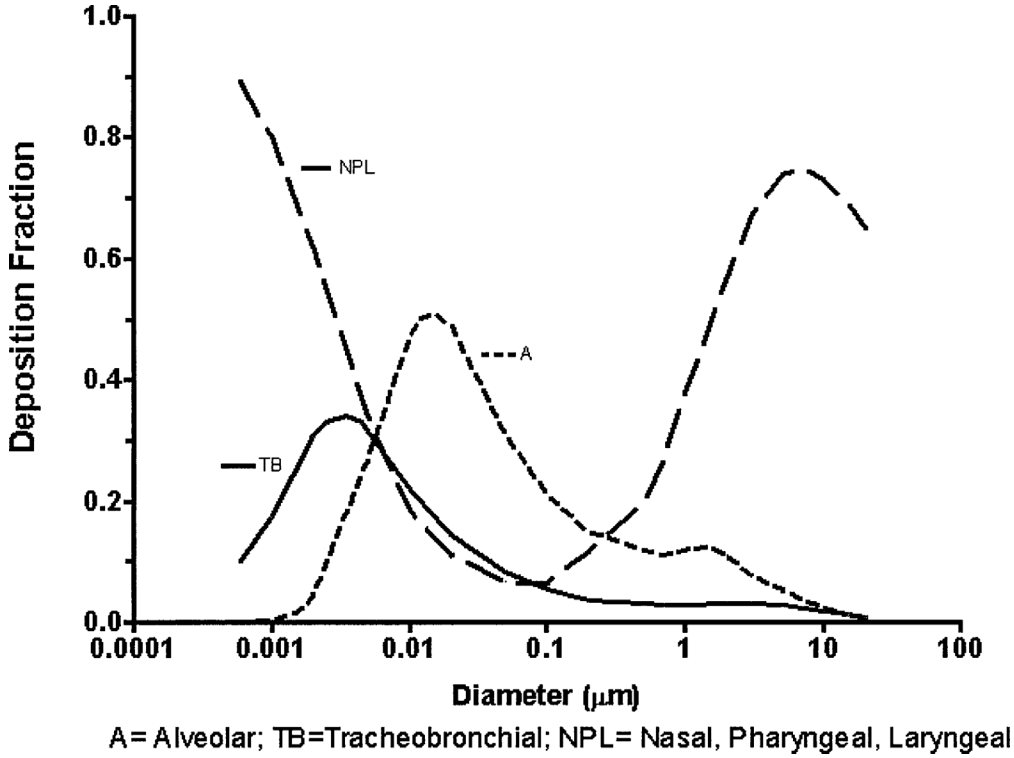

Figure 1.3: Depositions of inhaled fine and ultrafine particles in different region of the respiratory system from International Commission on radiological Protection ICRP (1994)

The respiratory system has its own defense mechanism of using alveolar macrophages to consume foreign inhaled objects. However, there is limited number of macrophages per alveolus which are easily overwhelmed by the sheer number of UFP. Therefore, during strong air-pollution episodes, the function of macrophages is impaired, and UFP are able to be retained for a longer time on the alveolar epithelium. Furthermore, given enough time, UFP can penetrate inside the alveolar epithelium by endocytosis.

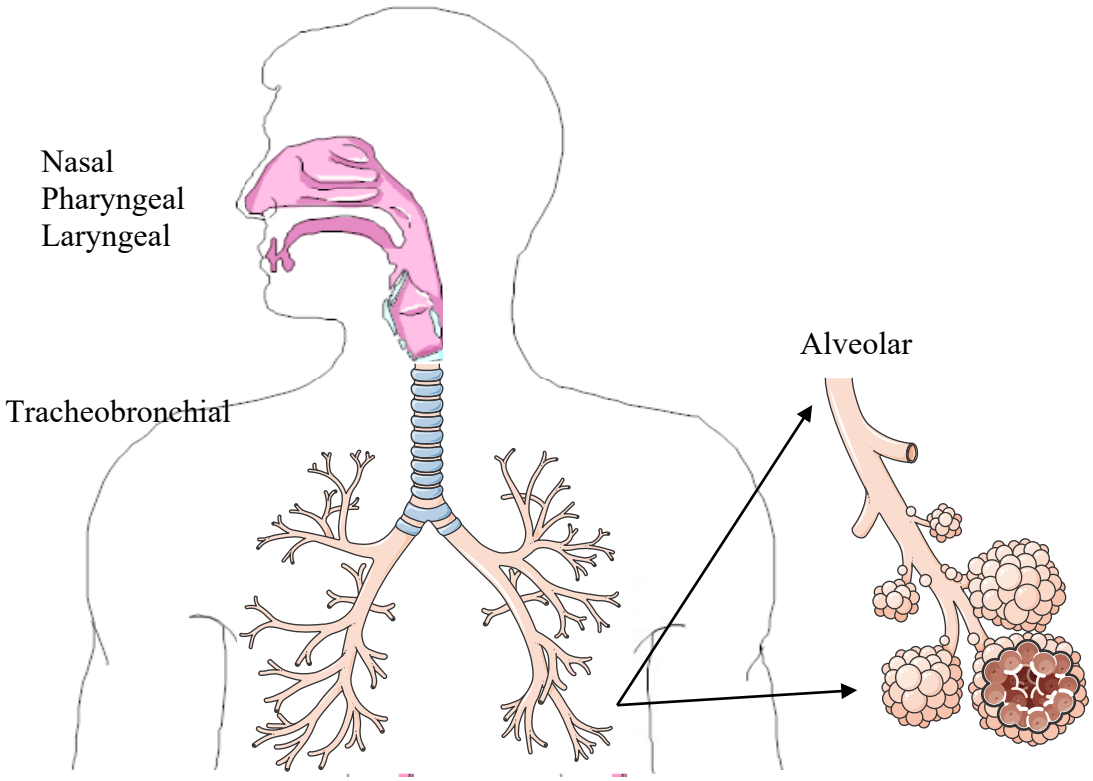

Figure 1.4 Deposition of UFP in respiratory system

After their deposition onto the alveolar epithelium, UFP will be transported further down to the gastrointestinal tract and on to other organs. In this mechanism, UFP are able to enter into the bloodstream and therefore to the central nervous system directly by means of alveolar endocytosis or indirectly by means of gastrointestinal tract [30].

The translocation of UFP into the epithelia is accompanied by a release of hydrogen peroxide or histamine [31]. This condition is known as oxidative stress, in which excessive amount of free radicals are released into the alveoli [32, 33]. Therefore, high exposure to ultrafine particles leads to systematic inflammation through oxidative stress and promotes the progression of atherosclerosis.

Particles that are deposited in the upper airways may be cleared within 24 hours. However, the clearance of UFP that are deposited deeper into the alveoli is a slower process; it involves phagocytosis, cell migration and mucociliary transport, processes that may take months or even years. [34]

1.5. Climate Effects of Ambient Aerosol Particles

Atmospheric aerosols influence the Earth's radiative balance directly and indirectly [35]. The direct effect of particles on climate results from scattering of the incoming solar radiation back to space by all particles, and absorption of solar radiation by elemental carbon particles. There are several additional ways, in which aerosol particles influence the radiative balance indirectly. Firstly, they can function as Cloud Condensation Nuclei (CCN) [36, 37] by allowing cloud and fog water droplets condense on their surface. Secondly, aerosol particles can influence the cloud droplet size distribution upon mixing with preexisting clouds [35].

With respect to radiative forcing, the aerosol indirect effect has the largest uncertainty and is poorly understood. The main uncertainty comes from the lack of understanding of effect of organic species on hygroscopic properties of aerosol particles. To make things even more complicated, the organic composition of aerosol particles is constantly changing because of oxidation by atmospheric OH, O_3 and NO_3 [38]. Upon oxidation, the organic coating becomes highly functionalized and potentially more hydrophilic. Therefore, the formation of aldehydes, carboxyls, alcohols, and other functional groups changes the optical and chemical properties of organic aerosols as well as their effectiveness as CCN [39, 40].

1.6. Observation of UFP in Indoor Environment

Several studies have identified cooking, cleaning, burning candles, vacuum cleaners, air fresheners and smoking as primary contributors to indoor airborne particulate matter. [41-44]. In addition, outdoor ultrafine particles can significantly contribute to indoor urban environment [45, 46]. Recently, other sources for indoor UFP were suggested to be potentially more potent. For example, stand-alone air purification devices for indoor use have gained widespread popularity in recent years, however, certain air purifiers emit ozone during operation, either intentionally or as a by-product of air ionization [47-50]. Ozone, a criteria air pollutant regulated by multiple health standards, represents a serious health concern by itself [51]. In addition, ozone can react with certain indoor surfaces [52-56] and indoor VOC [57-60] generating secondary products with potential adverse health effects. For example, terpene oxidation products are known eye and airway irritants [61, 62]. A series of experiments on major brands of air purifiers were conducted in indoor environment setup. Detailed results and findings of these experiments were discussed in details Chapters 5 and 6.

1.7. Thesis Objectives

The first part of this thesis focuses on hygroscopic properties of internally mixed inorganic/surfactant aerosol particles. The main goal of this work is to understand the relationship between the structure and hygroscopicity in ultrafine particles, and contrast their hygroscopic behavior to that of much better studied fine particles. Chapter 2 discusses a novel water uptake experimental setup that was designed and constructed specifically for this work. Chapter 3 discusses a set of detailed experiments on

hygroscopicity of 17 nm ultrafine particles composed of NaCl and surfactants AOT and SDS. Chapter 4 discusses the effects of particle size on its hygroscopic growth, and addresses mass transfer limitations. The second part of this thesis addresses a different aspect of UFP chemistry: their formation in indoor environments. Chapter 5 shows how organic ultrafine particles can be generated indoors by ionization air purifiers in the presence of certain VOCs. Chapter 6 addresses the kinetic analysis of competition between aerosol particle removal and generation by ionization air purifiers.

Chapter 2

2.1. Generation of Ultrafine Aerosol Particles

Electrospray is a soft ionization technique, wherein a solution containing analyte is pumped through a capillary needle maintained at a high voltage (2-3 kV) [63]. Modern applications of electrospray technique are mostly confined to mass-spectrometry because it represents a convenient way to extract ions from solutions with minimal fragmentation. However, under certain conditions, electrospray is also capable of generating ultrafine aerosol particles with a fairly narrow size distribution [64]. As a first step in this project, a home-build electrospray aerosol particle generator was constructed and optimized for the generation of mixed NaCl/surfactant particles. This setup is described in detail below.

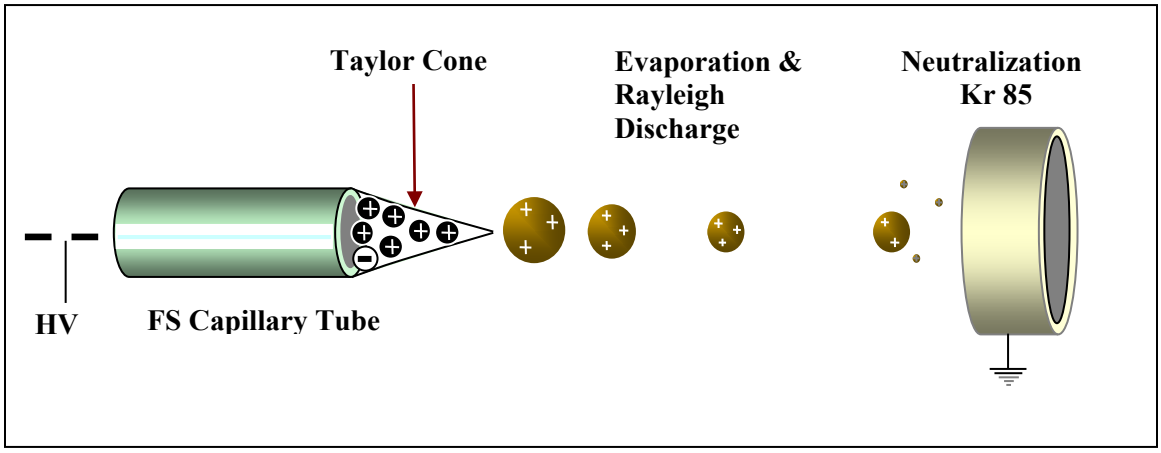

Figure 2.1: The primary droplets become unstable and may undergo Coulombic fission and evaporative ion loss.

The basic idea of the design is shown in Figure 2.1. The solution is supplied through a fused-silica capillary tube with a syringe pump. A sufficiently high electric field is established between the capillary tip and a bipolar neutralizer (Kr-85, 10 mCi TSI

Model 3054), drawing the solution outward and forming what is known as Taylor cone jet. The Taylor cone breaks up into smaller but highly charged primary droplets which then experience a sequence of evaporation and Rayleigh discharge steps [65].

Figure 2.1 also includes a simplified cartoon of the primary droplet evaporation. The initially generated droplets are about 100-500 nm in size, each carrying some 10^4-10^6 charges. As the solvent evaporates, surface charge density of the droplets increases. Once the surface charge density reaches the Rayleigh limit, wherein the electrostatic repulsion equals to the surface tension forces, the droplet surface becomes unstable. The ions repulsion that are on the droplet surface can eventually overcome the surface tension and produce satellite droplets having a small mass but carry a high overall charge [66-68]. However, the advantage of having a neutralizer is theorized to prevent a complete disintegration of the primary droplet into ions [69], which is valuable for mass-spectrometry but is a nuisance for aerosol particle generation.

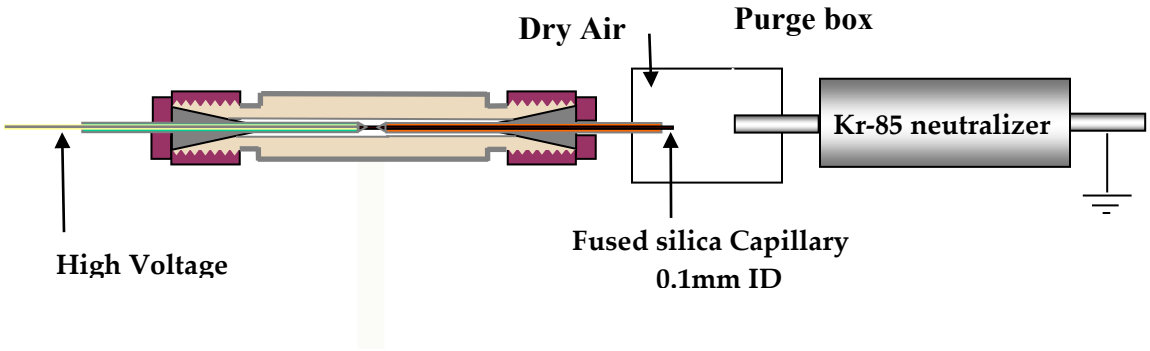

Figure 2.2: Electrospray aerosol particle generator setup

Figure 2.2 shows a schematic diagram of the aerosol particle generator constructed for this work. A syringe pump (KD Scientific) that was operated at 25-100

μL/hr, was capable to generate desired particles size. The capillary needle (250 μL Hamilton syringe) was maintained at a high voltage (2-3 kV). The stable cone jet was viewed by a microscope piece (x25 magnification). A range of (8-30) nm UFP can be easily generated by either varying the pumping flow rates, changing the inner diameter of fused silica capillary (25, 50 and 100μm ID), by varying solvents and solution concentrations.

For the purpose of testing the utility of this electrospray setup for generation of UHP containing surfactant molecules, 0.5g/l aqueous surfactant solutions of Sodium Dioctyl Sulfosuccinate (AOT) or Sodium Dodecyl Sulfate (SDS) were elertosprayed through a 25 μm ID fused-silica capillary tube. The structures of these surfactants are shown in Figure 2.3. The generated particles were characterized by Scanning Mobility Particle Sizer (SMPS TSI 3080).

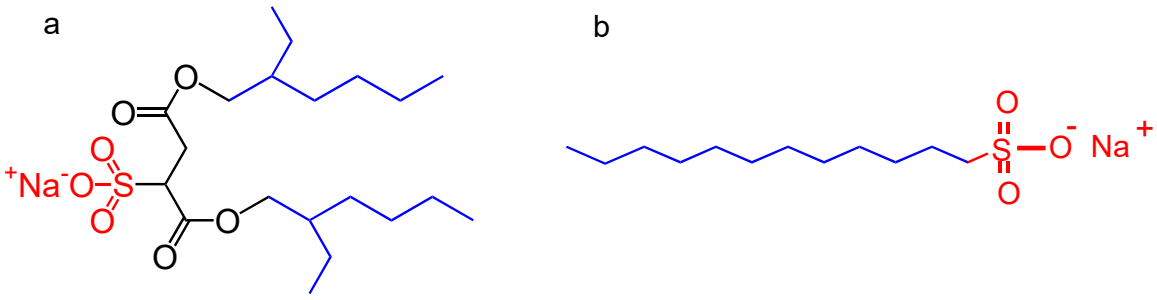

Figure 2.3: a) Sodium Dioctyl Sulfosuccinate (AOT). b) Sodium Dodecyl Sulfate (SDS)

Fig 2.4 shows a lognormal particle size distribution produced by electrospraying aqueous AOT. The distribution is centered at 17.0 nm and has a standard geometric deviation of 1.14. The total count corresponds to 1.0×10^6 particles per cm^3, which is more than enough for the hygroscopic growth experiments described below.

Particles were also collected on TEM grids and imaged under UHV conditions. Some of the resulting images are shown in Figure 2.5. For these experiments, the electrospray conditions were adjusted to produce larger particles (~25 nm in diameter). The imaged particles appear to retain their size under UHV conditions suggesting that they are free of solvents (presence of solvents in the particles is discussed in more detail in the following section). Typical parameters used for generation of aerosol particles by this electrospray source are listed in Table 2.1. Some of these conditions were optimized for maximal particle number concentration, whereas others were optimized for the best stability or the narrowest size distribution.

Table 2.1 Comparison of number, area and size for different particles

Solvent	Solute	Concentration	Optimal flow μL/min	Optimal Voltage	Particle count	Particle size (nm)
MeOH	NaCl	0.5 g/L	50	2100 kV	$1.0x10^6$	17.0
H2O	NaCl	3.0 g/L	70	2700 kV	$1.0x10^6$	17.0
MeOH /Chloroform	NaCl	0.5 g/L	50	3400 kV	$1.0x10^6$	17.0

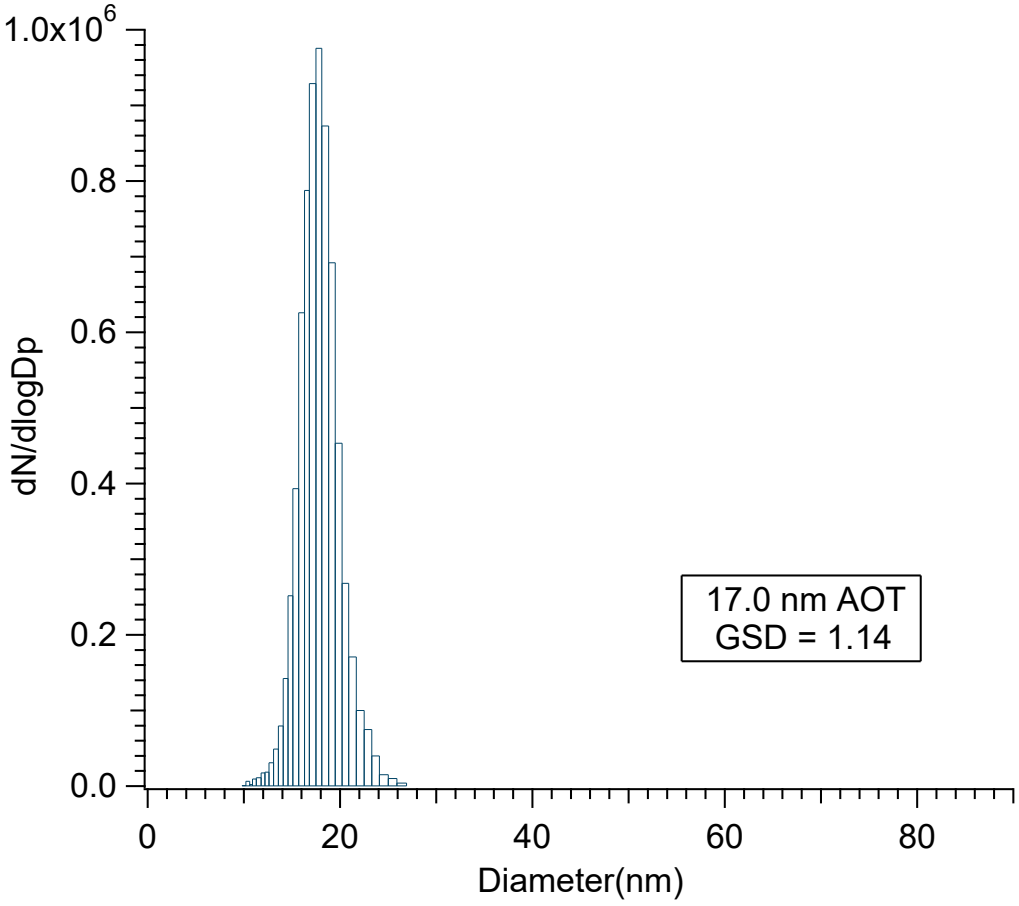

Figure 2.4: Particle size distribution of electrospraying an aqueous solution of 0.5 g/L AOT.

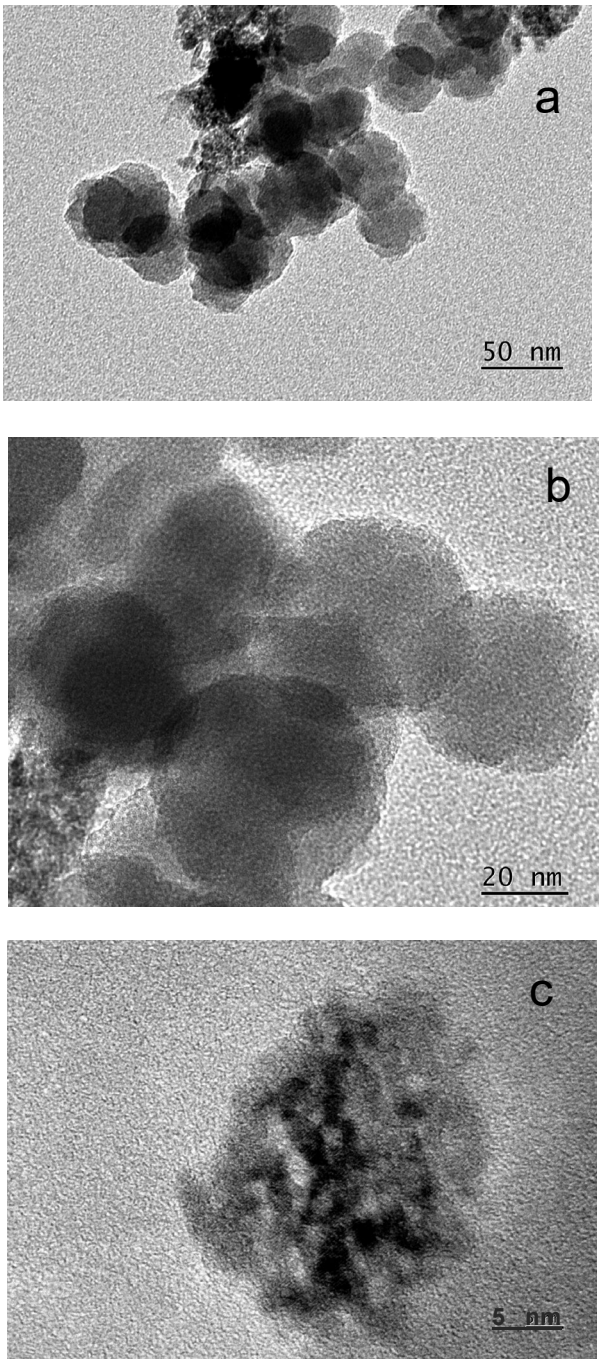

Figure 2.5: TEM images of AOT particle cluster in (a) and (b) at different magnifications. In panel (c), a single AOT particle is shown

2.2. Solvent Content of Generated UFP

The properties of solutions of surfactant molecules under electrospray conditions are not well established. To verify whether particles generated by our electrospray source contained residual solvent, two separate experiments were conducted. The first one was to measure the effect of laser vaporization on the particle size. The second was to measure the effect of conventional heating on the particle size.

For the laser experiment, a 0.1 g/L, mixture of NaCl with a probe molecule 2,5-dihydroxybenzoic acid (DHB) was electrosprayed to produce 21 nm particles. DHB is a well known molecule that is frequently used in MALDI because it absorbs 355nm radiation and efficiently converts absorbed energy into heat [70, 71]. This heat can be utilized to evaporate any solvent excess in the aerosol particle containing DHB.

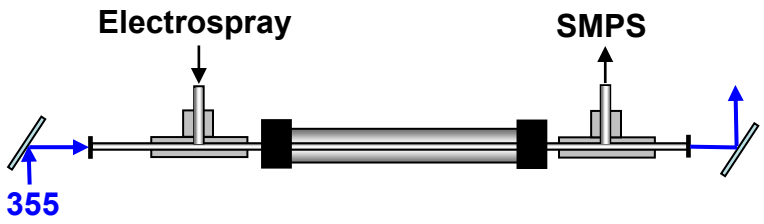

Figure 2.6: Experimental setup for laser heating of 21 nm particles consisting of NaCl/DHB.

Solution of NaCl/DHB was electrosprayed and was directed into the setup shown in Figure 2.5 at 0.3 SLM by using a dry air as a carrier gas. The particles were exposed to variable amounts of pulsed 355 nm radiation from a frequency tripled Nd: YAG laser (20

Hz, 10 ns pulse width). The generated particles had a size distributions centered at 21 nm with a Geometric Standard Deviations within GSD= 1.10. The size distributions were measured before and after the laser exposure, and compared to the most immediate scans when the laser was off.

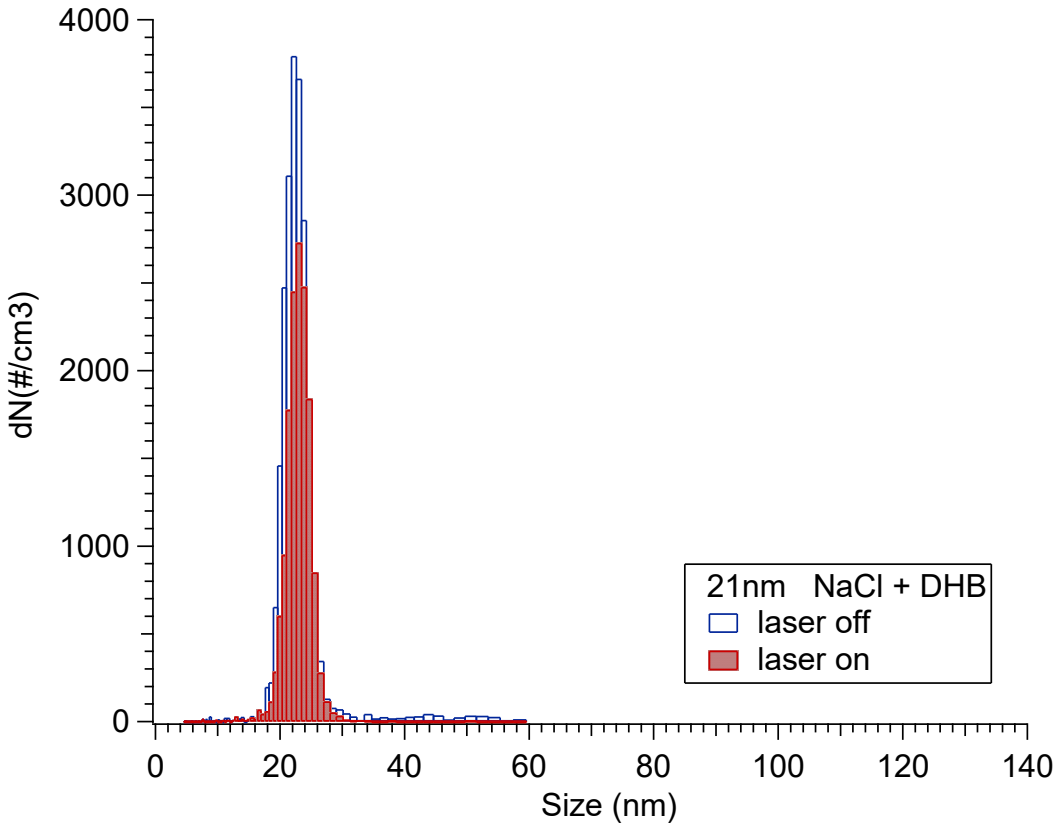

Figure 2.7: Size distribution for 21 nm particles of NaCl/DHB. When the laser is on, there is no significant decrease in size, but the particle count decreases.

No sign of particle size decrease was evident at pulse energies below 10 mJ/pulse. At higher pulse energy (30mJ/pulse), the particle size distributions decreased in total count, however, the distribution was still centered at 21 nm, indicating the laser completely vaporized a small fraction of particles. Further increase in the pulse energy resulted in total vaporization of all particles. Although these experiments were consistent

with solvent-free particles, they were not entirely conclusive because of the binary nature of the result (the laser either completely vaporized the particle or did nothing; no intermediate sizes were observed).

A second experiment was conducted by utilizing a tube furnace, and it tuned out to be more revealing. Solutions of pure NaCl, AOT and SDS were electrosprayed to generate particles of different sizes. The particles were directed into a heated 1/2" x 12" glass tube immediately followed by a diffusion dryer in order to minimize solvent recondensation back onto the particles after they come out of the furnace. The particle size distributions were compared before and after heating.

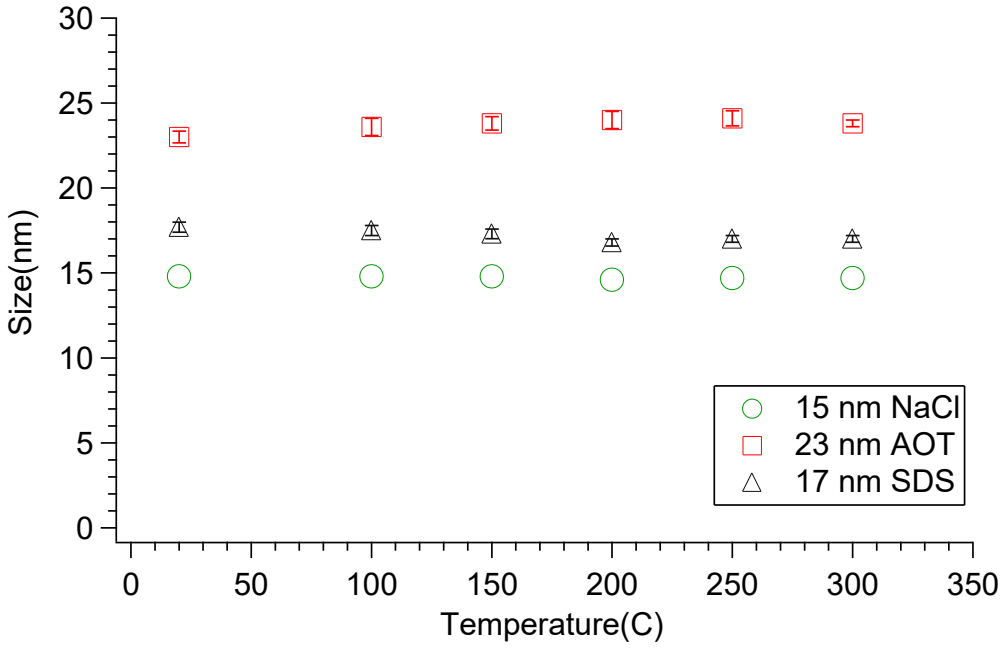

Figure 2.8: 15nm NaCl (circles), 23nm AOT (squares), 17nmSDS (triangles) are showing no apparent changes in size at different temperatures.

The experimental results are shown in Figure 2.8. Within the accuracy of SPMS size resolution, there was no evidence of size shift that would indicate further solvent evaporation up to 300 C^0 Celsius. We conclude from these experiments, that particles generated by the electrospray source are free of solvent molecules.

2.3. Hygroscopicity Experimental Setup

The main goal of this research project is to characterize hygroscopicity of ultrafine mixed soluble inorganic / surfactant ultrafine particles. To this end, we have constructed a Hygroscopic Tandem Nano-Differential Mobility Analyzer (HTNDMA), and used it to characterize hygroscopic activity of several different classes of ultrafine particles. Such tandem DMA techniques are widely used to study particle size changes due to water uptake [72-74]. The main components of this setup are two Nano-Differential Mobility Analyzers (NanoDMA) that are connected in series, conditioning section comprised of a combination of drying and humidification systems, and a condensation particle counter (CPC).

Throughout these experiments, the following protocol is adopted. Polydisperse particles that are generated by the electrospray source are dried and size selected by using the first NanoDMA. The monodisperse particles are then humidified to a desired relative humidity inside the conditioning section and finally are probed for a change in their particle size using a second NanoDMA. Details of all these steps are provided below.

2.3.1. Size Selection

The internally mixed ultrafine aerosol particles of NaCl and AOT or SDS surfactants were generated by electrospraying a 0.1 g/L aqueous solution of 100% NaCl (Aldrich) and 99.99% AOT (Fluka) or 99.99% SDS (Fluka). Solution analytes were dissolved in deionized water (OmniSolv, conductivity < 8 μΩ.cm) with variable relative weight concentrations of NaCl vs. surfactant. The source produced polydisperse particles, having geometric standard deviation <1.2 and particle counts of the order ~ 1.0×10^6 particles cm^{-3}. These particles were diluted with 3.0 SLM of filtered dry air, and were immediately neutralized by passing the flow through a bipolar neutralizer (Kr-85, 10 mCi TSI Model 3054), in order to establish a near Boltzmann charge distribution, with the most probable charge state centered at zero. Since their initial size was less than 20 nm, particles that remained charged after the neutralization were almost entirely comprised of singly charged particles; no multiply charged particles remained [75]. The generated aerosol particles were established to be solvent-free, and were assumed to be internally mixed after being electrosprayed, since their size distribution after deliquescence was unimodal. They were also assumed to have the same composition as the bulk solution mixture.

Fig 2.9 shows a detailed diagram of the experimental setup for manipulating the particles once they were generated. A flow of 0.3 SLM (standard liter per minute) of polydisperse aerosol particles was directed into the first Differential Mobility Analyzer (DMA1, TSI 3085) in order to narrow the size distribution. The applied DC voltage to the first NanoDMA and the internal flows both determine the mobility diameter of the selected particles. For instance, in order to change the particle size, the applied voltage

was adjusted while maintaining the same internal flows. The sheath air for DMA1 (3.0 SLM) was operated with a closed loop configuration, in which the excess air was filtered twice and was further dried with a Nafion dryer (PermaPure, MD-110), in order to maintain a stream of 3.0 SLM of clean dry air with an accurate and stable relative humidity of (%RH < 0.5). The polydisperse aerosol particles were size selected by applying a corresponding voltage.

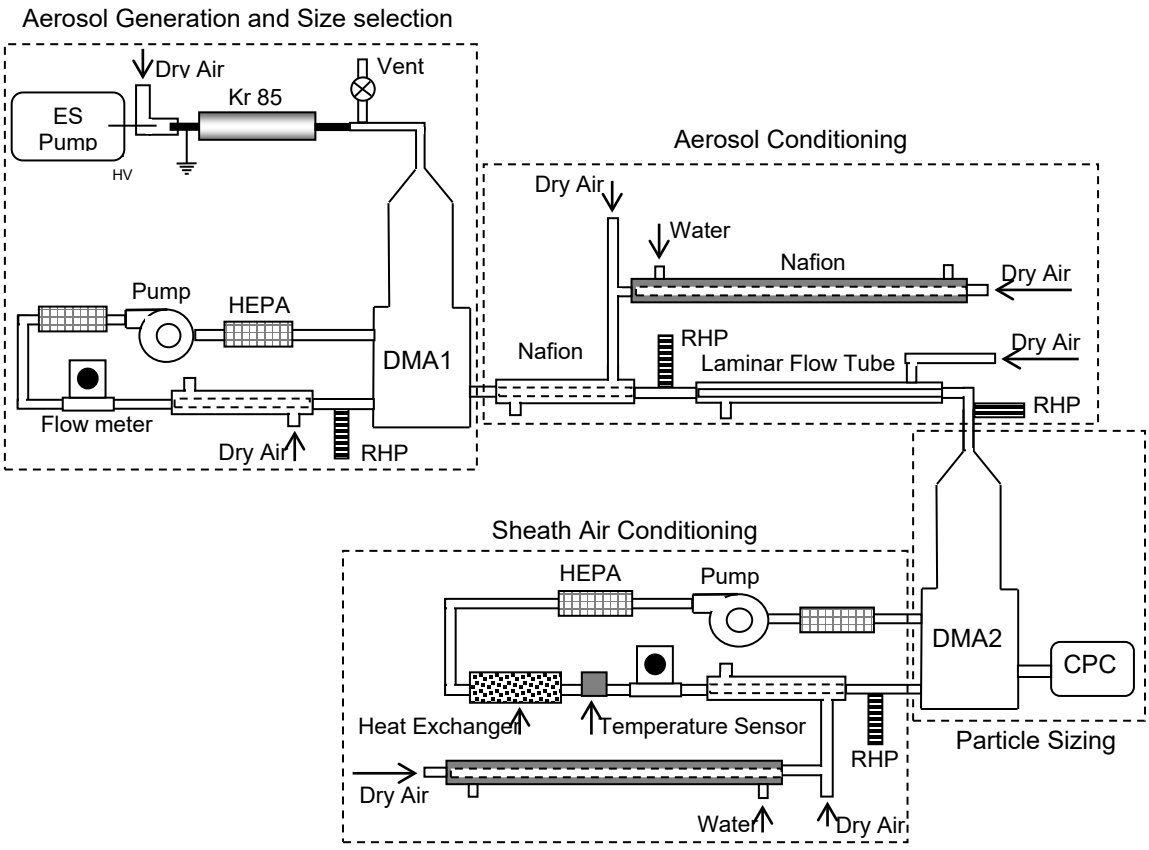

Fig 2.9: The experimental Hygroscopicity Tandem Nano Differential Mobility Analyzer (HTNDMA) constructed for this work.

A typical size distribution of particles before and after the size selection process is shown in figure 2.10

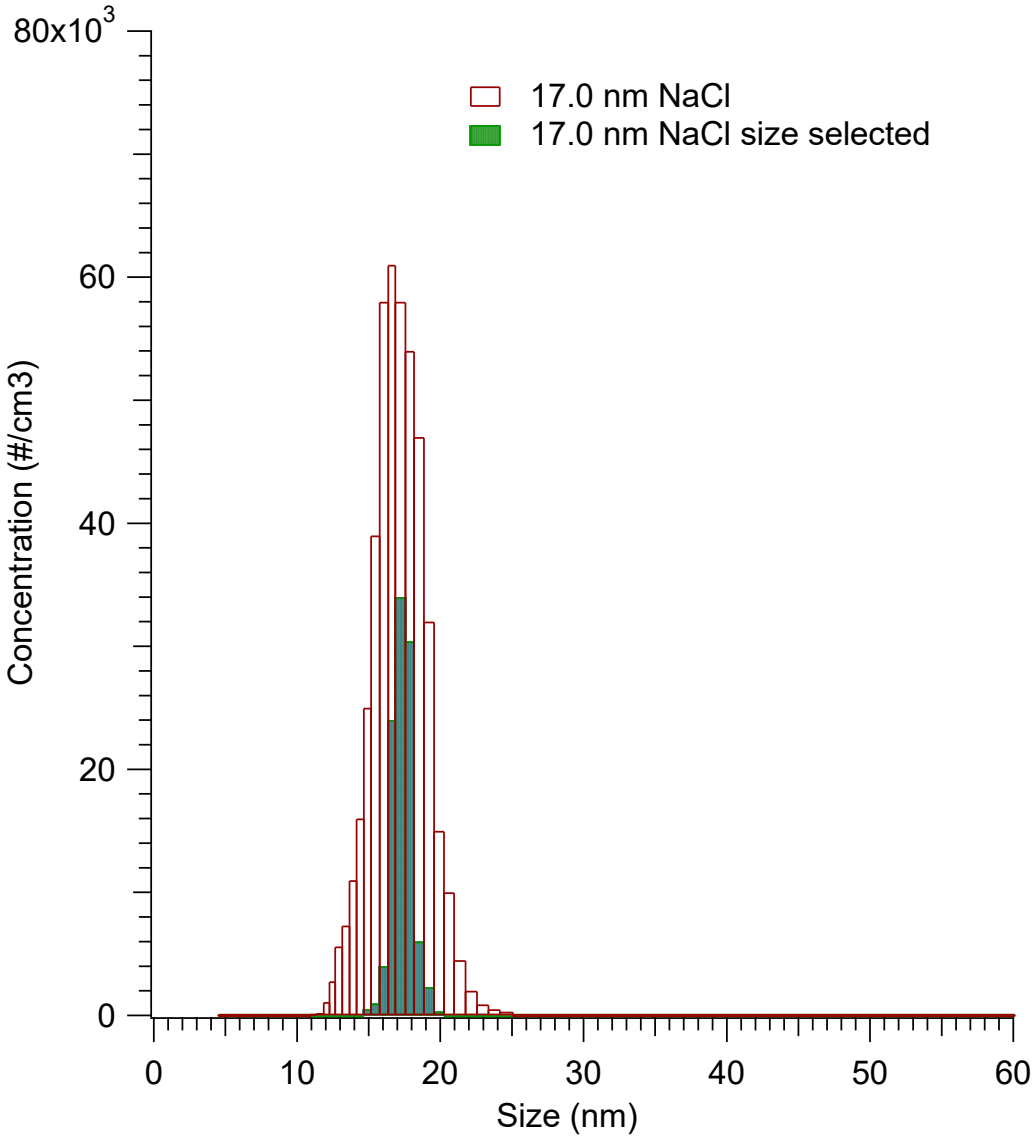

Figure 2.10: Size distribution for 17.0 nm NaCl particles before and after the process of size selection. 17.0nm NaCl particle distribution having Geometric Standard distribution of GSD =1.25 (red), after the second Nano-DMA, size distribution has GSD = 1.05 (green)

2.3.2. Aerosol Particles Conditioning

Once the particles were size selected, they were conditioned to achieve a desired relative humidity (RH). The conditioning of monodisperse aerosol particles was achieved by using a combination of a Nafion humidifier (PermaPure MD-110) and a laminar flow conditioner (a copper tubing with 1/2“ID that could be maintained at desired relative humidity). A rapid and stable adjustment of a desired relative humidity inside the Nafion humidifier was achieved by mixing different ratios of a highly humidified air flow (%RH > 95) and dry air flow as shown in Figure 2.9 The monodisperse aerosol particles experienced a relative humidity gradient inside the Nafion humidifier with a residence time of 1.35s. The relative humidity was monitored by Vaisala HMP237 probes. They were periodically calibrated against %RH of air above standard salt solutions (Vaisala ready saturated solutions) with an accuracy of ±1.0% for the low RH range (%RH < 50) and ± 2.0% for the upper RH range (%RH > 80).

For some experiments, a longer humidification time was desired in order to study possible mass transfer effects during hygroscopic particle growth [76]. In such cases, a laminar flow conditioner was used, where particles were exposed to a matching relative humidity with an additional residence time of 60 s. As relative humidity was increased, a necessary adjustment to an encountered relative humidity deviation between the inlet and outlet of the flow conditioner was made by introducing a laminar flow of dry air alongside the conditioner.

2.3.4. Sheath Air Conditioning and Particle Sizing:

Humidified particles were sized in the second DMA column. To ensure the proper operation of this column, the sheath air of the second DMA (3.0 SLM) had a closed loop configuration to allow an independent control of relative humidity. It was carefully conditioned in order to match the relative humidity of the incoming conditioned monodisperse aerosol particles stream. The RH was adjusted by mixing a humid (>95%) and a dry air flows in different proportions. The excess air was filtered twice and was heat exchanged to match the sheath air temperature. The relative humidity was monitored by a Vaisala HMP237 probe. The size distribution of the conditioned particles was measured with by DMA2 and the condensation particle counter (CPC, TSI 3025A). The total particle conditioning time (from DMA1 output to DMA2 output) was 67 s. All gas flows were periodically calibrated using a Gilian-type mass flow calibrator. The particle growth factors were measured by taking the ratio of the averaged mobility diameters for the dry particles with respect to their mobility diameters after being conditioned.

Chapter 3

3. Hygroscopicity of Ultrafine Particles

3.1. Introduction

Ultrafine organic aerosol particles (UFP; diameter < 100nm) are ubiquitous in the atmosphere. Despite their small mass and size, they are the most abundant of all particles in terms of their number concentration. While a significant fraction of these particles were found to contain organic surfactants [77-80], the effect of surfactants on hygroscopicity of ultrafine particles is not well characterized.

UFP are characterized by having an enhanced Kelvin effect and a greater surface energy contribution to the overall free energy of the particles. Their small size can drastically alter their hygroscopic behavior relative to larger particles with the same composition [73]. The effect of particle size becomes the most pronounced when the size approaches nanometer domain. To the best of our knowledge, the hygroscopicity of internally mixed nanometer-sized particles containing soluble inorganic salts and organic surfactants have not been investigated in the past.

3.2. Deliquescence

Deliquescence is defined as the phase transition that takes place upon adsorption of water vapor by a crystalline solid until it completely dissolves into a saturated solution. The deliquescence transition occurs when the free energy of the solid crystal equals the free energy of the droplet [81]. Upon deliquescence, the particle size undergoes a sudden

jump as shown in Figure 3.1. Particle growth factor is defined as the ratio of particle diameter at a given relative humidity (RH) to the diameter of the dry particle measured well below the deliquescence point. Upon decreasing the relative humidity a reverse phase transition from a dissolved to crystalline form takes place at so called efflorescence point. Efflorescence normally takes place at a lower RH than deliquescence because of kinetic limitations. Further increase in RH above the deliquescence point causes the deliquesced particle to absorb more water and grow further in size (Figure 3.1).

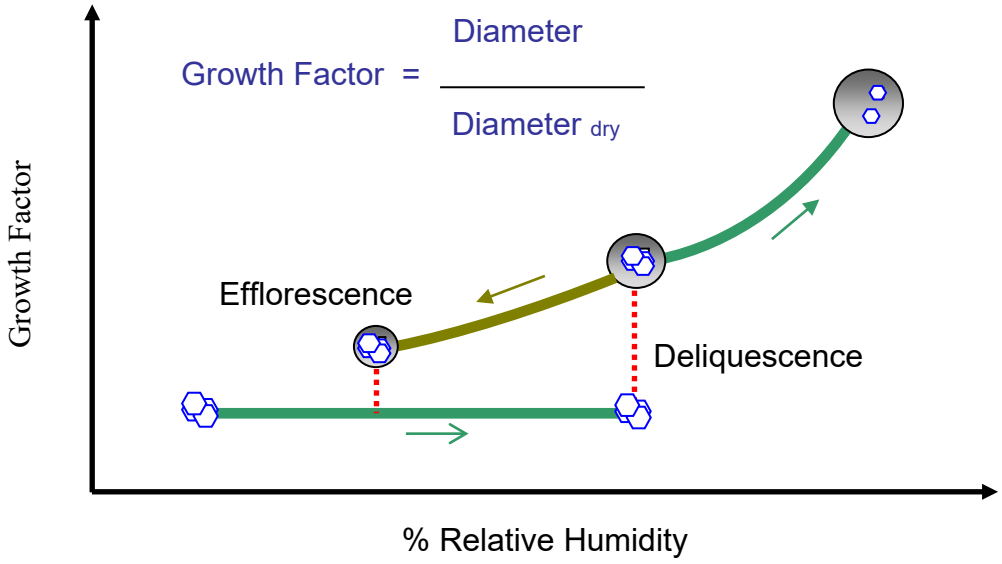

Figure 3.1: Deliquescence and efflorescence of pure crystalline compound

The water vapor content is usually defined by specifying percent relative humidity %RH:

$$RH = \frac{p}{p_0} \cdot 100\%$$

Where p is the partial water vapor pressure and p_0 is the equilibrium water vapor pressure for a given temperature. If water vapor is treated as an idal gas, the RH can be equated to the activity of gas-phase water molecules. A soluble inorganic salt having a well defined crystalline structure in a dry environment normally undergoes deliquescence and efflorescence at well defined relative humidity values[73].

According to thermodynamics, Gibbs free energy of the crystalline phase of any pure compound should be independent of activity of gas-phase water (we neglect a thin layer of surface water adsorbed on the crystalline surface).

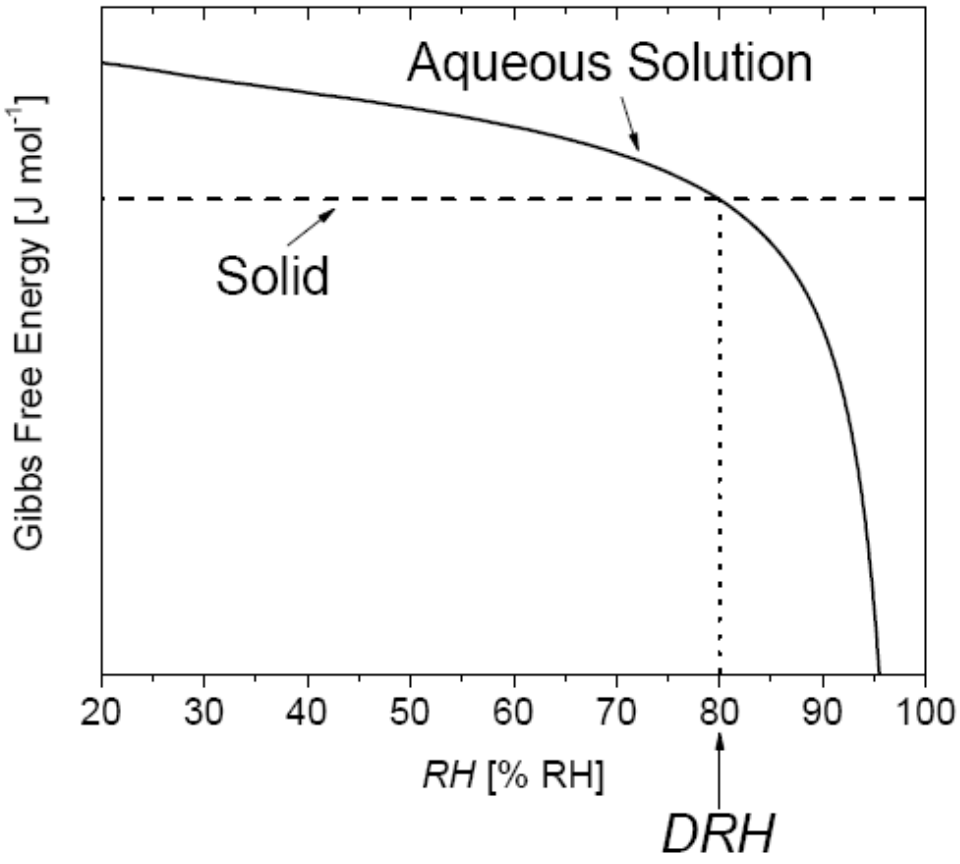

Figure 3.2: Phase transition of a single crystalline component [36]

However, Gibbs free energy of the same compound in solution is a function of its activity in that solution, which depends on RH as shown in figure 3.2[36]. Compounds generally undergo phase transition in order to accommodate for the lowest Gibbs free energy available for the system [36, 82]. The deliquescence transition occurs at the intersection of solid and solution curves shown in Figure 3.2. If the relative humidity is less than the deliquescence relative humidity (DRH), the crystalline phase is thermodynamically preferred. On the other hand, if relative humidity is greater than the DRH, the compound will exist in the solution phase.

3.3. Deliquescence in Binary Systems

Deliquescence phase transitions in binary systems are usually described assuming ideal behavior. However, mixtures of inorganic salts and surface active agents that are used in this work may or may not be ideal, and therefore experimental measurements presented here are needed in order to assess the deviations from the ideal behavior.

Figure 3.3 shows a typical deliquescence curve of an ideal mixture of two deliquescing components, KCl and NaCl. The system initially shows no water uptake until it reaches 72% RH, at which point the more soluble component (KCl) starts to dissolve to form a saturated aqueous solution that is in equilibrium with its own solid crystalline form. As %RH increases, the second component (NaCl) begins to dissolve, resulting in a coexisting of both solids that are in equilibrium with their saturated aqueous solution at 80% RH. At this point, a complete deliquescence for the mixture occurs. It has been observed by Tang et al [83] that the initial deliquescence of the mixed components

always occurs at a lower value than that for either one of the components. Above 80% RH, there are no more solids remaining, and the saturated droplet continues to grow.

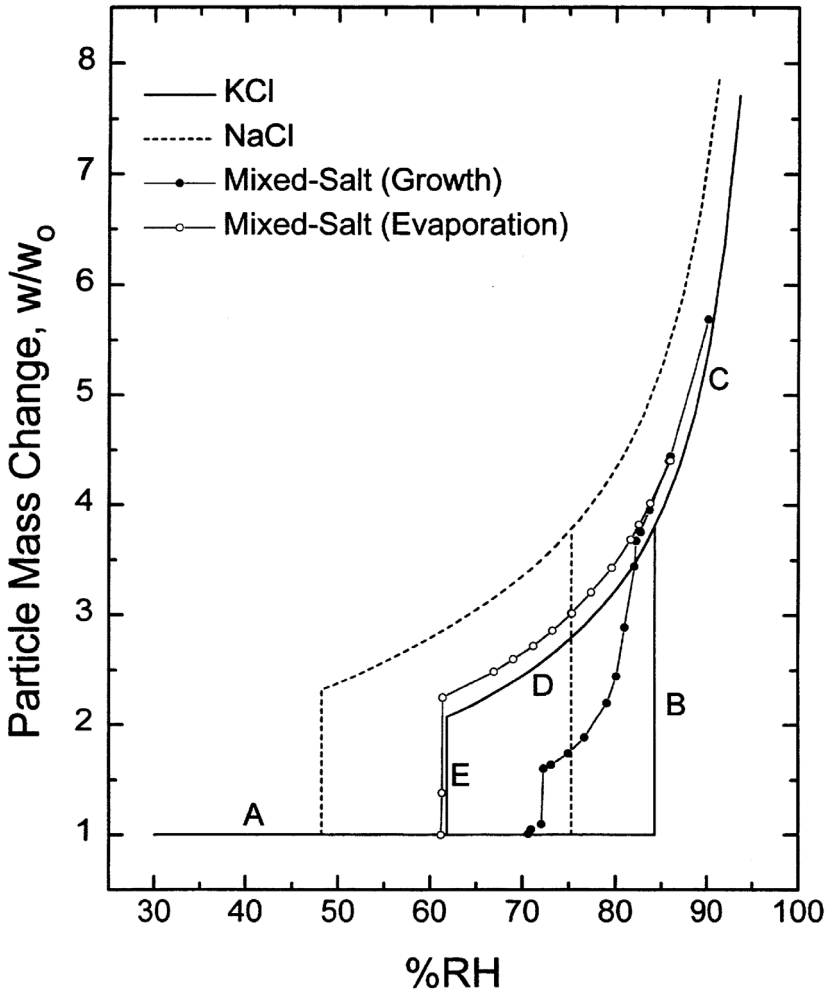

Figure 3.3: Example of a growth curve for a binary system of two deliquescent components. Particles are composed of mixed salt with 66% wt KCl and 34 wt% NaCl, Tang et al. [83]

A more atmospherically relevant model system to this work is particles composed of mixtures of soluble inorganic compound and poorly soluble organic compound. Investigations of these model systems are scarce. Our investigation in this chapter on nanometer-sized NaCl particles mixed with organic surfactant provides basis to such model.

3.4. Experimental

A more detailed experimental setup is described in Chapter 2. The following is a brief summary. Before size selection, the internally mixed ultrafine aerosol particles of NaCl and AOT or SDS surfactants were generated by electrospraying a 1.0 g/L aqueous solution of 100% NaCl (Aldrich) and 99.99% AOT, (Fluka) or 99.99% SDS, (Fluka). Solution analytes were dissolved in deionized water (OmniSolv, conductivity < 8 μΩ.cm) with variable relative weight concentrations of NaCl vs. surfactant. The polydisperse particles that were generated by the electrospray source had a geometric standard deviation <1.2 and particle counts in the range of ~ 1.0×10^{6} particles cm^{-3}. These particles were diluted with 3.0 SLM of filtered dry air, and were immediately neutralized by passing the flow through a bipolar neutralizer (Kr-85, 10 mCi TSI Model 3054).

The setup had an optional Nafion Dryer (PermaPure, MD-110) installed right before the first DMA to insure particles were completely dry. The generated particles were assumed to be internally mixed and were also assumed to have the same composition as the bulk solution mixture. Only 0.3 SLM of polydisperse aerosol particles were directed into the first Nano Differential Mobility Analyzer (Nano-DMA, TSI 3085). This was mixed with 3.0Lpm closed loop sheath air. A corresponding DC voltage to the first NanoDMA was applied and was finely adjusted to select a desired mobility diameter. By using Nafion humidifiers, size selected monodisperse particles were conditioned to have a desired relative humidity (RH). The relative humidity was monitored by Vaisala HMP237 probes. All the experiments in this section have a total conditioning residence time that was about 7 seconds. Humidified monodisperse particles

were sized in the second Nano-DMA that was preconditioned by using a closed loop configuration of 3.0 SLM sheath air, in order to match the relative humidity of the incoming conditioned particles.

The size distribution of particles was measured by scanning the voltage of the second Nano-DMA and was sent to a condensation particle counter (CPC, TSI 3025A). The hygroscopicity measurements of different mixtures of NaCl and AOT/SDS were reported in terms of growth factors. The growth factor is defined as the ratio of the humidified particle diameter to the dry particle diameter. The growth factors were compared to Zdanovskii-Stokes-Robinson (ZSR) model. Figure 3.8 shows a close up of the electrospray portion of hygroscopicity experimental setup.

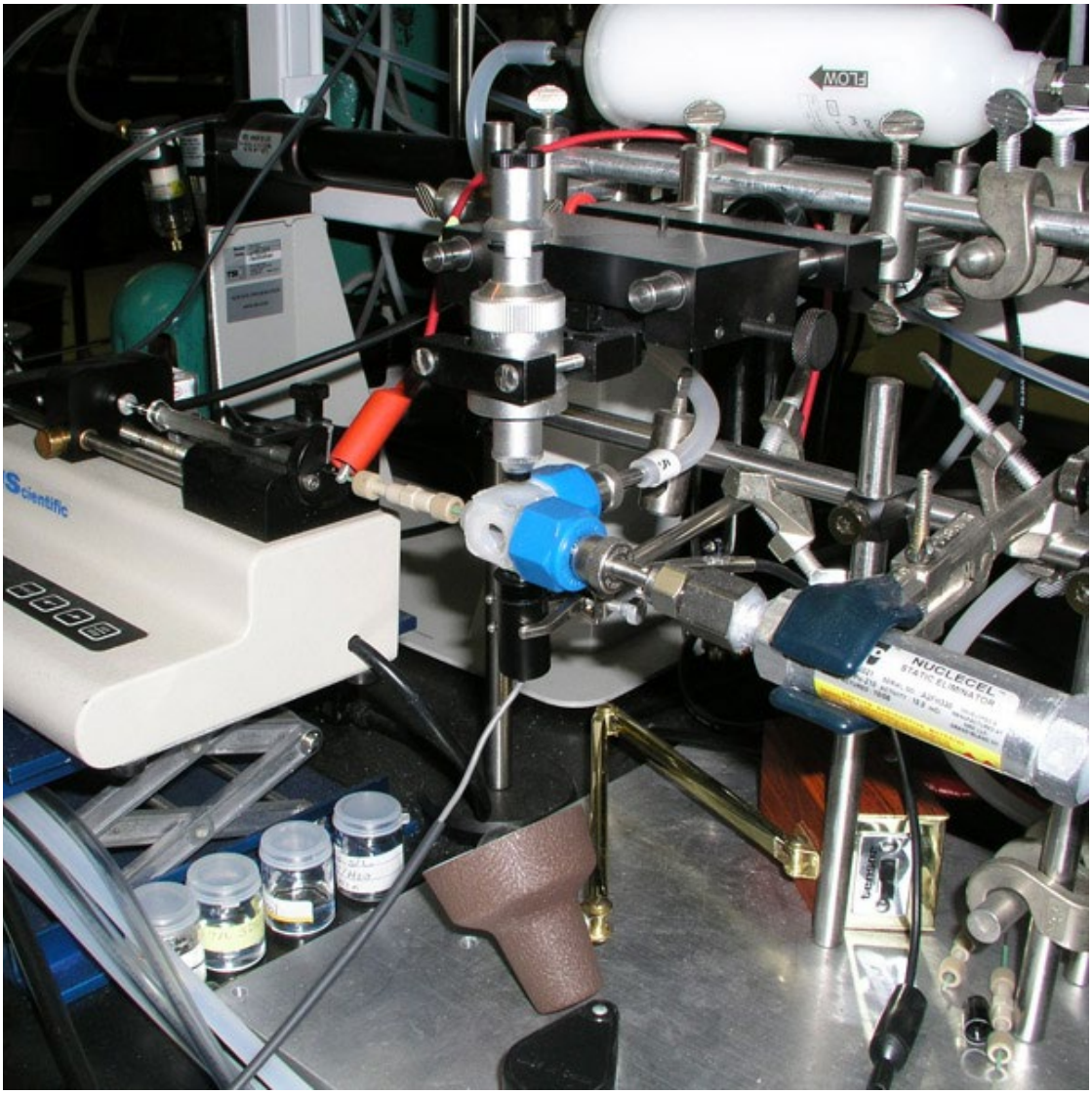

Figure 3.4: Electrospray portion of the experimental setup

3.5. Results and Discussion

3.5.1. The Growth Factor of Pure NaCl Particles

The measured growth factors of the dry 17.0 nm particles of pure NaCl were consistent and in good agreement with the results reported by Hameri [84] and Russell and Martin [73, 85]. Specifically, the growth factor of 17.0 nm NaCl particles was 1.0+/-0.05 with the experimental uncertainties until 70%RH (Figure 3.9). After this, the mean mobility diameter slightly increased due to some initial water adsorption onto NaCl particles [86]. This initial water coating created a metastable equilibrium at which water molecules deposited onto steps or edges of NaCl crystalline that caused a portion of crystalline population to prematurely increase in size.

It was somewhat counter intuitive to have an increase in the mobility-equivalent particle size early on before the deliquescent relative humidity, since the rounding of the NaCl edges was expected to result in a rather slight decrease in size, but perhaps the initial water adsorption process was accelerated at 78% relative humidity, at which a sudden increase in growth factor took place which indicating particle deliquescence during the passage of particles inside the second preconditioned DMA.

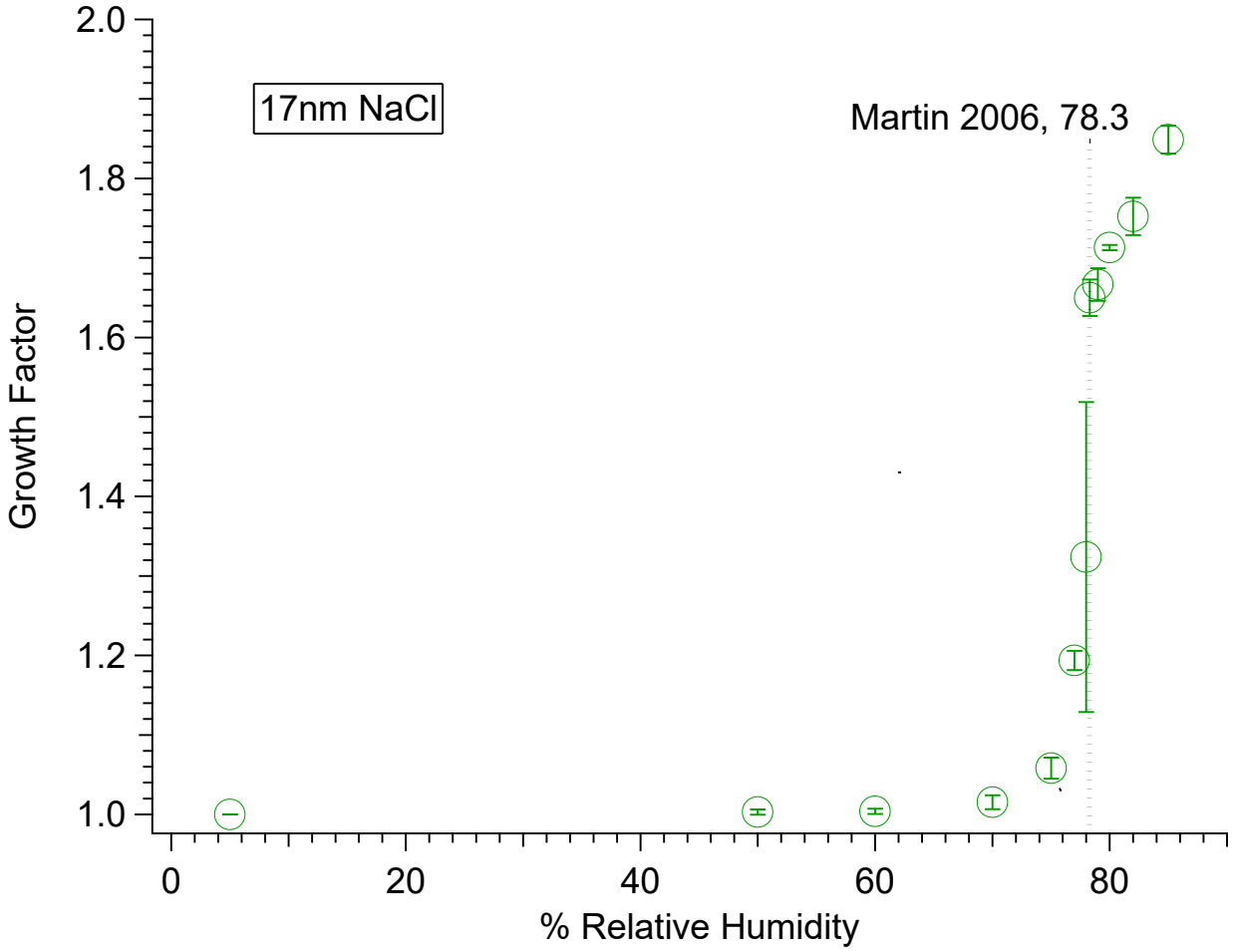

Figure 3.5: Growth factor for 17.0nm NaCl particles, in agreement with Martin results in 2006

3.5.2. The Growth Factor of NaCl Particles Internally Mixed with AOT

Figure 3.10 illustrates the experimentally measured growth factors for three different mixtures of NaCl with AOT at different relative weight concentrations (5%, 25% and 59% w/w) at a total conditioning residence time of 7 seconds. One major observation is non-promptness of the of the deliquescence transition. Upon increasing the weight fraction of the surfactant, the deliquescence relative humidity shifts to lower values relative to that of pure NaCl, corresponding to a shift in Gibbs free energy for the aqueous solution mixture of NaCl and AOT as the weight fraction of surfactant is increased according to figure 3.2.

After the deliquescence transition, there is an apparent decrease in the growth factor compared to NaCl. This suggests that surfactants at the particle-air interface impede the water mass transfer to the deliquescing $NaCl/H_2O$ solution inside the particle. It is also apparent that the decrease in growth factor was indirectly proportional to the weight fraction of the surfactant in the mixture.

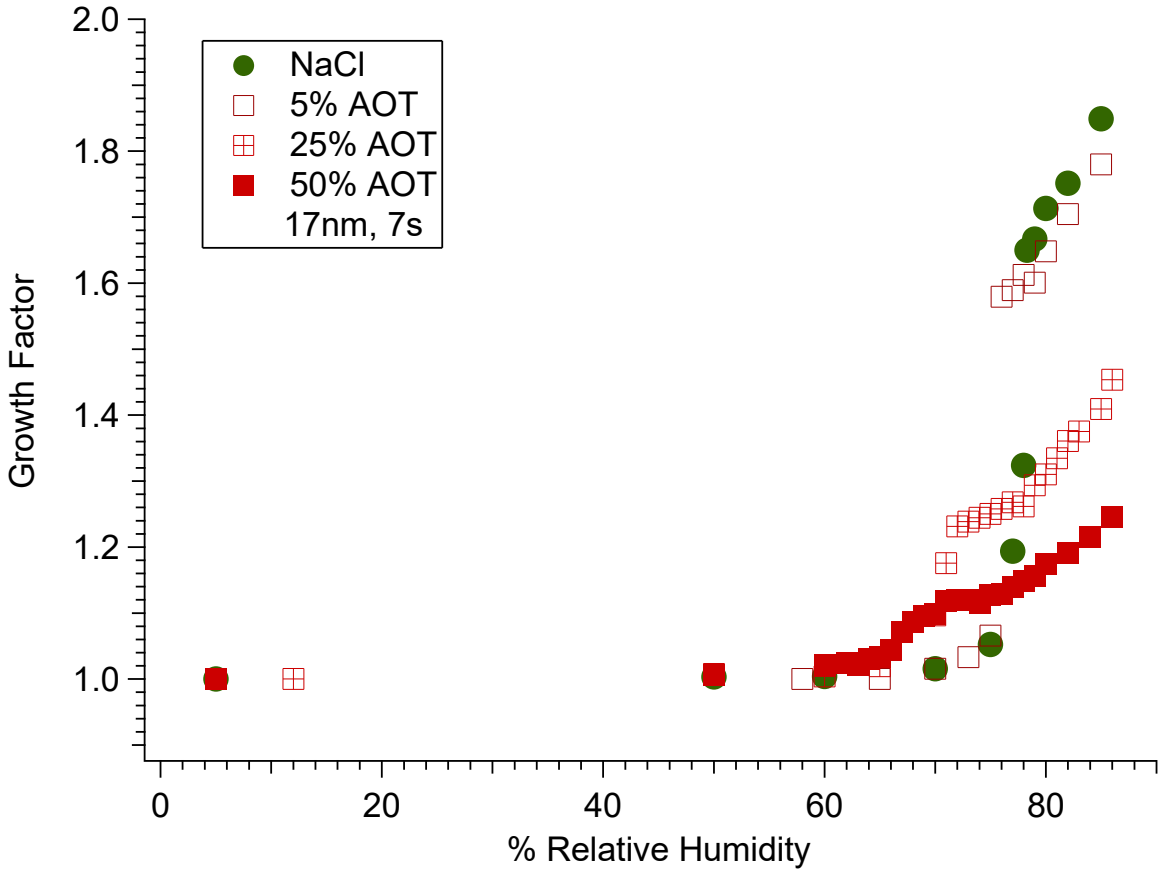

Figure 3.6: Growth factors for mixtures of 17nm particles of AOT and NaCl at different compositions, total residence time is 7.0 seconds

3.5.3. AOT vs. SDS as Surfactant

Figure 3.11 shows the comparison of growth factors for the particles of NaCl with AOT and NaCl with SDS having the same size and the same relative weight fraction. For both cases, the deliquescence relative humidity of 25% salt mixtures occurred at the same value of 70%RH. However, there were obvious differences immediately after deliquescence. For example, for the mixture of 25% SDS with NaCl, there was an

enhanced depression of growth factor right after deliquescence as compared to 25% AOT and NaCl mixture

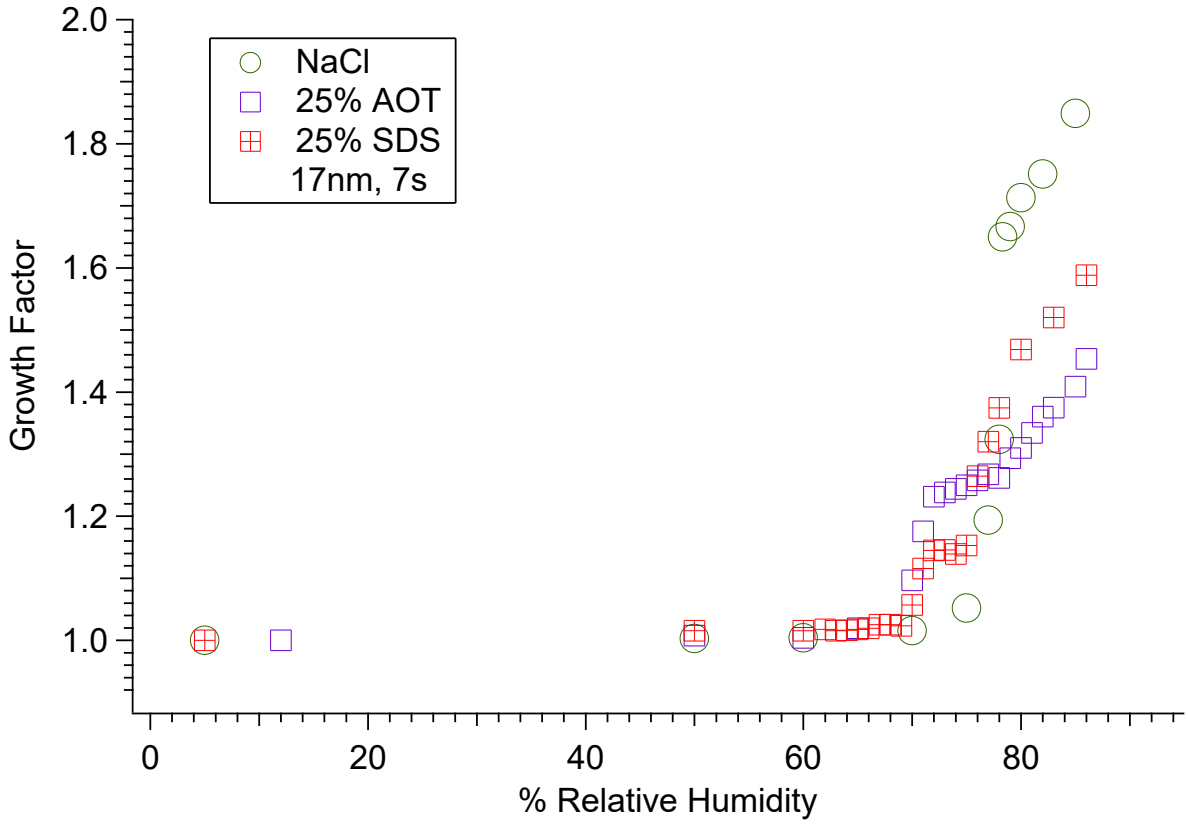

Figure 3.7: Comparing growth factors for 25% by weight of AOT with NaCl vs. SDS with NaCl, total residence time is 7.0 seconds

3.5.4. Zdanovskii, Stokes and Robinson (ZSR) Modeling of Hygroscopic Growth of Internally Mixed Particles

In the ZSR model of multi-component system, the hygroscopic growth factor (GF) can be estimated from the known GF values of its pure components and their volume fractions. ZSR model assumes that there are no interactions amongst the different mixture components; therefore, the hygroscopic growth of the internally mixed particles is an appropriately weighed sum of the hygroscopic growth factors of its components [87]. It also assumes an ideal mixing behavior with spherical particles having a shape factor of unity.

$$GF^3 = \varepsilon_1 GF_1^3 + \varepsilon_2 GF_2^3$$

Where ε_1 and ε_2 are the volume fractions of component 1 and 2 respectively. GF_1 and GF_2 are the growth factors for pure component 1 and 2. Figure 3.12 shows that ZSR modeling for a mixture of 5% AOT with NaCl was in reasonable agreement with the experimental results for the growth but it did not reproduce the deliquescence point correctly.

However, ZSR model for particles containing 25% AOT showed large disagreement with the experimental results on two counts: it missed the premature deliquescence, and it also incorrectly predicted the absolute value of the growth factor. This indicates that water uptake by NaCl and AOT cannot be regarded as independent.

Therefore, the best approach to modeling such system would be to consider structural characteristics of such mixed particles.

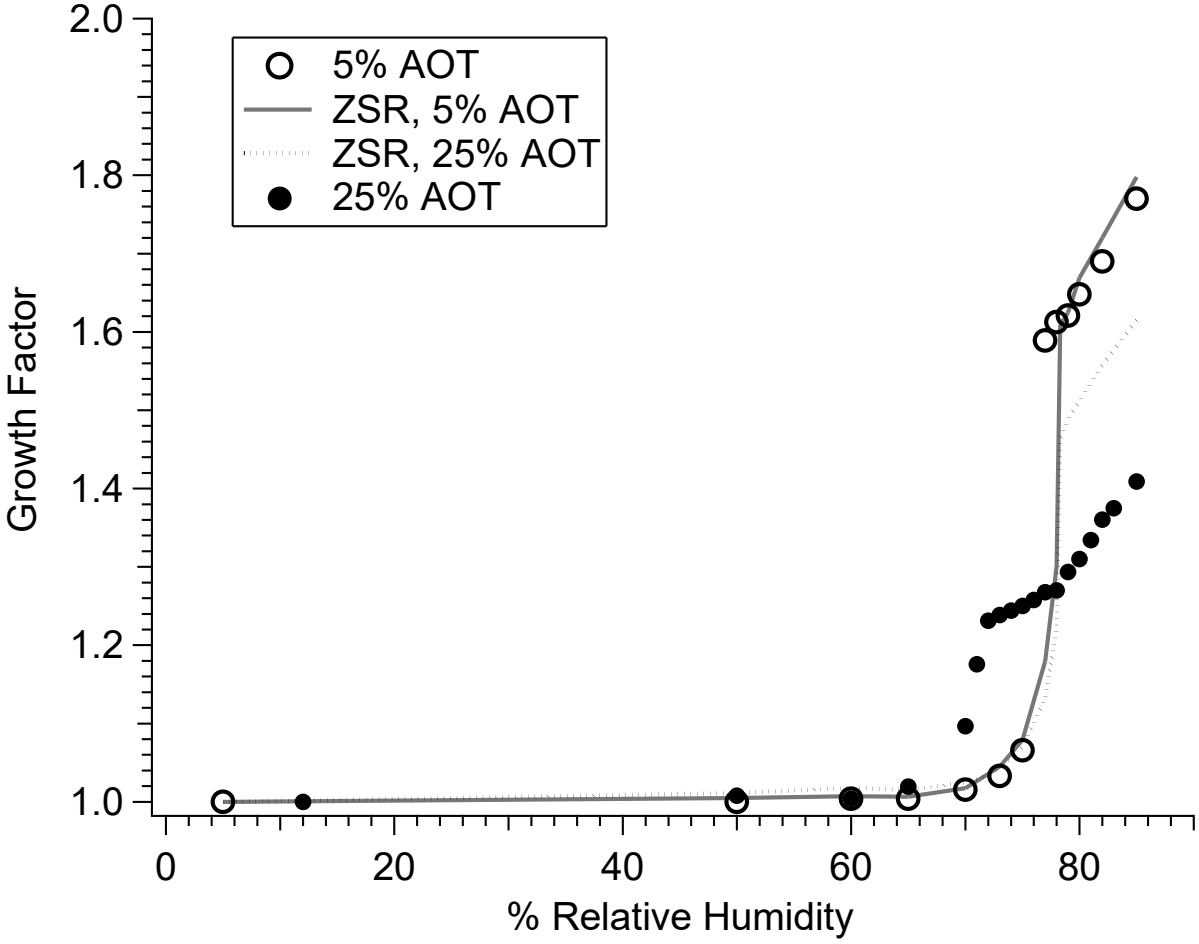

Figure 3.8: ZSR model of growth factors for NaCl/AOT particles

3.6. Conclusion

The growth factors of internally mixed 17.0 nm aerosol particles of NaCl and AOT or SDS surfactants were investigated at the total conditioning residence time of 7.0 seconds. The hygroscopic growth measurements were preformed using a Tandem Nano Differential Mobility Analyzer (Tandem-NDMA). Initial results for 25% w/w AOT with NaCl and 25 % w/w SDS with NaCl showed a growth factor depression as well as a shift in the deliquescence relative humidity to lower values compared to the pure NaCl particles. The experimental results presented above suggest that a small amount of surfactant is sufficient to cause a significant change in the water uptake by the inorganic soluble core.

Chapter 4

Effects of Mass Transfer and Size on Hygroscopicity of Internally Mixed Particles

4.1. Introduction

The rate of deliquescence of ultrafine aerosol particles can substantially alter both their potential role as cloud condensation nuclei (CCN) and its deposition rate in human respiratory system. One important concern in investigating hygroscopicity of ultrafine particles (UFP) is whether or not particles have actually attained final equilibrium during the measurement time. It has been well established that particles made of pure inorganics can achieve hygroscopic equilibrium within timescale of < 1 s [76, 88]. However, the presence of organic films on particles surface can increase the time required for particles to grow to their final equilibrium size [89-93] because organic films significantly reduce the rate of mass transfer across their gas-liquid interface. A second important concern is the enhanced Kelvin effect due to particles small size, i.e., increased equilibrium water vapor pressure about strongly curved surfaces. Indeed, there have been laboratory observations indicating that deliquescence relative humidity of UFP is a function of size for particles < 20 nm in diameter [73, 84]. In this work, the effects of mass transfer and size on deliquescence of aerosol particles are addressed.

4.2. Experimental

The experimental setup was previously discussed in Chapter 2. In order to increase the time during which the aerosol particles interact with humid air, an optional laminar flow tube (½" OD. Copper tube) was added to the setup immediately after the Nafion conditioner tube (fig 2.9), giving an additional residence time of 60 seconds, and thereby giving a total conditioning residence time of 67 seconds.

4.3. Results and Discussion

4.3.1. Mass Transfer Effects on Hygroscopicity of 17.0 nm NaCl Particles Internally Mixed with AOT or SDS

Figure 4.1 shows the growth factor of 17 nm NaCl particles containing 25% AOT by weight at two different residence times: 7 seconds and 67 seconds. In order to interpret these hygroscopicity measurements, it should be kept in mind that particle's growth factor is a function of particle's size, composition and shape. Therefore the rate at which the particle approaches deliquescence may depends on some or all of these variables. The first observation that can be made from Figure 4.1 is that by increasing the residence time from 7 seconds to 67 seconds, there is a reproducible shift in the growth factor curve. This strongly suggests that AOT/NaCl particles require more than 7 seconds achieving equilibrium with water vapor. This is in stark contrast to pure NaCl particles, which are know to equilibrate with waver vapor on millisecond time scales [76].

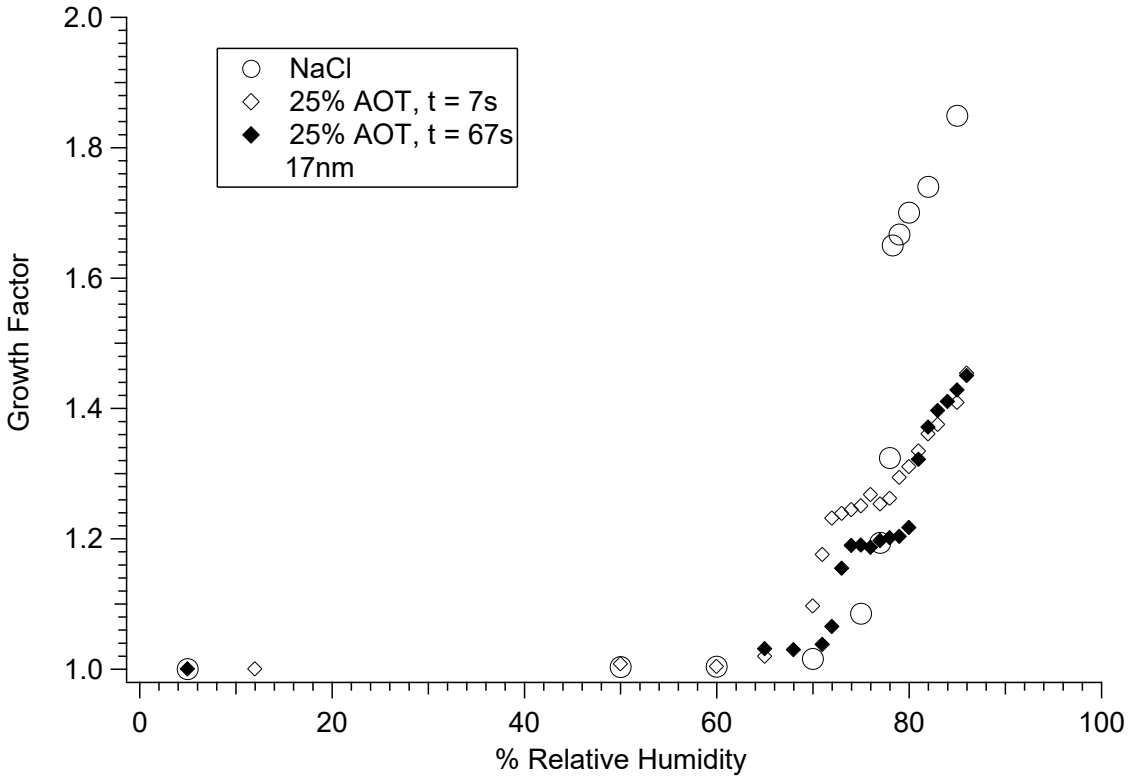

Figure 4.1: Growth factor of 17.0 nm NaCl with 25% AOT internally mixed particles at two different conditioning residence times 7 and 67 seconds.

More careful examination of figure 4.1 reveals a shift of the first deliquescence point to higher RH% values at increased residence times and simultaneous reduction in the growth factor achieved after the first deliquescence transition. At first, this observation is surprising. Indeed, we would expect that the particles should either grow more or maintain their size after spending more time in the humid air. Instead particles appear to become more compact when given a chance to interact with water longer. This observation suggests that the premature increase in size at 70% RH that achieved after 7

second residence is compensated for by some sort of slow rearrangement of the particle structure. This rearrangement must take place on time scale of tens of seconds.

One possible explanation of the observed growth factor suppression at longer residence times is the effect of new found equilibrium for the internally mixed particles at which more surfactants are found at the surface therefore decreasing water accommodation, and consequently dislodging some previously adsorbed water molecules.

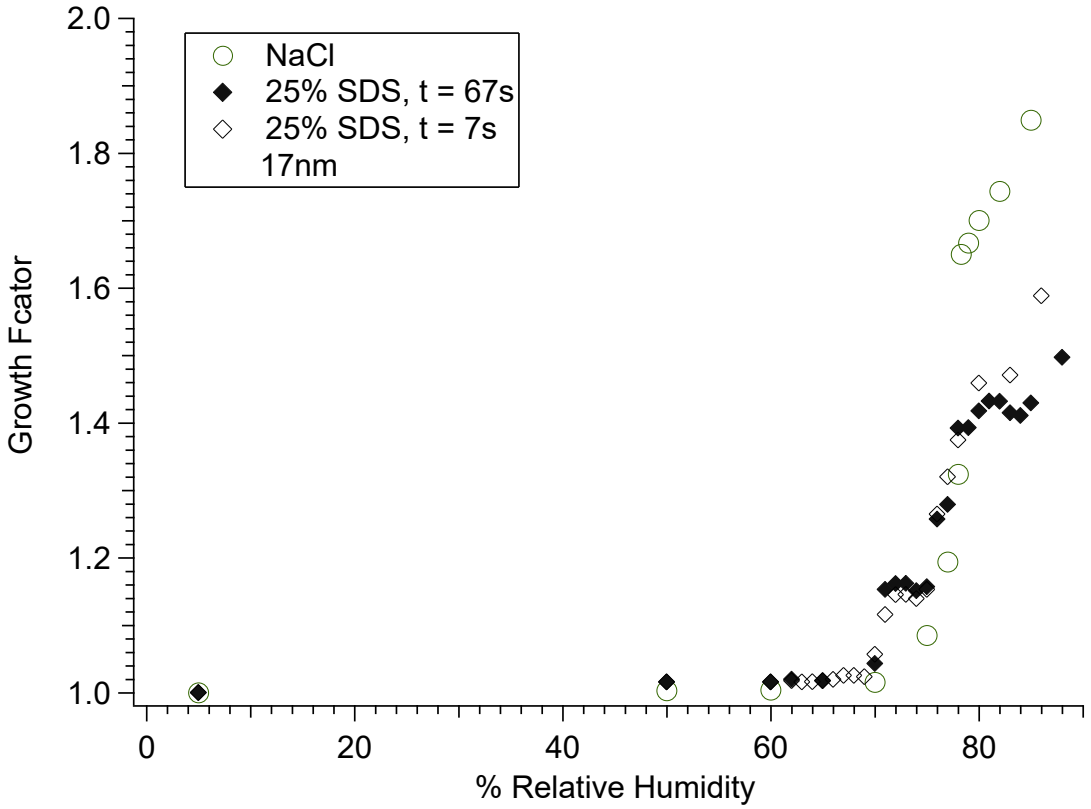

Figure 4.2: Growth factor of 17.0 nm NaCl with 25% SDS internally mixed particles at two different conditioning residence times 7 and 67 seconds.

Figure 4.2 shows the growth factor of 17 nm NaCl particles containing 25% SDS at two different residence times (7 and 67 seconds). As opposed to the previously considered case of NaCl/AOT particles, there seem to be a good correlation between the 7 s and 67 s curves. This implies that SDS/NaCl particles achieve equilibrium with water vapor in 7 seconds or less. We conclude that the nature of the surfactant has a large effect on the on the rate of water accommodation on nanometer-sized particles.

4.3.2. Size effects on hygroscopicity

Ultrafine particles with diameters less than 10 nm are not expected to have a well defined surface compare to 17 nm particles described previously.. Therefore they should be regarded as large molecular clusters whose hygroscopic properties strongly depend on the relative placement of their constituent molecules. By studying the particle size effects on the hygroscopic growth factor one can gain indirect information on particle morphology. To this end, the following section compares the hygroscopic growth of 9 and 17 nm particles with the same relative NaCl/surfactant composition.

4.3.2.1. The Growth Factor of 9.0 nm NaCl Particles

Before discussing the results for mixed 9 nm NaCl/surfactant particles, it is useful to examine the data for pure NaCl particles (Figure 4.3). In general, the measured growth factors of the dry 9.0 nm particles of pure NaCl were consistent and in good agreement with the results reported by Hameri [84] and Russell and Martin [73, 85] at 6 seconds

conditioning residence time. The mean mobility diameter displayed a slight increase below the deliquescence point due to some initial water adsorption onto NaCl particles [86], followed by restructuring of the deliquescing crystal. This initial water coating creates a metastable state at which water molecules are deposited onto steps or edges of NaCl crystalline causing an apparent increase in aerodynamic size. Between 80-83% relative humidity, there is a sudden increase in particle growth factor indicating particle deliquescence.

.

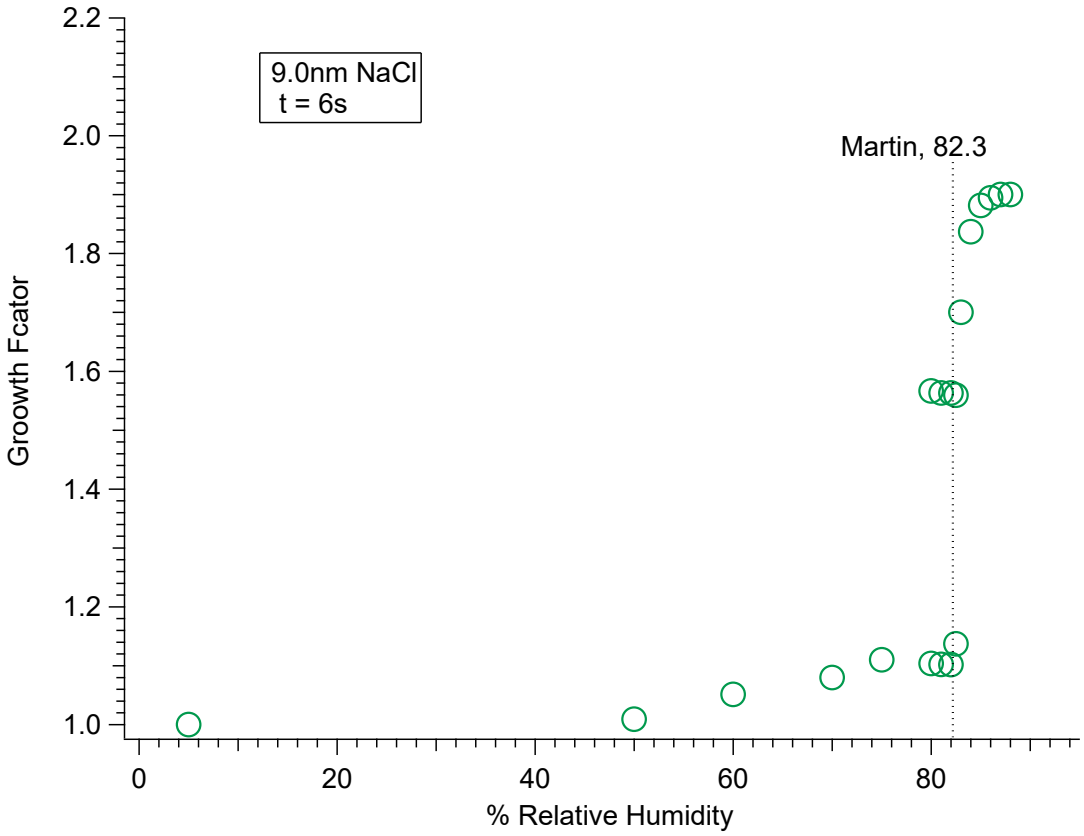

Figure 4.3: Growth factor of 9.0 nm NaCl particles at conditioning residence time of 6 seconds.

Similar to observation described in Hameri et al. [94], we observed that the particles do not deliquesce all at once. Close to the deliquescence point the size distribution actually becomes bimodal, with some particles already deliquesced and some

still retaining their pre-deliquescence size. The full deliquescence for all 9.0 nm particles occurred at 82.3%RH.

4.3.2.2. The Growth Factor of 9.0nm NaCl Particles Internally Mixed with AOT or SDS

The 9.0 nm internally mixed particles of NaCl with surfactants were generated by electrospraying 3.0 g/L solution of 25 % AOT or 25% SDS at about 3000 VDC spraying potential and by utilizing a 50 μm fused silica capillary tube. Figure 4.4 shows the results. The 25% AOT/NaCl particles displayed graduate uptake of water with no evidence of clear deliquescence transitions below 90%RH. This is clearly different from the growth factors for 17 nm 25% AOT/NaCl particles (Figure 4.1).

Experimental difficulties with stability of humidity probes precluded us from getting reliable data above 90%RH. Contrary to AOT, the 25% SDS particles gradually increased in size until 78%RH where they picked up a different rate of increase. At this experimental level there was no evidence that particles have achieved equilibrium and attained their final size increase, therefore it was necessary to investigate the effects of residence time on growth factors.

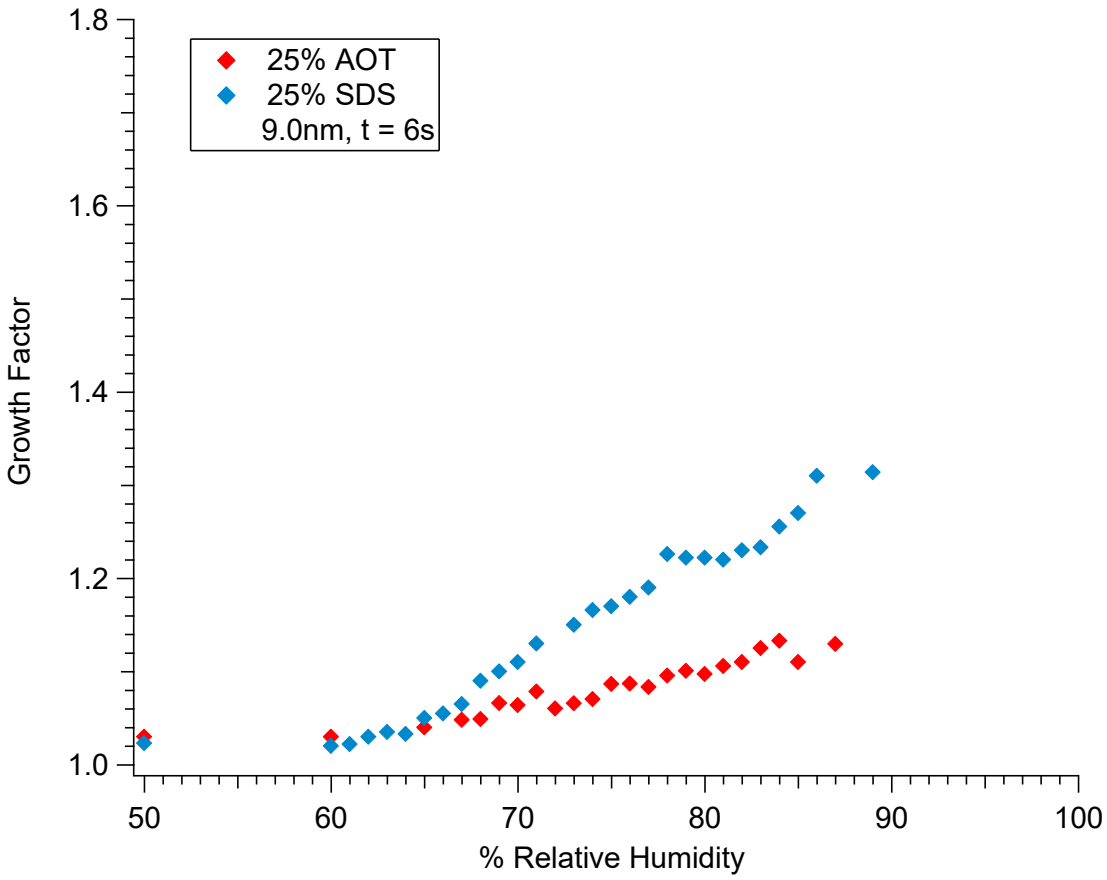

Figure 4.4: Growth factor of 9.0 nm NaCl with 25% AOT and 25% SDS internally mixed particles at conditioning residence time of 6 seconds.

4.3.2.3. Mass Transfer Effects on Hygroscopicity of 9.0 nm Internally Mixed with AOT or SDS

Figure 4.5 shows that increasing the conditioning residence time from 6 seconds to 66 seconds had no effect on the growth factor curve of the 9.0 nm internally mixed particles of 25% AOT with NaCl within 90% RH range. Within the signal-to-noise of the measurement (0.02 growth factor units) the growth curves are identical. Also shown in Figure 4.5 is the growth curve for pure AOT particles and pure NaCl particles of the same size. Similarly to pure AOT, the mixed AOT/NaCl particles display no clear

deliquescence transitions. However, the mixed particles do pick up more water than the pure AOT ones.

The situation for the 9.0 nm internally mixed particles of 25% SDS with NaCl was very different. SDS/NaCl particles exposed to water for 6 seconds displayed a relatively featureless growth curve. At longer interaction times, a clear deliquescence transition appeared which is an increased suppression of the growth curve between 76-82% RH. What is surprising is that this behavior is completely opposite to 17 nm particles, in which SDS/NaCl growth factor was unaffected by the residence time, whereas that of AOT/NaCl particles was.

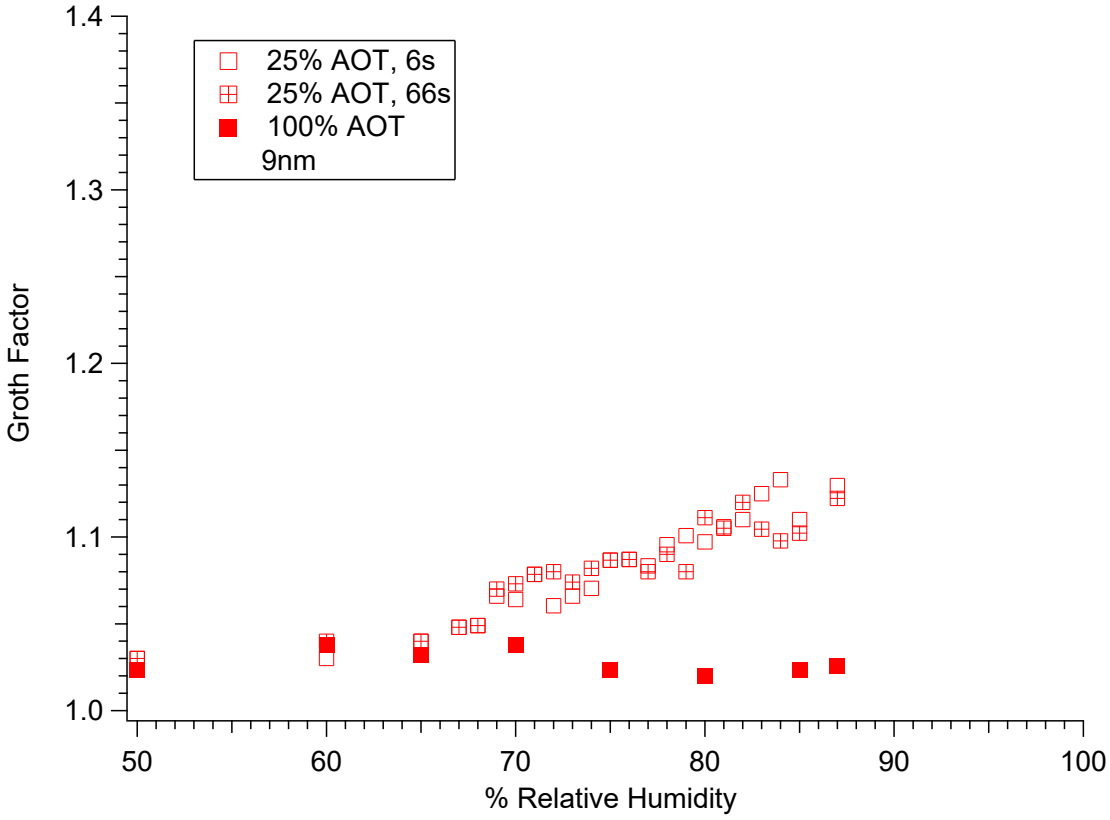

Figure 4.5: Growth factor of 9.0 nm NaCl with 25% AOT internally mixed particles at two different conditioning residence times 6 and 66 seconds.

The increased suppression in growth factor that occurred immediately after increasing residence time can be interpreted as the following: upon increasing residence time, there should be some form of particle structural rearrangement after which more surfactants are now accessible at the surface of the particle. At this instance, a new equilibrium is talking place since surfactants are now been giving more time to spread out at the particle surface.

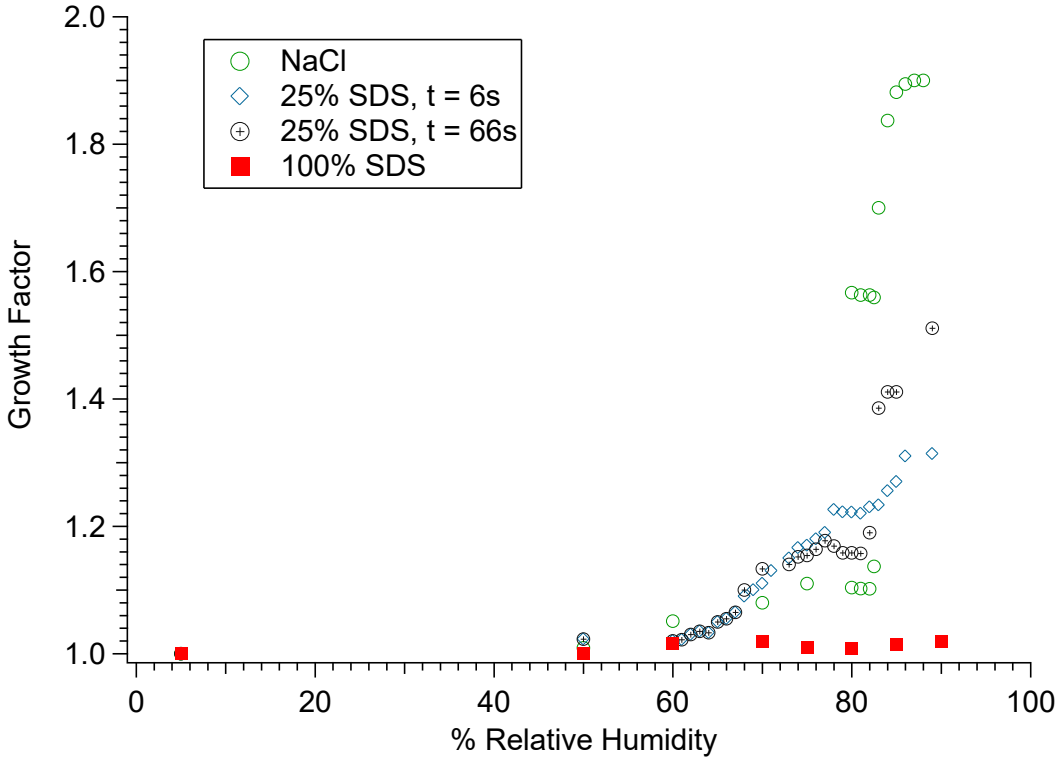

Figure 4.6: Growth factor of 9.0 nm NaCl with 25% SDS internally mixed particles at two different conditioning residence times 6 and 66 seconds.

As the next step in the discussion, let us consider possible structures of mixed particles of different surfactant/NaCl composition and size. The simplest assumption we

can take is that the particles have a core shell structure shown in figure 4.8, wherein the NaCl is at the core and organic surfactants are distributed on the surface. Furthermore, the core is assumed to be spherical (probably not true for NaCl, which prefers to form cubic crystals). With this model, the diameter of NaCl core can be estimated from Equation 1.

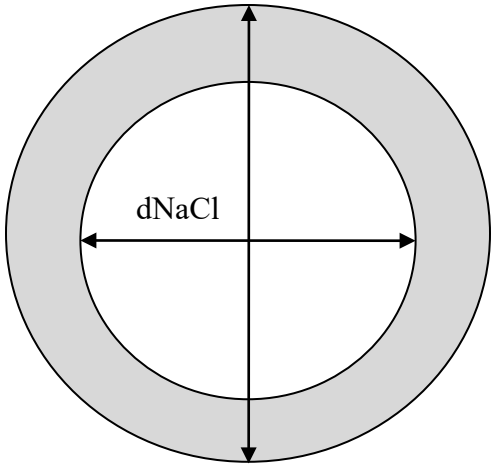

Figure 4.7: Core- Shell Model of NaCl mixed with Surfactant

$$d_{NaCl} = \left(\frac{w_{NaCl} \rho_{AOT} d_{particle}^3}{\rho_{NaCl} - (\rho_{NaCl} - \rho_{AOT}) w_{NaCl}} \right)^{\frac{1}{3}} \qquad \text{Eq.1}$$

Here, W_{NaCl} is the weight fraction of NaCl, $d_{particle}$ is the overall particle diameter, ρ_{NaCl} and ρ_{AOT} are the densities of NaCl and AOT respectively. Calculations for the possible number of surfactants that are inside the shell are shown in table 4.4.

By looking at table 4.4, for 17.0 nm NaCl particles mixed with 25% surfactants, the number of AOT molecules that are available inside the shell (fig 4.8) are comparable to number of AOT that can be accommodated at the surface. However, 17.0 nm particles with 25% SDS in table 4.4 have less surfactant molecules available than what can be

accommodated at the surface. Therefore, based on these calculated results, one would predict to observe more hygroscopic growth for 25% SDS molecules due to partial surface coverage with surfactants compared to 25% AOT molecules. However, both 25% AOT and 25% SDS show similar hygroscopic growth above 80% RH as in fig.4.1 and 4.2, indicating that the 17.0 nm internally mixed particles of surfactants- NaCl may not necessary adopt the core-shell model at the onset of the electrospray process on one hand. On the other hand, if one compares calculated values in table 4.4 for 9.0nm particles for mixtures of 25% AOT and 25% SDS, it is very clear that both would have much less number of surfactants inside the shell than what could be accommodated at the surface, therefore one would predict similar hygroscopic growth factors. However, the growth factors obtained for 9.0nm particles of 25% AOT and 25% SDS in figure 4.4 clearly show that 9.0 nm of 25% SDS particles have greater growth factor than 25 % AOT particles, indicating once again that the internally mixed particles at the onset of electrospray do not actually adopt a core-shell model.

Table 4.1 Density and cross sectional area used in the calculations[95, 96]

Density of NaCl (g/cm^3) =	2.165
Density of AOT (g/cm^3) =	1.1
Area per AOT head =	0.37nm^2
Density of SDS (g/cm^3) =	0.4
Area per SDS head =	0.25nm^2

Table 4.2: AOT and SDS possible accommodation for 9.0 nm and 17.0 nm diameter. The # AOT and #SDS molecules that can be accommodated at the particle surface were calculated using first order approximation (particle surface area divided by the area per surfactant head group in table 4.3)

%AOT	%W NaCl	Diameter of NaCl (nm)	AOT thickness (nm)	# AOT molecules inside shell	# AOT molecules that can be accommodated at surface
0	1	17.0	0	0	0
5	0.95	16.451	0.275	362	2125
25	0.75	14.369	1.316	1529	1622
50	0.5	11.829	2.585	2559	1099
100	0	0.000	8.500	3859	0

%SDS	%W NaCl	Diameter of NaCl (nm)	SDS Thickness (nm)	# SDS molecules inside shell	# SDS molecules that can be accommodated at surface
0	1	17.0	0.000	0	0
5	0.95	15.637	0.681	476	3073
25	0.75	12.055	2.472	1382	1826
50	0.5	9.150	3.925	1813	1052
100	0	0.000	8.500	2148	0

%AOT	%W NaCl	Diameter of NaCl (nm)	AOT Thickness (nm)	# AOT molecules inside shell	# AOT molecules that can be accommodated at surface
0	1	9.0	0.000	0	0
5	0.95	8.709	0.145	54	596
25	0.75	7.607	0.696	227	454
50	0.5	6.262	1.369	380	308
100	0	0.000	4.500	573	0

%SDS	%W NaCl	Diameter of NaCl (nm)	SDS Thickness (nm)	# SDS molecules inside shell	# SDS molecules that can be accommodated at surface
0	1	9.0	0.000	0	0
5	0.95	8.279	0.361	71	861
25	0.75	6.382	1.309	205	512
50	0.5	4.844	2.078	269	295
100	0	0.000	4.500	319	0

4.4. Conclusion

Based on the results of Chapter 4, it was clearly shown that unless the deliquescence relative humidity is at equilibrium, hygroscopicity measurements could be potentially compromised by mass transfer effects. The time needed for these particles to grow to their final size depends on the structure and size of the mixed organic/ inorganic particles. Perhaps the largest single question is the observed hygroscopic retardation effect for 17.0 nm 25% AOT upon increasing residence time. To this end, more experiments would have to be preformed in order to account for this unexplained effect. Another set of experiments would also be required in order to ascertain the assumption that the initial mixture composition was actually maintained at the onset of electrospray.

Further studies are also required in order to explore the lack of water activity for 9.0 nm particles of 25%AOT compared to 25% SDS. It was speculated that either the initial composition of 25 % AOT for 9.0 nm was not maintained at the onset of electrospray or that AOT surfactants were capable to encapsulate NaCl and therefore retarding its hygroscopicity.

Chapter 5

Quantification of Ozone Levels in Indoor Environments Generated by Ionization and Ozonolysis Air-Purifiers

Abstract

Indoor air-purifiers are advertised as safe household products for health conscious individuals, especially for those suffering from allergies and asthma. However, certain air-purifiers produce ozone during operation, either intentionally or as a by-product of air ionization. This is a serious concern because ozone is a criteria air pollutant regulated by health-related federal and state standards. Several types of air-purifiers were tested for their ability to produce ozone in various indoor environments at 40-50% relative humidity, including office rooms, bathrooms, bedrooms, and cars. Ozone levels generated by personal wearable air-purifiers were also tested. In many cases, ozone concentrations were well in excess of public and/or industrial safety levels established by the EPA, CARB, and OSHA. Simple kinetic equations were obtained that can predict the steady-state level of ozone in a room from the air-purifier's ozone emission rate and the first-order decay rate of ozone in the room. The additively of ozone levels generated by independent ozone-generators was experimentally demonstrated.

5.1. Introduction

5.1.1. Indoor Air-Purifiers and Ozone.

Due to growing air pollution problems in urban areas, indoor air purification has gained widespread popularity in recent years, with a large variety of indoor air-purifiers being available to the public [97]. The main targets of indoor air purification are odorous VOCs (Volatile Organic Compounds), dust, pollens, and airborne particles, which are suspected exacerbates of respiratory health problems [98-101]. From an operational standpoint, there are three basic types of air-purifiers: i) air filtration; ii) air ionization; iii) ozonolysis of air impurities. Household use of certain air ionization and ozonolysis air-purifiers has raised serious concerns because they produce ozone, a criteria air pollutant, either as a by-product of air ionization or intentionally.

Most air ionization (ionic) devices work by charging airborne particles and electrostaticaly precipitating them on metal electrodes. Ionic air-purifiers are available in a broad spectrum of designs including large units for household use, smaller units for use in bathrooms, refrigerators and closets, units intended specifically for cars, personal wearable units, ionic brushes, shoe cleaners, toothbrush disinfectors, etc. Depending on the design, some ionic air-purifiers can emit ozone with a rate of a few milligrams of ozone per hour (mg/hr), which is comparable to the amount of ozone emitted by dry-process photocopiers during continuous operation [102, 103].

Ozonolysis air-purifiers typically produce several hundred mg/hr of ozone with a goal of oxidizing VOCs in indoor air. However, ozone reacts exceedingly slowly with most saturated VOCs [104]. Ozonolysis half-lives of common VOCs found indoors are

days or even years at 100 ppb (parts per billion) of ozone [59]. Ozone reacts considerably faster with VOCs containing unsaturated carbon-carbon bonds [104, 105]. found in cooking oils, air fresheners, cleaning products, etc. [59, 106], and with certain polycyclic aromatic compounds [107], found in household materials (e.g., pigment dyes in carpets). However, these reactions produce carboxylic acids, epoxides, organic peroxides, aldehydes, and ketones as stable products, some of which may result in adverse health effects [61, 62, 108-110]. Ozone + unsaturated VOC reactions are known to produce OH as an intermediate [111-114], which further contributes to the diversity of oxidation products. Ozone treatment may affect the particle size distribution but it generally does not reduce the overall concentration of particles in the air. In fact, new ultrafine particles are likely to be created if an ozonolysis air-purifier is used in a room with a large concentration of gaseous unsaturated VOCs, such as terpenes [60, 115, 116].

The level of ozone required to efficiently kill bacteria is also harmful to humans. Indeed, the US Environmental Protection Agency (EPA) provided a comprehensive assessment of the effectiveness and health consequences of ozone generation indoors stating that "at concentrations that do not exceed public health standards, ozone is generally ineffective in controlling indoor air pollution" [117]. Reviews by Boeniger [118] and Weschler [59] similarly concluded that "ozone is not a practical and effective means of improving indoor air quality". The California Air Resources Board (CARB) issued an official statement in early 2005 expressing a serious concern about ozone-generating air-purifiers and recommending the public avoid using these devices [119]. In February 2005, CARB released a draft report to the California Legislature on indoor air pollution which stated that "Air cleaners that intentionally generate ozone should not be

used indoors. Independent studies by US EPA, the Consumers Union, and others have shown that ozone-generating air cleaners do not effectively destroy microbes, remove odor sources, or reduce pollutants enough to provide any health benefits" [48].

5.1.2. Ozone Health-Effects and Regulations.

The detrimental health effects of ozone are well known and have been extensively reviewed [34, 51, 120-124]. In addition to directly affecting humans breathing ozone-polluted air, ozone can react with indoor surfaces [52-54, 59, 125] such as carpets, linoleum, clothing, furniture, etc., releasing volatile oxidation products that may have adverse health effects [61, 110]. For example, aldehydes are readily produced in reactions between ozone and C=C double bonds in fatty acid residues, which are found in a number of detergents [40, 126-128]. Carpets were also shown to release a number of volatile aldehydes in the C1-C13 size range upon ozone treatment which may change the odor perception [55, 56, 129, 130].

Existing US health-related standards for ozone are reviewed in Table 5.1. The National Institute for Occupational Safety and Health (NIOSH) established the Immediately Dangerous to Life or Health Concentrations (IDLH) ozone level at 5 ppm and Permissible Exposure Limit (PEL) at 100 ppb. The Occupational Safety and Health Administration (OSHA) established a PEL of 100 ppb for an 8-hour exposure and Short-Term Exposure Limit (STEL) of 300 ppb for a 15-min exposure. The US EPA classified ozone as a criteria pollutant and established national ambient air quality standards (NAAQS) of 120 ppb for 1-hour exposure and 80 ppb for 8-hour exposure. The California state government has just introduced new 8-hour AAQS at 70 ppb [131] (the California 1-hour-average ozone standard is 90 ppb). In California, a stage-one smog

alert is issued whenever the ambient concentration of ozone is in excess of 200 ppb. Ozone levels of 350 ppb and 500 ppb correspond to stage-two and stage-three smog alerts, respectively.

In spite of the existing concerns about ozone-generating air-purifiers, no government-imposed restrictions on the use of such devices in occupied spaces currently exist[48]. The US Food and Drug Administration (FDA) limits the concentration of ozone produced by medical devices operated in closed spaces to 50 ppb [132] but this limit does not strictly apply to indoor air-purifiers. The US EPA website states that "no agency of the federal government has approved these devices for use in occupied spaces" [117]. The main objectives of this work are to: i) verify whether ozone-generators such as ionic air-purifiers can produce levels of ozone in excess of public health standards; ii) quantify the steady-state ozone levels generated by air-purifiers in several representative indoor environments; iii) develop a simple phenomenological model that can be used to predict the steady-state ozone level generated by an air-purifier in a closed space; iv) test the effect of operating ozone-generating air-purifiers in rooms with pre-existing ozone sources. The following sections describe the experimental procedure, key results, and implications of these measurements.

5.2. Experimental

Ozone concentration was measured with Ebara Jitsugyo EG-2001 high-accuracy ozone monitor, which provided ozone mixing ratio referenced to 1 atm and 295 K conditions with a 1 ppb resolution. The linearity and accuracy of this instrument was verified by cross-referencing it against two home-made absorption cells operating on the

253.65 nm mercury line (base-*e* absorption cross section of O_3 at 253.65 nm is 1.136×10^{-17} cm^2) [133]. The calibration showed that EG-2001 is accurate to better than 5% for all the ozone mixing ratios of interest. Before each measurement, the instrument was allowed to warm up for 2-3 hours to achieve better stability. The instrument automatically re-zeroed itself every 3 minutes by passing the sampled air flow through a built-in scrubber. It continuously displayed ozone mixing ratio averaged over 1 second interval between re-zeroing cycles. The drift in the output between re-zeroing cycles did not exceed 3 ppb. As all the measurements were done close to atmospheric pressure and room temperature, no explicit temperature or pressure corrections were made.

5.2.1. Air-Purifier Ozone Emission Rates.

The ozone emission rate was measured for each air-purifier inspected in this work. For these measurements, the air-purifier was placed in a sealed Teflon bag filled with a known volume of dried air (400-700 L; relative humidity < 5%). A fan was placed inside the bag to ensure rapid mixing. The ozone monitor withdrew air from the bag at a rate of 1.5 SLM (standard liters per minute) and returned it to the bag in a closed-loop circuit through all-Teflon gas lines. Although a small amount of ozone was destroyed by the instrument during re-zeroing cycles, the ozone destruction rate was not fast enough to compete with other ozone emission and removal processes in the measured volume. In a typical measurement, the air-purifier was turned on and the build-up of ozone with time was recorded. The concentration was logged every 0.5-5 minutes depending on the rate of ozone concentration increase. A slightly modified procedure was used for highly efficient ozone generators. These were turned on for a preset period of time (20-30

seconds) and turned off. The resulting ozone concentration increment was then recorded after the air in the Teflon bag was well mixed. The procedure was reiterated several times for repeatability.

When the concentration of ozone in the bag reached a certain level, typically 500-1000 ppb, the air-purifier was turned off and the decay of ozone concentration was recorded. Ozone concentration typically dropped with exponential lifetime of 3-5 hours because Teflon is relatively unreactive towards ozone. The resulting data were analyzed, as described in the kinetics section below, to extract the ozone emission rate. The results of the measurements are summarized in Table 5.2.

5.2.2. Measurements in Rooms.

Several types of indoor environments were examined (Table 5.3) including: i) two medium-size office rooms in the Rowland Hall building on campus of the University of California at Irvine; ii) medium-size bathroom; iii) small bathroom; iv) small furnished carpeted bedroom. The last three rooms were located in a 3 year old house in Irvine, California. All measurements were done in rooms with doors and windows closed. In some measurements, forced air circulation from the building ventilation system was present. The amount of admitted air was varied from measurement to measurement to control the decay rate of ozone from the room. In rooms with forced ventilation, the air exchange rate was estimated from the time it took to fill a plastic bag of known volume through the air intake vent. No measurements of air exchange rates were performed in rooms without forced ventilation. The ozone monitor, which was installed in an adjacent room, was withdrawing and returning air at 1.5 SLM through Teflon tubes. The rate of

ozone removal by the instrument (during its re-zeroing cycles) was always negligible compared to other ozone emission and removal processes in the room. A large fan was placed in the room for better circulation of air to avoid significant ozone concentration gradients across the room volume.

During the measurements, the air-purifier was turned on and the ozone concentration build-up was traced until either a steady-state concentration level was reached or the concentration exceeded the levels deemed to be safe for occupants of neighboring rooms and offices. After that, the air-purifier was turned off and the decay rate of ozone in the room was measured.

5.2.3. Measurements in Cars.

A few measurements were performed in a stationary unoccupied car, Lexus ES 250, 1991, outfitted with leather seats and carpeted floors. The car was positioned in a driveway with its doors and windows closed. The ozone monitor was installed in a nearby garage and it withdrew air from the car at 1.5 SLM through a Teflon line. The measurements were done at dusk hours at a temperature of about 15°C to avoid possible artifacts from inhomogeneous heating of the vehicle by the sun and to minimize the effect of variations in the ambient ozone level. No measurements of air exchange rate were performed.

5.2.4. Personal Air-Purifiers.

Personal air-purifiers (PAPs) were tested in a way that is similar to a previous study of PAPs by CARB researchers.[50] The PAP was suspended from a ring stand and ozone concentration was sampled a certain distance away from the PAP (typically 10 cm) through a Teflon tube withdrawing air at 1.5 LPM. In initial experiments, the ring stand was positioned on a bench in a laboratory with a lot of air currents (because of two fume hoods withdrawing air from the room and forced ventilation admitting air to the room). In subsequent tests, the ring stand was surrounded by a large Plexiglas cylinder to minimize the effect from the strong lateral air currents in the lab. A few additional measurements were done using a human-sized stuffed doll wearing a PAP around its neck, with ozone level being sampled next to the doll's "mouth" (10 cm away from PAP).

5.3. Results and Discussion

5.3.1. Air-Purifier Ozone Emission Rates.

Figure 5.1 provides an example of measurements of ozone emission rates by air-purifiers under dry-air conditions. For PZ6 Air, which is a fairly powerful ozone generator, the observed ozone concentration in a 700 L Teflon bag reaches 5 ppm in just 10 minutes. The concentration increase appears to be linear in time with no visible signs of saturation. For SI633, which is a much less efficient ozone producer, the rate of increase is also linear but considerably slower. The observed concentration profiles can be fitted to the kinetics model described below ($[O_3](t) \approx k_{source} \times t$ for small t) to obtain the air-purifier ozone emission rates in mg/hr.

An example of ozone concentration decay taking place after the air-purifier is turned off is given in Figure 1b. The observed decay profile deviates slightly from the single exponential dependence. It is somewhat better described as a second-order loss at concentrations above 200 ppb suggesting that the loss of ozone on Teflon surfaces is not a first-order process. Indeed, ozone reactions on hydrophobic soot [134] and self-assembled organic monolayers [128] are known to be governed by a Langmuir-Hinshelwood mechanism. It is possible, that decomposition of ozone in a Teflon bag follows a similar mechanism, wherein ozone molecules participate in a rapid adsorption-desorption equilibrium with the surface, with a very slow $O_3 + O_3$ surface reaction removing the ozone. There was no evidence of the second order ozone loss in normal environments (rooms); all decays could be fit to a single exponential decay within the measurement uncertainties.

Table 5.2 reports the ozone emission rates measured in a Teflon chamber in dry air with RH (relative humidity) <5%. All measurements use the highest air-purifier settings. Although the measurements are quite repeatable for one and the same air-purifier, it is not appropriate to place well defined error bars on these values without testing multiple copies of the same model. Two identical units were available for SI627, with one producing 0.17 mg/hr and the other 0.24 mg/hr of ozone (30% difference in the ozone emission rates). The measured ozone emission rates should be treated as approximately representative values for a given class of air-purifiers.

As the ozone emission rate by air-purifiers can be affected by RH, the effect of RH was tested on 2 ionic air-purifiers, SI637 and SI627. The ozone emission rates for both models decrease at higher RH; the effect is stronger for SI637. Specifically, SI637

produces 2.2, 1.9, and 1.4 mg/hr of ozone at RH of 5, 30, and 60%, respectively. The output of SI627 drops from 0.24 mg/hr at RH = 5% to 0.18 mg/hr at RH = 60%. The RH dependence of the ozone emission rates for other air-purifiers was not explicitly measured. It is expected that air-purifiers generating ozone by an electrical discharge (every model in Table 5.3 except PZ6 Air) should reduce their ozone emission rates somewhat at elevated RH.

The effect of particulate matter on SI637 ozone emission rate was investigated by purposely injecting NaCl aerosol particles into the Teflon bag (roughly 10^5 particles per cm^3 with a mean particle diameter of 0.2 μm). Presence of particles caused no significant change in the ozone emission rate suggesting that ozone production and particle ionization processes are fairly independent of each other in ionic air-purifiers. The effect of particles on the performance of ozonolysis air-purifiers was not explicitly investigated in this work.

For certain air-purifiers, the ozone emission rate was specified by the manufacturers. With the exception of Ioncare personal air-purifier which was advertised to produce 44 mg/hr as opposed to the measured rate of 0.5 mg/hr, the measurements were within a factor of 3 of the specifications. For EZ-COM air-purifier, the measured rate of 68 mg/hr is a factor of 1.7 larger than its 40 mg/hr manufacturer's rating. The PZ6 Air-purifier had been used for an unknown number of hours prior to this study, which may account for its lower output of 42 mg/hr compared to its 125 mg/hr rating. Pro 420 model produced 132 mg/hr instead of the quoted 420 mg/hr. After the manufacturer replaced the unit (initially believed to be defective), the replacement performed at a

similarly low 137 mg/hr level. XT-400 model generated ozone at a measured rate of 220 mg/hr compared to its 400 mg/hr rating.

5.3.2. Ozone Measurements in Rooms.

Sample measurements of emission of ozone by air-purifiers operated in rooms and offices are shown in Figures 5.2, 5.3, and 5.4. In all examined cases, the ozone concentration in the room increases to some steady-state level after the air-purifier is turned on. It decreases exponentially to the background level after the air-purifier is turned off. The steady-state ozone concentration and the rate with which ozone is removed from the room depend on the specific environment. Table 5.3 provides a comprehensive listing of all air-purifier/environment combinations examined in this work.

Figure 5.2 shows sample results for unventilated bathrooms. Bathrooms are uniquely different from other kinds of indoor environments in that they have a relatively small volume, little or no furniture, and fairly unreactive surfaces (ceramic tile, glass, enamel painted walls, etc.). As a result, even weak ozone generating appliances can be rather effective in building up large ozone concentrations in bathrooms. For example, Figure 2a shows that SI637, which has an ozone emission rate of 2.2 mg/hr in dry air, can easily maintain levels of ozone in excess of 150 ppb in a small bathroom. EZ-COM, a 30 times more powerful ozone generator, only needs about 15 minutes to reach the OSHA STEL ozone level of 300 ppb in a larger bathroom (Figure 5.2b). For this specific measurement, the steady-state level was not reached because of safety issues (a strong smell of ozone was detected in the adjacent rooms). The extrapolated steady-state value in Figure 2b is in excess of 1 ppm.

Figure 5.2 also illustrates the effects of environmental variables on measurements in rooms. The SI637 measurement in Figure 5.2a took about 10 hours from 9.30 in the morning till 20.00 in the evening on a Christmas day. The temperature in the bathroom was about 5 °C higher in the afternoon (between about 12.30 and 15.00) compared to that in the morning and evening hours. This small temperature variation had a visible effect on the rate of ozone decomposition on the room surfaces. Indeed, the observed exponential lifetime for the first decay in Figure 5.2a is about 20 min as opposed to 29 min for the second decay measured later in the evening. As a direct result of this temperature variation, the steady-state level achieved in the afternoon is somewhat lower than that in the evening. The temperature variation is also responsible for the observed decline in the steady-state ozone level between 12.30 and 13.00.

Figure 5.3 shows the result of using the same air-purifiers, EZ-COM and SI637, in a ventilated furnished office room. Because of the increased room volume, larger available area for ozone surface decomposition reactions, and presence of forced air ventilation with an air exchange rate of about 5 room volumes per hour, the observed increase in the steady-state ozone level is not as dramatic as in bathrooms. SI637 increases ozone level by about 9 ppb. EZ-COM is capable of driving the ozone concentration up by about 240 ppb, which is higher than both 1-hour and 8-hour EPA NAAQS standards. The loss of ozone from the air after the generator is turned off is considerably faster: the exponential lifetimes measured from data in Figure 5.3a and 3b are 13±3 and 12±2 min, respectively. This is essentially identical to the time needed for the ventilation to displace one room volume (measured to be 12±1 min from the rate of filling a plastic bag of calibrated volume through the air inlet) suggesting that the removal

of ozone from the office in this particular case is dominated by physical rather than chemical loss. More measurements in offices will be discussed after introducing the kinetic model.

5.3.3. Car Air-Purifiers

Two car air-purifiers were tested as described in the experimental section. The observed ozone concentration behaved similarly to the results obtained in rooms: an increase in the steady-state concentration during the air-purifier's operation, and an exponential decline after the air-purifier is turned off. The observed ozone decay rate was very rapid (lifetime ~ 2 min) presumably because of the presence of a number of reactive surfaces inside the car (leather upholstery, carpet floors, rubber, insulation, etc.) and also because of a relatively facile exchange of air between the car interior and the outside (not quantified in this work). As a result, the incremental ozone concentration increase caused by the air-purifier was relatively small: below 10 ppb (Table 5.3).

5.3.4. Personal Air-Purifiers

In addition to experiments with air-purifiers designed for rooms and cars, several tests were done with personal air-purifiers (PAPs). The previous findings of CARB researchers [50] that PAPs can expose the wearer to ozone levels in excess of public health standards were fully confirmed by the present work. For example, in tests with Ioncare PAP worn by a human-sized doll, peak ozone concentrations near its "mouth" were as high as 700 ppb and average concentrations were in excess of the EPA 1-hour NAAQS standard of 120 ppb. The concentrations were highly variable and depended strongly on the pattern of air drafts in the room. Figure 5 shows the result of using

Ioncare PAP in a quiet air environment, wherein the air currents are controlled solely by diffusion. One can see that the ozone level was quickly brought up to 120 ppb above the PAP. The results of Figure 5 were obtained with a 10 cm separation between the PAP and the ozone meter sampling inlet; the measured concentration increased rapidly as this distance was reduced, in agreement with the results of Ref. [50].

5.4. Kinetic Treatment.

The ozone concentration time dependence and steady-state level observed in experiments in closed volumes such as rooms, cars, and Teflon bags can be described by a simple model. The linearity of the initial ozone concentration rise in Teflon bag measurements (Figure 1) suggests that the production of ozone by an air-purifier is a zero-order process with respect to ozone:

$$\text{Air} \rightarrow \text{O}_3 \qquad \frac{d[\text{O}_3]}{dt} = k_{source}(cm^{-3}s^{-1}) = 1.23\times10^{11}\times\frac{Rate\,(mg/hr)}{V(cu.ft.)} \qquad (1)$$

The measured ozone emission rates for several air-purifiers are reported in Table 5.2. The zero-order assumption was observed to be valid for all air-purifiers listed in Table 5.2 for ozone mixing ratios in the ppb - low ppm range. The conversion factor in Eq. (1) is valid for 1 atm, 25°C, and for volume measured in the units of cubic feet (1 foot = 30.48 cm). Eq. (1) implicitly assumes that the rate of mixing of air within the room volume, *V*, is considerably faster than the rate of ozone removal from the room. This condition was satisfied for all measurements reported here (except for measurements with PAPs).

The loss of ozone from the room is in principle a complicated process because of the presence of multiple surfaces with varying degree of reactivity towards ozone

(including the body of the air-purifier itself), complicated pattern of air mixing in the room, and coupling between air-transport and surface kinetics [135]. However, in present measurements in closed, well-mixed indoor environments the observed ozone decay could be described as a first-order process to an excellent degree of approximation (i.e., there were no apparent deviations from the first-order kinetics within the measurement uncertainties):

$$O_3 \rightarrow \text{products} \qquad \frac{d[O_3]}{dt} = -k_{loss}(s^{-1})[O_3] \qquad (2)$$

The decay rate constant, k_{loss}, is a combination of physical removal due to the air exchange, chemical removal due to heterogeneous reactions on surfaces, and chemical removal due to reactions with air impurities.[59] In cases when the wall loss dominates, the decay rate-constant can be related to the deposition velocities customary reported in the research literature on surface decay rates:

$$k_{loss} = \frac{1}{V}\sum A \times \upsilon_d \qquad (3)$$

where A is the surface area, υ_d is the deposition velocity of ozone on that particular type of surface, and the summation extends over all available surfaces in the room.

The inverse of the decay rate constant, k_{loss}^{-1}, can be viewed as the characteristic lifetime of ozone in a given environment. It can range from several hours in a highly unreactive Teflon bag (e.g., 5 hours in Figure 1) to just a few minutes in a well-ventilated office (Table 5.3). The decay rate constants measured here (Table 5.3) are consistent with previous measurements of similar parameters in houses and offices [59, 136]. In well-ventilated, sparsely furnished rooms the ozone decay rate is observed to be very close to the air exchange rate, which suggests that the decay is dominated by physical removal of

ozone from the room. However, when the air exchange rate is slow or the room contains reactive surfaces, the observed decay rate should be faster than the air exchange rate. In this case, the removal is mostly due to the chemical reactions with the surfaces and/or with gas-phase organics. The effect of air exchange and transport-limitations on concentrations of indoor air pollutants is discussed in more detail in Refs. [106, 135].

Eq. (1) and (2) can be integrated to give the ozone concentration build-up after the air-purifier is turned on (assuming very low background ozone concentration):

$$[\mathrm{O_3}](\mathrm{t}) = \frac{k_{source}}{k_{loss}}\left(1 - e^{-k_{loss}t}\right) \qquad (4)$$

The ozone concentration builds up from zero to a steady-state value in which the emission rate is exactly balanced by the decomposition rate:

$$[\mathrm{O_3}]_{\mathrm{ss}} = \frac{k_{source}}{k_{loss}} \quad \text{or} \quad [\mathrm{O_3}]_{\mathrm{ss}}(ppb) = \frac{300 \times Rate\,(mg/hr)}{k_{loss}(\mathrm{min}^{-1}) \times V(cu.ft.)} \qquad (5)$$

Once again, Eq. (5) is valid only when the rate of mixing of air within the room volume is considerably faster than the rate of ozone removal from the room. The conversion factor in Eq. (5) is equal to 300 purely by accident; it is valid for the conditions of 1 atm, 25°C, and the specified set of units. In cases where the ozone loss is dominated by the wall decomposition, the product $k_{loss} \times V$ in the denominator can be equivalently replaced by the product of the deposition velocity and the room surface area, $A \times \upsilon_d$.

After the air-purifier is turned off, the ozone concentration decays exponentially

$$[\mathrm{O_3}](\mathrm{t}) = [\mathrm{O_3}]_{\mathrm{ss}}\, e^{-k_{loss}t} \qquad (6)$$

with the decay rate constant, k_{loss}. Figures 2-4 provide clear examples of this behavior. Except for measurements inside Teflon bags, no significant deviations from the single exponential decay were observed in this work.

5.4.1. Verification of the Kinetic Model.

Eq. (5) has several interesting ramifications. For example, it confirms the suggestion of Ref. [50] that the effect of putting several ozone generators in the same room is additive, with contributions of each generator to the total steady-state ozone concentration being proportional to its ozone emission rate. Indeed, if there is an additional source of ozone present, e.g., from a steady intake of polluted air from the outside or from another ozone-generating device inside, it will create a background concentration of ozone, $[O_3]_{bg} = \frac{k_{ext}}{k_{loss}}$, where k_{ext} is the effective zero-order rate constant for the background source and k_{loss} is the first-order ozone decay rate constant for the room (or any other closed space in question). A simple exercise in kinetics shows that turning on an air-purifier with ozone emission rate constant k_{source} will further increase the steady-state ozone concentration to $[O_3]_{ss} = \frac{k_{ext} + k_{source}}{k_{loss}} = [O_3]_{bg} + \frac{k_{source}}{k_{loss}}$. The last term in this equation is exactly equal to the steady-state level of ozone that the air-purifier would have produced in the absence of the background ozone source.

This additivity of contributions from different ozone sources was explicitly tested by running two air-purifiers in the same room at the same time. Figure 4 shows the result for operating Pro-420 in a ventilated office for an hour, followed by simultaneously operating Pro-420 and XT-400 for another hour, followed by operating XT-400 for another hour. The measured steady-state levels of ozone for individual air-purifiers (corrected for the small background level of 8 ppb) are 307 ppb (Pro-420 only) and 276 ppb (XT-400). The uncertainties in the measured steady-state values are about 5 ppb. The

sum of these values, 584 ppb, is essentially identical to the steady-state level of 582 ppb measured during the Pro-420 and XT-400 concurrent operation.

To further test the predictive power of Eq. (5), Figure 5.6 compares incremental $[O_3]_{ss}$ measured in experiments (Table 5.3) with $[O_3]_{ss}$ calculated from the room volume, measured decay rate constant for the room, and the air-purifier ozone emission rate measured in separate experiments in a Teflon bag. The data in Figure 6 reflect the results obtained for several ionic and ozonolysis air-purifiers operated in cars, offices, bathrooms, and bedrooms. The ozone emission rates of air-purifiers in Figure 5.6 span 2 orders of magnitude (from 0.4 mg/hr to 357 mg/hr in dry air). Nevertheless, the agreement between the measured values and those predicted from the simple kinetic model can be regarded as excellent over the entire range of environmentally relevant ozone concentrations (10 – 1000 ppb).

Possible sources of scatter in Figure 5.6 include: i) use of ozone emission rates for dry air (Table 5.2) instead of those for the actual RH in the room (in this work, RH was 40±5% in offices and 50±10% in the house); ii) uncertainties in measuring k_{loss} (10-20%); iii) and air-transport limitations. The last source refers to either inhomogeneous or insufficiently rapid mixing of air across the room volume by the fan. These two conditions required for the validity Eqs. (1) and (5) are not always trivial to meet in actual environments because of the presence of furniture, sharp room corners, temperature and pressure gradients across the room, and non-uniform distribution of ozone deposition velocities on the room surfaces. In spite of all these limitations, the model performs quite well; the largest deviation between measured and observed steady-state concentrations in Figure 6 is by a factor of 2.

5.4.2. Implications of the Model.

In the absence of indoor ozone-generating sources, indoor ozone concentration is known to track the outdoor ozone concentration [59]. The observed ratios of indoor-to-outdoor ozone levels (I/O) are generally in the range of 0.1-0.7 [59], with larger values correlating with higher air exchange rates between the inside and outside. Operation of an ozone-generating air-purifier can make the I/O ratio considerably larger than 1, with the incremental increase in indoor ozone level being directly proportional to the air-purifier ozone emission rate. Therefore, people occupying rooms with an operating ozone-generating air-purifier are more likely to be exposed to levels of ozone in excess of the public health standards. Depending on the way the air-purifier is used, the exposure level can be as high as the equivalent of Stage-1 or even Stage-2 smog alert (Figures 5.2-4). For reference, the last Smog-2 alert in the South Coast Basin, which includes Los Angeles, occurred in 1988, and there was only one Smog-1 alert in this area between 1999 and 2003 [137].

Eqs. (3) and (5) suggest that the increase in ozone concentration driven by an air-purifier should be inversely proportional to the total room surface area in the limit when the ozone removal from the room is dominated by the wall loss, and the surfaces in the room have similar reactivity towards ozone (i.e., similar ozone deposition velocities). Everything else being equal, operation of an ozone-generating air-purifier in rooms with smaller floor areas (i.e., bathrooms) should produce higher steady-state levels of ozone. In the limit when the ozone removal is dominated by air-exchange, the steady-state increase in ozone level is inversely proportional to the room volume instead of the total

surface area. Again, the prediction is that operation of an air-purifier in smaller rooms should result in larger ozone level rises. Data in Table 3 fully confirm these predictions.

As a final note, Eq. (5) can be of some potential value for future regulatory decisions affecting ozone-generating appliances and for checking compliance with already existing regulations. Consider an example of a calculation of the maximal ozone emission rate for a medical device subject to the Code of Federal Regulations 21 CFR 801.415 set forth by the US Food and Drug Administration in 1976. According to the code, such a device should not generate ozone at a level in excess of 50 ppb in an "enclosed space intended to be occupied by people for extended periods of time".[132] Assuming that the device is to be operated in a 2000 cu. ft. enclosed space characterized by an ozone lifetime of 30 min, one calculates 11 mg/hr for the maximal ozone emission rate under such conditions. The chief advantage of Eq. (5) is that one does not need to conduct actual measurements of ozone concentrations to obtain the steady-state level of ozone resulting from the device. Indeed, the room volume and surface area can be easily measured, ozone emission rate is an intrinsic property of the device, and the ozone decay rate can be estimated from deposition velocities for surfaces used in construction. Tables of ozone deposition velocities are available from multiple sources, e.g., Ref. [53, 59, 125].

5.5. Conclusions

Operation of an ozone-generating air-purifier in a closed indoor environment results in an increase in the steady-state ozone concentration that is directly proportional to the air-purifier's ozone emission rate. Depending on the mechanism of ozone removal from the room, the magnitude of the increase is inversely proportional to either the surface area of the room (the loss is dominated by heterogeneous removal on surfaces) or the total volume of the room (the loss is dominated by air-exchange). In either case, the largest increase in the steady-state ozone level is anticipated for small, poorly ventilated rooms, especially if they are constructed from materials with low reactivity towards ozone. In such rooms, even a device with an ozone emission rate of a few milligrams per hour can maintain an ozone level in excess of public health standards. The ozone level generated by an air-purifier is in addition to the normal indoor ozone level resulting from the air exchange between inside and outside. Therefore, persons operating ozone-generating air-purifiers in their houses and/or offices may be more frequently exposed to ozone levels in excess of the health standards compared to an average person living in the same area.

Table 5.1. Health-based standards for ozone mixing ratio in the air established by the US government. The acronyms are explained in the introduction.

Agency	Standard	Exposure time	Mixing ratio (ppb)
US EPA	NAAQS	1-hour average	120
US EPA	NAAQS	8-hour average	80
CARB	California AAQS	1-hour average	90
CARB	California AAQS	8-hour average	70
NIOSH	IDLH	-	5000
NIOSH	PEL	15-min	100
OSHA	PEL	8-hour average	100
OSHA	STEL	15-min	300
CARB	Stage 1 smog alert	-	200
CARB	Stage 2 smog alert	-	350
CARB	Stage 3 smog alert	-	500

Table 5.2. Ozone emission rates for air-purifiers tested in this work. Ionic and ozonolysis air-purifiers are listed on the top and bottom of the table, respectively. The rates were measured in a Teflon bag in dry air with RH<5%. Only a single instrument of each type was tested except for SI627 and PRO 420, where two units were available. All air-purifiers were new except for PZ6 Air. All measurements used the highest device settings, where applicable.

Air-purifier name	Model number	O_3 emission rate (mg/hour)
SI (= Sharper Image) Quadra Silent Air-Purifier	SI637	2.2
SI Personal Air-purifier	SI736	0.30
SIIB Pet Brush	SI688	0.71
SI GP Car Air-purifier with Ultraviolet Germicidal Protection	SI710	0.74
SI Dashboard (Plug-In) Ionizer	SI629	0.40
SI Car Air-purifier	SI633	0.48
SI Electrostatic Air Cleaner for Bathrooms & Small Spaces	SI627	0.17 / 0.24
SI Air Freshener 2.0 for Bathrooms & Small Spaces	SI717	0.16
Ioncare Personal Air-purifier	Ioncare PAP	0.50
EZ-COM Air-purifier (rated at 40 mg/hr)	EZ-COM	68
Air-Zone® XT-400 (rated at 400 mg/hr)	XT-400	220
Prozone® Air-purifier (rated at 125 mg/hr)	PZ6 Air	42
o3ozoneTM PRO 420 Ozone Generator (rated at 420 mg/hr)	PRO 420	132 / 137

Table 5.3. Measurements of steady-state ozone concentrations during operation of selected air-purifiers in various environments. The ozone emission rates refer to dry air; they are listed for reference only. Different $[O_3]_{ss}$ and k_{loss} values are reported for the same room/air-purifier combinations because the air exchange rate in the room was varied from test to test by partially blocking the air intake. Uncertainties in k_{loss} are about 10% (σ). The air exchange rates were quantified only for selected measurements in offices.

Environment	Floor area sq.ft. (m^2)	Volume cu.ft. (m^3)	Air exchange rate $(k_{air})^{-1}$ (min)	Air-purifier	Rate (mg/hour)	Measured $[O_3]_{ss}$ increase (ppb)	Measured $(k_{loss})^{-1}$ (min)
Bathroom A	23 (2.1)	207 (5.9)	-	SI637	2.2	135	20
			-	SI637	2.2	165	29
			-	SI627+SI717[a]	0.40	40	53
Bathroom B	46 (4.3)	370 (10.4)	-	EZ-COM	68	Stopped at 450[b]	18
			-	SI637	2.2	22	11
Bedroom	125 (11.6)	1110 (31.4)	-	EZ-COM	68	260	30
Office A	138 (12.9)	1245 (35.2)	12	EZ-COM	68	240	12
			12	PRO 420	132	320	10
			12	SI637	2.2	9	13
			12	PZ6 Air	42	120	11
Office B	120 (11.1)	957 (27.1)	11	PZ6 Air	42	140	9.3
			11	PRO 420	137	340	9.2

			11	EZ-COM	68	180	9.5
			-	PRO 420	137	650	12
			-	PRO 420	137	290	6.3
			-	PRO 420	137	310	8.4
			-	SI637	2.2	12	12
			-	PRO 420	137	307	7.7
			-	PRO 420 + XT-400[a]	357	582	7.7
			-	XT-400	220	276	7.7
Lexus ES250	-	~50 (1.4)[c]	-	SI633	0.48	6	~2
	-		-	SI710	0.74	9	~2

[a] Operated simultaneously

[b] The steady-state was not reached for safety reasons (See Figure 2b)

[c] Estimated

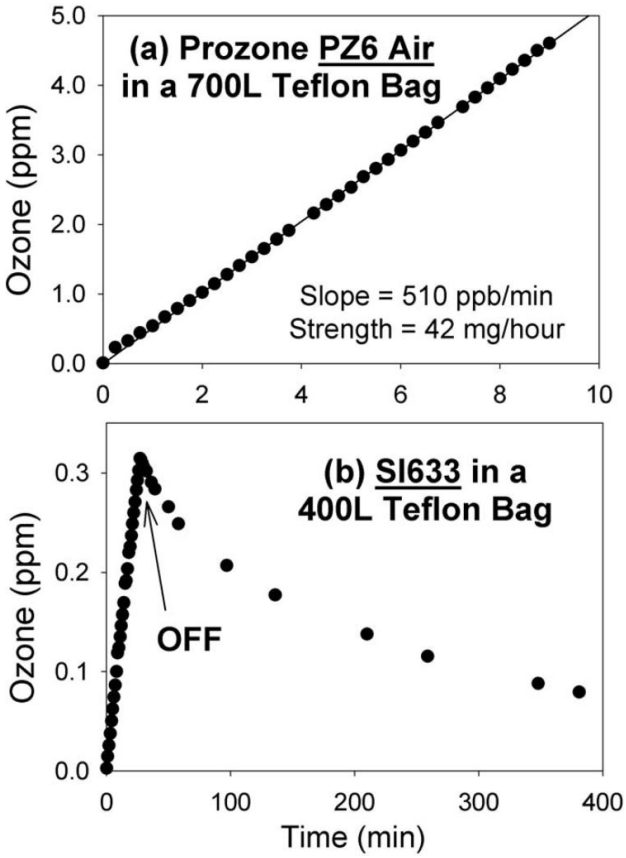

Figure 5.1: Sample measurements of ozone emission rates for PZ6 Air and SI633. Ozone concentration build-up is measured in a Teflon bag of a known volume after turning the air-purifier on. The initial concentration rise is linear, $[O_3] \approx k_{source} \times t$. The lifetime of ozone in the Teflon bag after the air-purifier is turned off is very long, with a lifetime of almost 5 hours.

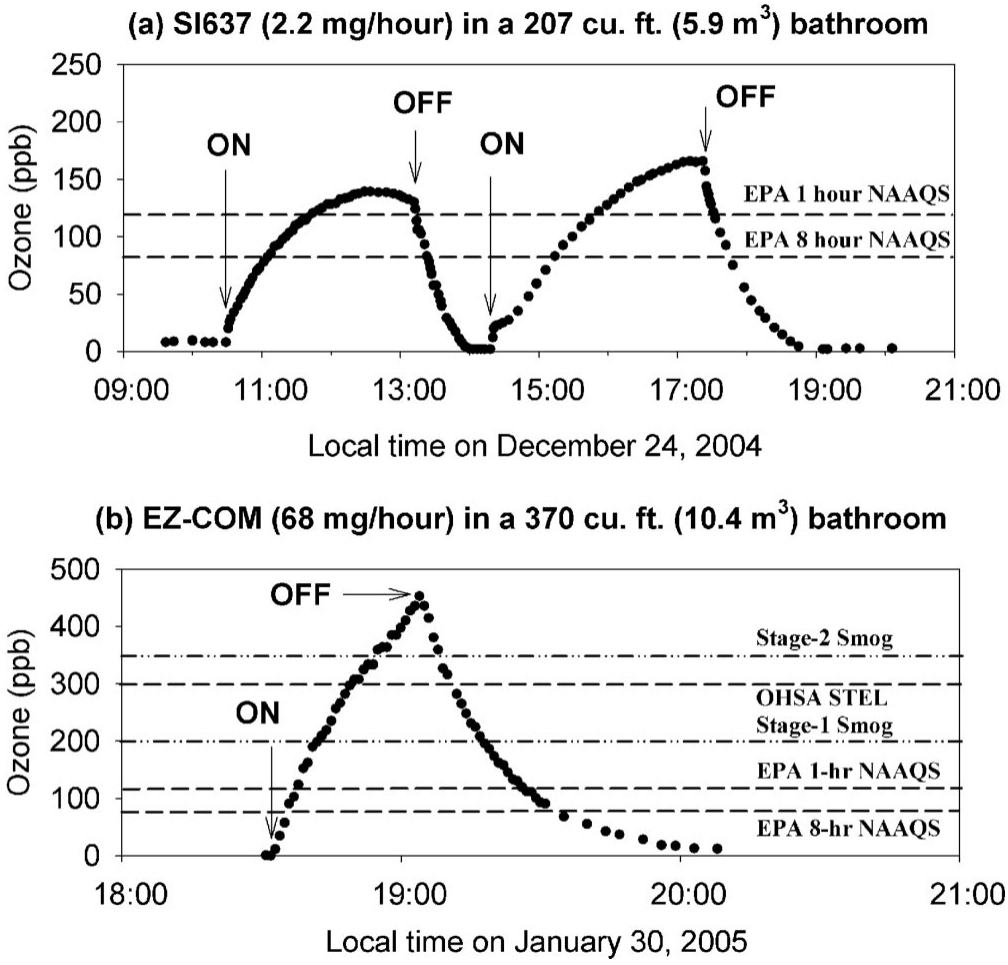

Figure 5.2: Sample measurements in bathrooms: (a) SI637 operated in a small bathroom; (b) EZ-COM operated in a larger bathroom. No forced ventilation is used in both cases. Dashed lines correspond to EPA 1-hour (80 ppb), EPA 8-hour (120 ppb), and OSHA STEL (300 ppb) standards. Dash-dotted lines are Stage-1 (200 ppb) and Stage-2 (350 ppb) smog alerts.

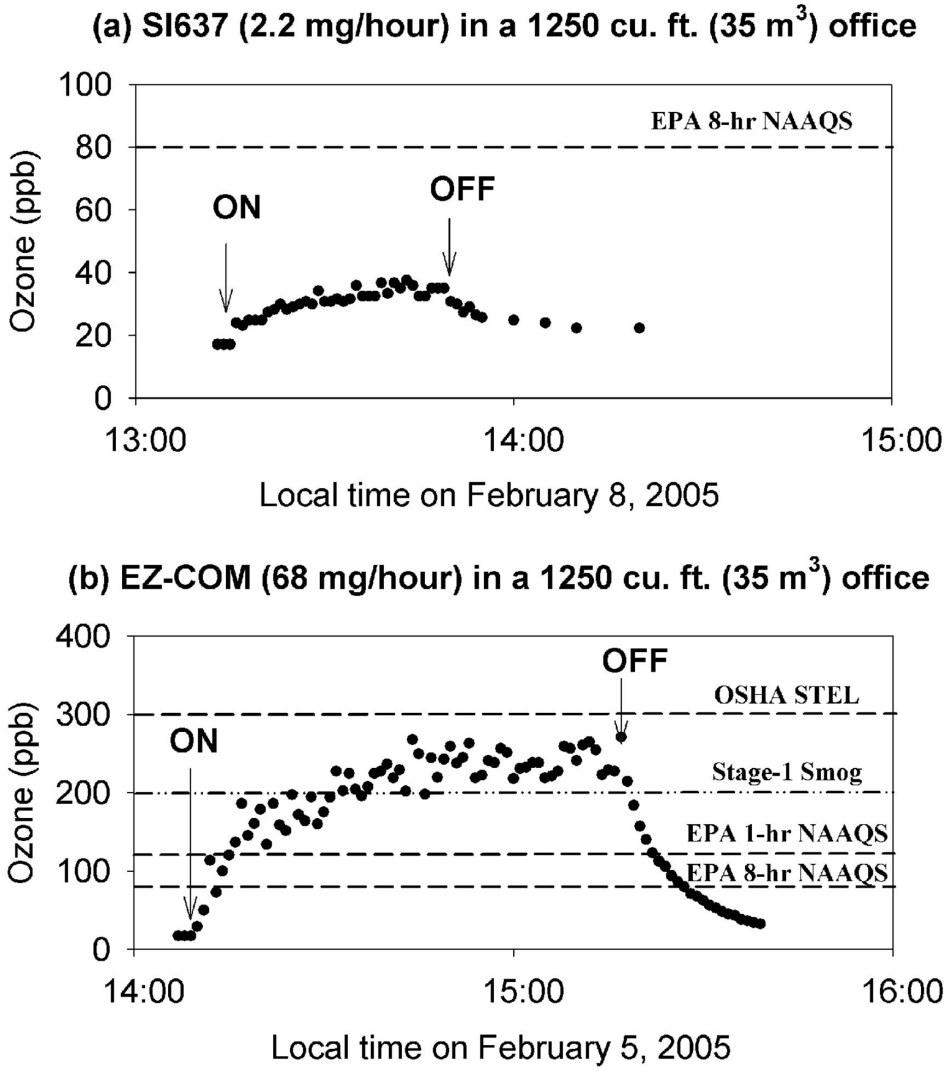

Figure 5.3: Sample measurements in ventilated office rooms: (a) SI637 operated in an office room; (b) EZ-COM operated in the same room. The air exchange rate is one room volume every 12 minutes. Dashed lines correspond to EPA 1-hour (80 ppb), EPA 8-hour (120 ppb), and OSHA STEL (300 ppb) standards. Dash-dotted line is Stage-1 Smog alert level (200 ppb).

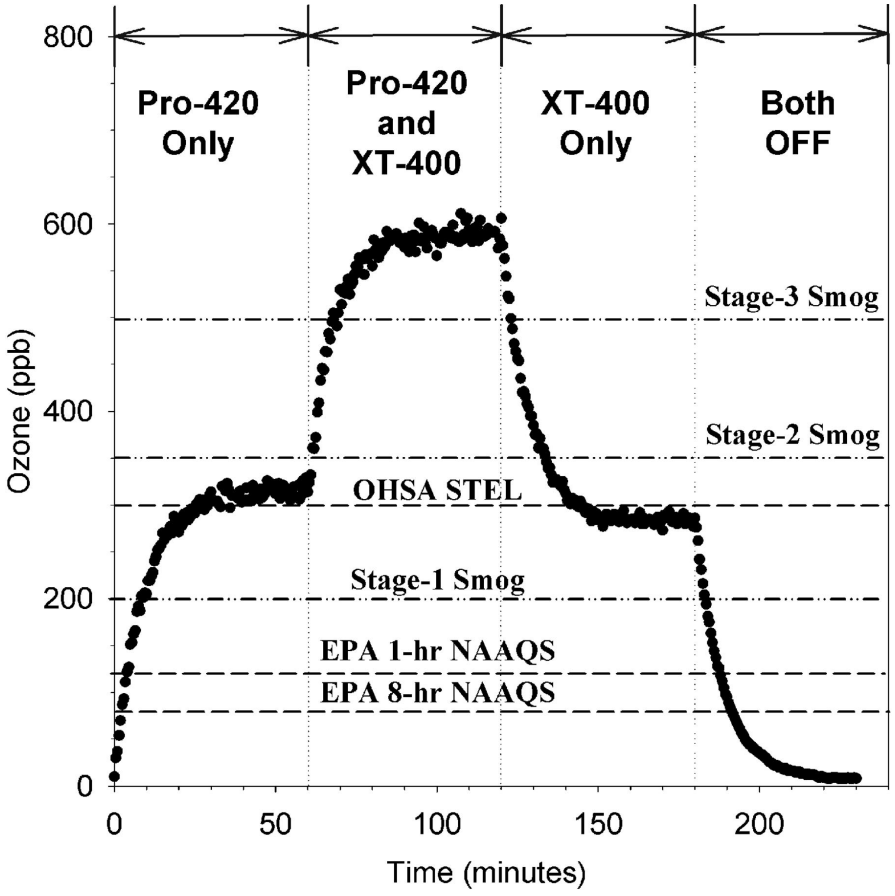

Figure 5.4: Back-to-back operation of two different air-purifiers in the same office. First, Pro-420 is turned on for 60 min, followed by Pro-420 and XT-400 both on for the next 60 min, followed by XT-400 on for the next 60 min, followed by the decay of ozone after everything is turned off. Dashed lines correspond to EPA 1-hour, EPA 8-hour, and OSHA STEL standards. Dash-dotted lines are California Stage-1, -2 and -3 smog alerts.

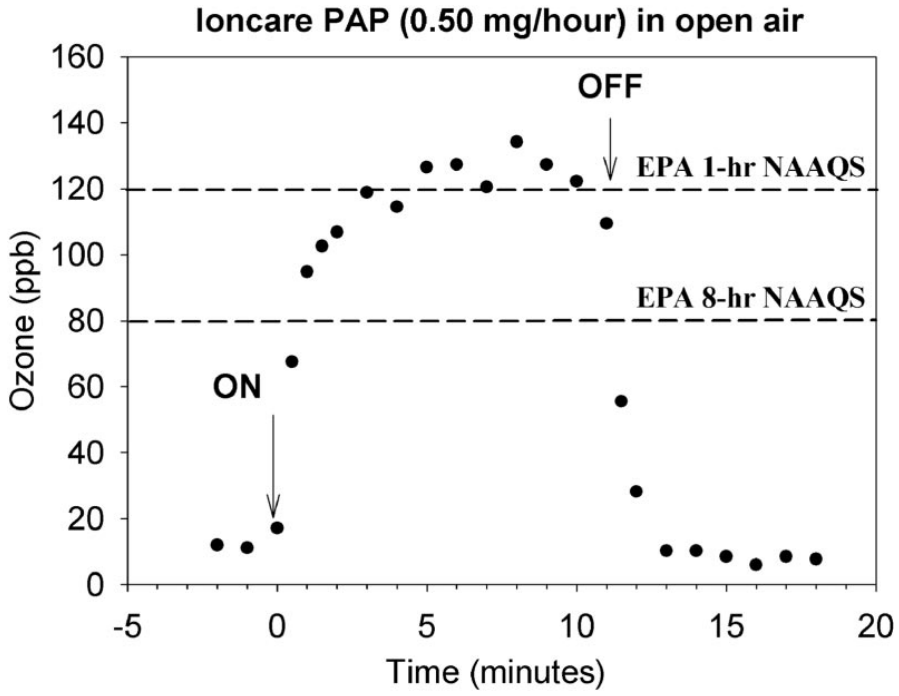

Figure 5.5: Sample measurement for Ioncare PAP. Sampling takes place 10 cm above the PAP. Dashed lines correspond to EPA 1-hour (80 ppb) and EPA 8-hour (120 ppb) standards.

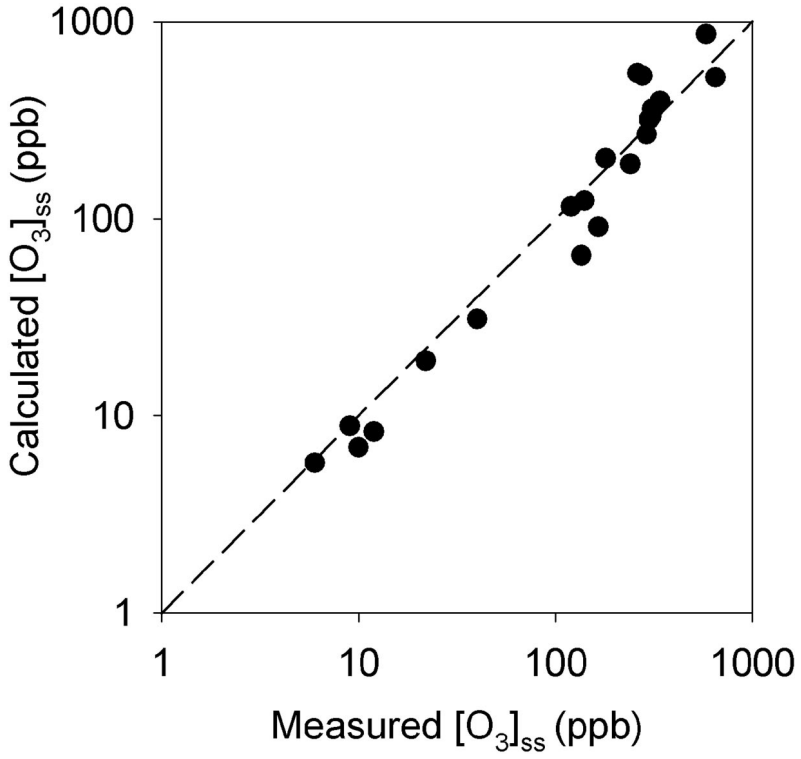

Figure 5.6: Comparison of the measured steady-state ozone concentrations with those calculated using Eq. (5) from the decay rate constants, air-purifier ozone emission rates, and room volumes. The plot includes all data from Table 3. The sources of the scatter are discussed in the text.

Chapter 6

Kinetic analysis of competition between aerosol particle removal and generation by ionization air purifiers

Abstract

Ionization air purifiers are increasingly used to remove aerosol particles from indoor air. However, certain ionization air purifiers also emit ozone. Reactions between the emitted ozone and unsaturated volatile organic compounds (VOC) commonly found in indoor air produce additional respirable aerosol particles in the ultrafine (<0.1 μm) and fine (<2.5 μm) size domains. A simple kinetic model is used to analyze the competition between the removal and generation of particulate matter by ionization air purifiers under conditions of a typical residential building. This model predicts that certain widely-used ionization air purifiers may actually *increase* the mass concentration of fine and ultrafine particulates in the presence of common unsaturated VOC, such as limonene contained in many household cleaning products. This prediction is supported by an explicit observation of ultrafine particle nucleation events caused by the addition of d-limonene to a ventilated office room equipped with a common ionization air purifier.

6.1. Introduction

Ultrafine (diameter < 0.1 μm; $PM_{0.1}$), fine (< 2.5 μm; $PM_{2.5}$), and coarse (< 10 μm; PM_{10}) aerosol particles significantly contribute to the toxicity of urban air pollution [138, 139]. The adverse health effects of particulate matter (PM) include exacerbation of asthma symptoms [99, 101], cardiovascular problems [140, 141], increased mortality [29, 100], and increased incidence of lung cancers [142, 143]. To address the health impacts of airborne PM, the Environmental Protection Agency (EPA) established the national ambient air quality standards for $PM_{2.5}$ at 15 $\mu g/m^3$ (annual mean) and 65 $\mu g/m^3$ (24-hour mean). The standards for PM_{10} are 50 $\mu g/m^3$ and 150 $\mu g/m^3$, respectively. No official standards for ultrafine particles have been established yet in spite of the increasing evidence for their toxicity and innate ability to penetrate into the blood circulation [144].

A significant fraction of urban PM can be classified as secondary organic aerosol (SOA) produced by oxidation of volatile organic compounds (VOC) [104]. A particularly important group of aerosol-forming VOC are terpenes [145, 146], a class of hydrocarbons emitted by coniferous plants, and used extensively as additives to many household cleaning products. The SOA yields, reaction mechanisms, and particle composition have been extensively studied for oxidation of α-pinene, β-pinene, limonene, and other monoterpenes in smog chambers under atmospherically relevant conditions [147-158] and in simulated indoor environments [60, 115, 116, 145, 146, 159, 160]. The observed SOA yields resulting from oxidation by ozone can be quite high (> 50% by mass), but the yields depend in a complicated way on multiple factors including presence of NO_x, presence of OH scavengers, concentration of preexisting aerosol particles, concentrations of reactants, humidity, temperature, radiation level, and reaction time.

Stand-alone air purification devices for indoor use have gained widespread popularity in recent years. However, certain air purifiers emit ozone during operation, either intentionally or as a by-product of air ionization [47-50]. Ozone, a criteria air pollutant regulated by multiple health standards, represents a serious health concern by itself [51]. In addition, ozone can react with certain indoor surfaces [52-56] and indoor VOC [57-60] generating secondary products with potential adverse health effects. For example, terpene oxidation products are known eye and airway irritants [61, 62].

Ionization air purifiers present an interesting dilemma in this respect. On one hand, they remove PM from the air. On the other hand, ozone emitted by certain ionization air purifiers in the presence of unsaturated VOC increases both the mass and number concentration of aerosol particles. The main objective of this study is to verify whether the mass emission rate of fine and ultrafine PM resulting from an ionization air purifier operation can exceed the purifier's PM removal rate under conditions characteristic of a private residence.

6.2. Experimental

A common residential ionization air purifier (IAP) was used in experiments. A commercial ozone generator (OG) marketed as an "air cleaner" despite its lack of any particle filtration capabilities, was used for comparison. Rates of ozone emission and particle removal (Table 6.1) for these two devices were quantified as described in the supporting section.

The measured ozone emission rates for the IAP and OG are 2.2(2) mg hr^{-1} and 108(14) mg hr^{-1}, respectively. Parentheses contain 2σ uncertainties in the last significant digits.

IAP works by capturing a certain fraction of particles from the air passing through the purifier. The particle capture probability, γ, is related to the first-order particle removal rate constant, k_{ap}, the mass flow rate through the air purifier, F, and room volume, V, as follows:

$$k_{ap} = \frac{\gamma F}{V} \qquad (1)$$

The γF product, which is related to the clean air delivery rate (CADR) of the air purifier, can be used to predict the effective particle removal rate constant in a well-mixed room of an arbitrary volume. The measured value of γF (see supporting information) is 342(20) SLM = 20(1) m^3 hr^{-1} for the IAP. This value of γF was measured for particles that were predominantly in the 0.15-0.30 μm size range. This work assumes that γF value is the same for all particle sizes of interest. It is certainly possible that IAP has different efficiencies for ultrafine and course particles [161] but this is not going to strongly affect the main conclusions of this work. OG was found to have no measurable effect on the particle count ($\gamma F \approx 0$) because it has no built-in particle filtration capabilities.

The actual tests were performed in a sparingly furnished office room with a floor area of 11.1 m^2, and overall volume of 27.1 m^3. The floor material was linoleum, the walls were painted drywall, and the ceiling consisted of industrial fiberglass ceiling tiles. The room was ventilated through an HVAC system with a measured whole air exchange rate of ~5 hr^{-1}. This exchange rate is higher than for an average private residence but typical for an office room. The air purifiers were positioned on the floor in the middle of the room. The ozone monitor and particle counters were installed in an adjacent room and air was sampled approximately 1 m away from the air purifiers.

A scanning mobility particle sizer (SMPS) was used to measure the particle size distribution in 0.010-0.90 μm size range, and a laser particle counter sampled particles in the 0.15-5.0 μm size range. A large fan was placed in the room for a better mixing of the air across the room volume. The time to acquire one particle size distribution with SMPS was 7 min; that for laser particle counter was 5 min. In a typical run, the data were logged with a Labview-based program for 5-20 hours with the air purifier turned off and then for another 5-20 hours with the air purifier turned on. At certain time intervals, a measured quantity of d-limonene vapor (5-60 mg) was injected in the room at a rate of 3 mg min^{-1} for a brief period of time.

6.3. Kinetic model

The following model is used to describe concentrations in a single well-mixed indoor environment that exchanges air with the exterior atmosphere:

$$\frac{d[\mathrm{X}]}{dt} = \kappa_X \lambda [\mathrm{X}]_{out} + \frac{E_X(t)}{V} + R_X - \lambda[\mathrm{X}] - k_{rX}[\mathrm{X}] - \frac{S}{V}\upsilon_{dX}[\mathrm{X}] \qquad (2)$$

[X] and $[X]_{out}$ are concentrations of species X indoors and outdoors, respectively; λ is the whole air exchange rate; κ_X is outdoor-to-indoor penetration efficiency; V is the volume; S is the interior surface area; E_X is the emission rate for X by all indoor sources; R_X is the combined rate of production of X by gas-phase chemistry; k_{rX} is an effective first-order rate constant for the removal of X by chemical reactions; υ_{dX} is the deposition velocity of X on indoor surfaces. The constantsλ, k_{rX}, and $k_{dX} = \frac{S}{V}\upsilon_{dX}$ all have units of inverse time,

κ_X is unitless, and [X] has mass concentration units (μg m^{-3}) to simplify comparison of concentrations of gas-phase and aerosolized species.

Three species are included in the model: ozone, an unsaturated VOC (d-limonene), and PM. Ozone is emitted indoors by the air purifier, and also penetrates from outdoors by means of air exchange. Aerosol particles are brought indoors by the HVAC system, and also chemically generated via reaction

$$\mathrm{VOC} + \mathrm{O_3} \rightarrow \chi\mathrm{PM} + \text{volatile organics} \qquad (3)$$

where χ is the mass yield of aerosol resulting from the ozonolysis of VOC. The model implicitly assumes that all involatile products of VOC oxidation by ozone quickly partition themselves in the particle phase. The aerosol particles are not differentiated by size or composition; reaction (3) is simply assumed to increase the total mass concentration of PM in the room volume.

With these assumptions, the time evolution of ozone, reactive VOC, and aerosol concentrations can be written as follows.

$$\frac{d[\mathrm{O_3}]}{dt} = \lambda\kappa_{O3}[\mathrm{O_3}]_{out} + \frac{E_{O3}}{V} - \left(\lambda + k_{dO3} + k_r[\mathrm{VOC}]\right)[\mathrm{O_3}] \qquad (4)$$

$$\frac{d[\mathrm{VOC}]}{dt} = \lambda\kappa_{VOC}[\mathrm{VOC}]_{out} + \frac{E_{VOC}}{V} - \left(\lambda + k_{dVOC} + k_r[\mathrm{O_3}]\right)[\mathrm{VOC}] \qquad (5)$$

$$\frac{d[\mathrm{PM}]}{dt} = \lambda\kappa_{PM}[\mathrm{PM}]_{out} + \chi k_r[\mathrm{VOC}][\mathrm{O_3}] - \left(\lambda + k_{dPM} + k_{ap}\right)[\mathrm{PM}] \qquad (6)$$

In the last equation, we separated the removal of aerosol particles by wall deposition (k_{dPM}) and by the air purifier (k_{ap}). The latter can be calculated from equation (1). These equations will be used below to simulate the indoor VOC, PM, and ozone concentrations either analytically or numerically.

6.4. Results

6.4.1. Steady-state kinetic model

In the experiments and simulations described here, and also in many realistic indoor environments, the ozone removal is often dominated by either air exchange or surface deposition. Gas-phase reactions normally make a much smaller contribution to the ozone removal rate. Under such conditions, the term k_r[VOC] in equation (4) can be neglected compared to λ and k_{dO3}. With this simplifying assumption, the equations can be easily solved in steady-state (ss) for the case of time-independent emission rates E_{O3} and E_{VOC}. The steady-state concentration of ozone depends on whether the air purifier is turned on or off:

$$[O_3]_{ss}^{ON} \cong \frac{E_{O3}/V + \lambda\kappa_{O3}[O_3]_{out}}{\lambda + k_{dO3}} \qquad (7)$$

$$[O_3]_{ss}^{OFF} \cong \frac{\lambda\kappa_{O3}[O_3]_{out}}{\lambda + k_{dO3}} \qquad (8)$$

This dependence propagates into the steady-state concentrations of VOC and aerosol particles.

$$[VOC]_{ss}^{ON/OFF} \cong \frac{\lambda\kappa_{VOC}[VOC]_{out} + E_{VOC}/V}{\lambda + k_{dVOC} + k_r[O_3]_{ss}^{ON/OFF}} \qquad (9)$$

$$[PM]_{ss}^{ON/OFF} = \frac{\lambda\kappa_{PM}[PM]_{out} + \chi k_r[O_3]_{ss}^{ON/OFF}[VOC]_{ss}^{ON/OFF}}{\lambda + k_{dPM} + k_{ap}} \qquad (10)$$

The time it takes for the concentrations to approach their steady state values is inversely proportional to the corresponding removal rates, i.e., values in the denominators

of equations (8-10). For the base conditions listed in Table 2, these times are 0.3 hr, 1.4 hr, and 2 hr for ozone, particles, and VOC, respectively.

To quantify the effect of the air purifier on particle concentration in the room, we define an efficiency parameter K, as the ratio of the steady-state PM concentrations obtained when the air purifier is turned on to that when it is off.

$$K = \frac{[PM]_{ss}^{ON}}{[PM]_{ss}^{OFF}} = \frac{\lambda + k_{dPM}}{\lambda + k_{dPM} + k_{ap}} \times \frac{\lambda \kappa_{PM} [PM]_{out} + \chi k_r [O_3]_{ss}^{ON} [VOC]_{ss}^{ON}}{\lambda \kappa_{PM} [PM]_{out} + \chi k_r [O_3]_{ss}^{OFF} [VOC]_{ss}^{OFF}} \qquad (11)$$

Operation of an effective air purifier should result in conditions corresponding to $K<<1$. When $K>1$, the device actually makes more particles than it removes, thus acting as a net particle emitter. The situation with $K=1$ corresponds to the exact cancellation of the particle removal and generation rates.

The first term in this equation describes the effect of the air purifier in the absence of any indoor chemistry.

$$K_{base} = \left(1 + \frac{k_{ap}}{\lambda + k_{dPM}}\right)^{-1} \qquad (12)$$

The more effective is the air purifier the smaller is the values of K_{base}. It is close to unity for an ineffective air purifier ($k_{ap} << \lambda + k_{dPM}$). A similar parameter was used to characterize air cleaners in Ref. [162].

The second term in equation (11) corresponds to the effect of indoor particle generation from the VOC oxidation by ozone. It is unity for air purifiers that emit no ozone and/or for rooms containing negligible amounts of reactive VOC, but it can be substantially larger than unity if both ozone and reactive VOC are present. In such cases,

the effect of indoor chemistry can make the overall value of $K>1$ (air contamination) even if $K_{base}<1$.

We have calculated values of K for a typical indoor environment as a function of the ozone emission rate and clean air delivery rate from the air purifier (γF). Table 2 lists the calculation parameters. The outside ozone, PM, and unsaturated VOC concentrations are 30 ppb, 10 μg/m^3, and 0 μg/m^3, respectively , characteristic of reasonably clean air. The whole air exchange rate λ=0.5 hr^{-1} comes from an analysis of multiple residences [163, 164]. The value k_{dO3}=2.8 hr^{-1} is adopted for a typical surface removal rate constant for ozone [59, 136]. The corresponding rate constant for particles is k_{dPM}=0.2 hr^{-1}, a value suitable for a sparsely furnished room [163, 165]. It is known that particle deposition rates depend on particle size [161, 165] but this dependence is not explicitly considered in this model to in order to keep it simple. All penetration efficiencies are set to κ=1 (setting them to smaller values would only make the predicted K higher).

The VOC emission rate is assumed to be E_{VOC} =5 mg/hr (this corresponds to the evaporation of 0.5 g of a cleaning solution containing 1% limonene in one hour). This value is comparable to the combined emission rate of aerosol-forming terpenes in realistic indoor environments [57, 160]. The rate constant for the reaction between VOC and ozone correspond to that for limonene [104]. The aerosol mass yield is difficult to estimate as it depends in a complicated way on the preexisting PM concentration, concentrations of reactants, and many other factors. This model assumes that χ=1, but we also show results for an order of magnitude reduction in the yield. Surface deposition of VOC is neglected. The ozone emission rate is varied over the range expected for a typical ionization air purifier, 0-10 mg/hr [49].

Figure 6.1 shows the calculated K=1 curves for several different scenarios. Everything above the K=1 curves corresponds to K<1 (air purification) and everything below the curves corresponds to K>1 (air contamination). In addition to the base conditions listed in Table 2, Figure 1 also presents calculations for $[O_3]_{out}$, $[PM]_{out}$, or air exchange rate, λ, scaled by one order of magnitude. Although it is not directly obvious from equation (11), an increase in $[PM]_{out}$ by a certain factor is exactly equivalent to a decrease in the VOC emission rate, E_{VOC}, or to a decrease in the aerosol mass yield, χ, by the same factor. For example, the bottom curve in panel (b) is equivalent to the base conditions with χ changed to 0.1, a more realistic SOA yield for low concentrations of reactants [166].

Ozone-free air purifiers fall on the vertical axes (E_{O3} = 0) in Figure 1. They are always characterized by $K \leq 1$ as predicted by equation (12). Pure ozone-generators fall on the horizontal axes (γF = 0), and always have $K \geq 1$. The ionization air purifiers that both remove particles and emit ozone represent the most interesting case. For example, the IAP used here (γF = 20(1) m^3 hr^{-1} and E_{O3} = 2.2(2) mg hr^{-1}) falls slightly below the K=1 curve for the base-case scenario. With the predicted value of K=1.12, this device would not act as a purifier under the base conditions listed in Table 2. Decreasing the outside concentrations of PM or ozone, decreasing the air exchange rate, or increasing the indoor VOC emission rate would make the situation even worse.

6.4.2. Indoor SOA nucleation events

Aerosol particle generation was tested for both IAP and OG in a 27.1 m^3 office room. Figure 2 shows a sample data run. Operation of OG normally increased the ozone steady-state concentration by some 250 ppb above the 5 ppb background. Operation of IAP increased it by about 5-15 ppb above the background, in rough proportion to its ozone emission rate [49]. The triangles in Figure 2 indicate the time when a certain amount (5-60 mg) of limonene vapor was injected into the room.

Continuous operation of IAP in the absence of limonene resulted in a slight (< 20%) reduction in the average particle concentration. For the 27.1 m^3 room volume, the expected particle removal rate constant by IAP is k_{ap} = 0.76 hr^{-1}. The measured air exchange rate for this room is $\lambda \sim 5$ hr^{-1}. Neglecting the particle wall deposition, equation (12) predicts 10-15 % reduction in the particle count, in agreement with our observations. As expected, operation of OG had no detectable effect on the particle concentration.

Injections of limonene into the room during operation of either OG (injections 1-4 in Figure 6.2) or IAP (injections 5-6) reproducibly increased the particle number concentration by 1-2 orders of magnitude. On the contrary, injections of limonene without operating air purifiers (e.g., injection 7 in Figure 2) produced little change in the particle concentration; a small increase was observed only in 10-15% of such injections. Very infrequently, a spontaneous increase in the particle number concentration would occur (Figure 6.2). These spontaneous bursts were of an external origin, and penetrated into the room through the HVAC system.

The limonene injection rate (3 mg min^{-1}) was higher than one could expect for a typical indoor source. However, the injection lasted only a short time, and the total mass

of injected limonene was comparable to what one could get from a room cleaning using a limonene-containing cleaning solution [159].

Steady-state ozone concentration decreased at most 10-20% for a short period of time following the injection. (The spikes in $[O_3]$ in Figure 6.2 are artifacts resulting from the contribution of particles to the overall UV-absorption sensed by the ozone monitor.) This small effect on the ozone concentration is due to the relatively small rate of reaction (3). Indeed, an instantaneous 10 mg limonene injection into the 27.1 m^3 room volume would correspond to the initial concentration of 1.6×10^{12} molecules /cm^{-3}. Even at this high concentration, the VOC+O_3 reaction's contribution to the ozone removal rate is only 1.2 hr^{-1}. The air exchange rate, $\lambda \approx 5$ hr^{-1}, and ozone deposition rate, $k_{dO3} = 2.8$ hr^{-1} [59, 136] are considerably higher. The effect of VOC on the ozone concentration is expected to be even smaller if VOC are emitted over an extended period of time. The same arguments were used to justify neglecting the k_r[VOC] term in equation (4) in the steady-state model described above.

Figure 6.2(c) shows the total particle mass concentration computed from the particle size distribution assuming spherical particles with a density of 1 g/cm^3. While limonene injections 1-4 occurring at $[O_3]_{ss}$ = 250 ppb produce clear peaks in the total particle mass concentration, injections 5-6 occurring at 10-15 ppb ozone increase the number but not the total mass of the particles. This is a clear indication that the limonene oxidation products not only condense onto pre-existing particles but also nucleate homogeneously. A similar conclusion was reached in a chamber study of ozone reacting with selected household products [160]. The resulting new particles are in the ultrafine size domain (≈ 0.1 μm), and therefore do not significantly contribute to the total mass.

Figure 6.3 shows a filled contour plot of two particle bursts corresponding to injections 1 and 2 in Figure 2. In the first case, corresponding to the addition of 15 mg limonene over 5 min, the particle size distribution peaks below 0.1 μm. In the second case, corresponding to the addition of 30 mg limonene over 10 min, the resulting particle size distribution is bimodal, reflecting complicated particle nucleation and growth dynamics. The structure of these particle bursts bears a resemblance to the particle nucleation events frequently observed outdoors [167-169]. The main difference is that the size distribution evolves considerably faster under the present conditions of large concentrations of reactants and fast air exchange rates.

Figure 6.4 displays the time evolution in the particle size distribution resulting from an addition of 15 mg limonene in 5 minutes into the room with IAP turned on. Each size distribution took 6 minutes to acquire, with SMPS scanning in the direction of increasing particle diameter. New particles appear immediately after the limonene addition. They grow from their initial diameter of 0.02-0.03 μm to about 0.08-0.1 μm before being driven out of the room by the HVAC air flow.

6.4.3. Model evaluation

The observed particle bursts were fitted to the kinetic model described above in one of the following ways. The first approach was a numeric solution of equations (4-6) using a stiff differential equation solver. The injection of limonene was treated as a 3 mg min^{-1} limonene source turned on for a certain period of time. The second approach was an analytical solution of equations (4-6), under the simplifying assumptions of an instantaneous jump in VOC concentration by the amount of $[VOC]_{added}$ (i.e., the amount

that is added over the entire injection period), and a constant ozone concentration in the room. Once again, the second assumption means that $[O_3]_{ss}$ is not strongly affected by the presence of limonene. The resulting solutions are:

$$[\mathrm{VOC}](t) = [\mathrm{VOC}]_{ss}^{ON} + [\mathrm{VOC}]_{added}\, e^{-k_{VOC}t} \tag{13}$$

$$[\mathrm{PM}](t) = [\mathrm{PM}]_{ss}^{ON} + \frac{\chi k_r [\mathrm{VOC}]_{added} [\mathrm{O_3}]_{ss}^{ON}}{k_{PM} - k_{VOC}} \left(e^{-k_{VOC}t} - e^{-k_{PM}t} \right) \tag{14}$$

k_{VOC} and k_{PM} are the effective rate constants for the removal of VOC and PM, respectively,

$$k_{VOC} = \lambda + k_{dVOC} + k_r [\mathrm{O_3}]_{ss}^{ON} \tag{15}$$

$$k_{PM} = \lambda + k_{dPM} + k_{ap} \tag{16}$$

The initial steady-state concentrations are calculated from equations (7-10). Figure 6.5 shows the results of the simulations. The experimental data points represent the total mass concentration of particles following an injection of 15 mg limonene over 5 minutes into the room with an operating IAP. Because the particles are small, the total mass is calculated only for particles below 0.12 μm in diameter under the usual assumptions of particles' sphericity and unit density. The simulation parameters (Table 6.2) are explicitly measured, estimated, or taken from the literature. For example, the outdoor particle concentration, $[PM_{0.12}]_{out}$ = 0.55 μg m^{-3}, is chosen to match the background particle mass concentration for particles with D_p < 0.12 μm for that particular measurement. The only adjustable parameter in the fit is the mass yield of aerosol particles, χ.

Figure 6.5 shows that both exact and approximate simulations provide a satisfactory fit to the data. The fitted mass yield of aerosol particles is χ=0.13 for this

particular measurement. The fitted yield becomes higher for elevated $[O_3]_{ss}$ and/or larger amounts of injected limonene. This explains why the particle bursts resulting from injections 1-4 in Figure 6.2 are stronger than the ones from injections 5-6. These results are in qualitative agreement with published chamber studies of SOA yields, which find that the yields increase with the concentration of both VOC and O_3 [147, 166, 170, 171].

6.5. Discussion

Concerns about ozone-emitting air purifiers have been and continue to be raised by scientists and government officials [47, 49, 50, 59, 118]. Thus, in a recent report to the California Legislature, the California Air Resources Board officially recommended that the public avoid using these devices indoors [48]. This important report reviewed both direct and indirect health effects of the artificially elevated indoor ozone concentrations.

This paper evaluates a simple kinetic model that can be used to quantify the indirect effect of ozone-VOC chemistry on the level of indoor PM. This model includes only three chemical species but it grasps all the key elements of the ozone-VOC chemistry. It should be directly applicable under conditions when the reactive VOC emissions are dominated by one molecule or by several molecules with comparable reactivities towards ozone. In more complicated VOC emission scenarios, the model can be expanded to include multiple SOA-forming reactions between ozone and VOC.

The most striking prediction of the model is the small magnitude of the air purifier's ozone emission rate needed to significantly increase the PM level in the air under realistic indoor conditions. Indeed, under the base conditions listed in Table 2, an air purifier with $E_{O3}/\gamma F$ ratio exceeding ~ 0.1 mg m^{-3} (i.e., 0.1 mg of ozone emitted into

every cubic meter of air processed by the air purifier) may *increase* the respirable PM mass concentration instead of reducing it as advertised by the manufacturer. It is also of concern that this condition is actually fulfilled by IAP used in this work: an appliance that had a broad commercial availability as recently as 2005. Reduction of the ozone emission rate (ideally to zero level) and increasing the air flow through the air purifier are the most important factors for achieving the maximum possible reduction in the indoor PM level. Operation of ozone-emitting air purifiers in indoor environments with elevated concentrations of unsaturated VOC should be avoided.

Table 6.1. Parameters of commercial IAP (ionization air purifier) and OG (ozone generator) used in the tests. Measurements of ozone emission rates and particle removal rates are described in the supplementary information section.

	IAP	OG
Purchase date	2004	2004
Model	SI637	Crystal Air Pro 420
O_3 emission rate (mg/hr) ($\pm 2\sigma$)	2.2±0.2	108±14
Clean air delivery rate, γF ($m^3\ hr^{-1}$)	20±1	0

Table 6.2. Kinetic model parameters. The third column lists the base parameters used for steady-state calculation of the air purifier efficiency, *K*, from equation (11). The forth column lists parameters used in the simulation of particle bursts observed in the office room with operating IAP. $[PM]_{out}$ refers to the $[PM_{all\ sizes}]$ and $[PM_{0.12}]$ in columns 3 and 4, respectively.

Parameter	Definition	Base values for calculation of *K*	Values for simulation of particle bursts
V	Room volume	50 m^3	27.1 m^3 (measured)
$[O_3]_{out}$	Outside ozone	30 ppb	5 ppb (measured)
$[PM]_{out}$	Outside PM	10 μg m^{-3}	0.55 μg m^{-3} ($[PM_{0.12}]$)
$[VOC]_{out}$	Outside VOC	0.0 μg m^{-3}	0.0 μg m^{-3} (assumed)
λ	Air exchange rate	0.5 hr^{-1}	5.0 hr^{-1} (measured)
k_{dO3}	Ozone surface deposition	2.8 hr^{-1}	1.0 hr^{-1} (estimated)
k_{dPM}	PM surface deposition	0.2 hr^{-1}	0.2 hr^{-1} (assumed)
k_{dVOC}	VOC surface deposition	0.0 hr^{-1}	0.0 hr^{-1} (assumed)
k_r	VOC+O_3 rate constant	2.0×10^{-16} cm^3 s^{-1}	2.0×10^{-16} cm^3 s^{-1}
χ	Aerosol mass yield	1.0	0.13 (fitted)
κ_X	All penetration efficiencies	1.0	1.0 (assumed)
E_{VOC}	VOC indoor emission rate	5 mg hr^{-1}	5 min pulse @ 3 mg hr^{-1}
E_{O3}	Ozone indoor emission rate	Variable 0-10 mg hr^{-1}	2.2 mg hr^{-1} (SI637)
γF	Clean air delivery rate	Variable 0-100 m^3 hr^{-1}	20 m^3 hr^{-1} (SI637)

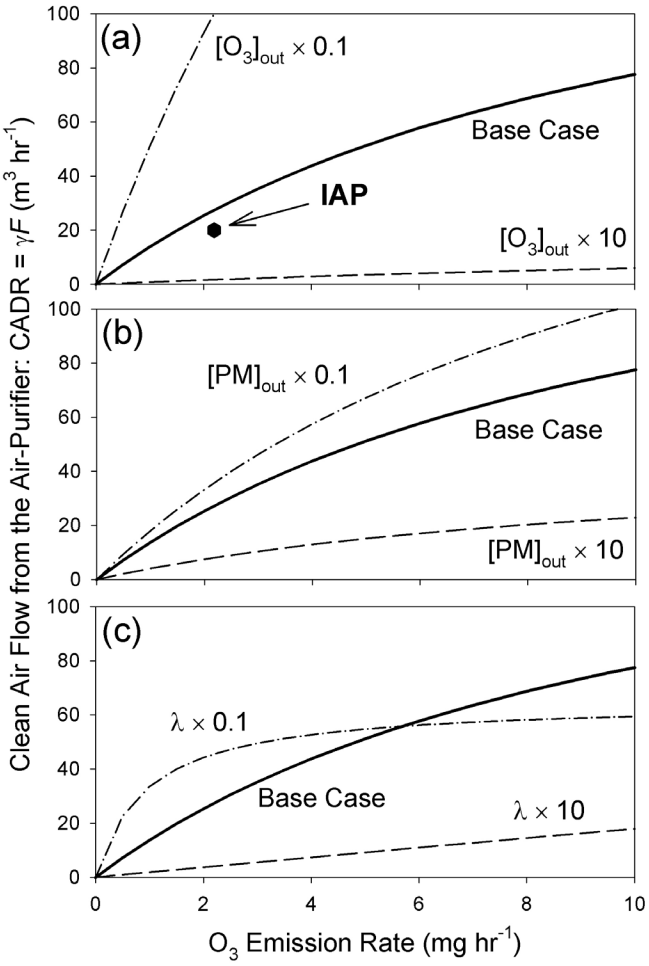

Figure 6.1 Conditions resulting in an exact cancellation of particle generation and removal by ozone-emitting air purifiers. Solid lines are K=1 curves for the base conditions listed in Table 2. Areas above and below the K=1 curves correspond to air purification (K<1) and contamination (K>1), respectively. Panels (a), (b), and (c) display K=1 curves for tenfold deviations from the base conditions in $[O_3]_{out}$, $[PM]_{out}$, and λ, respectively. An increase in $[PM]_{out}$ is exactly equivalent to a decrease in E_{VOC} or χ by the same factor. Panel (a) includes the parameters of the IAP used in this work.

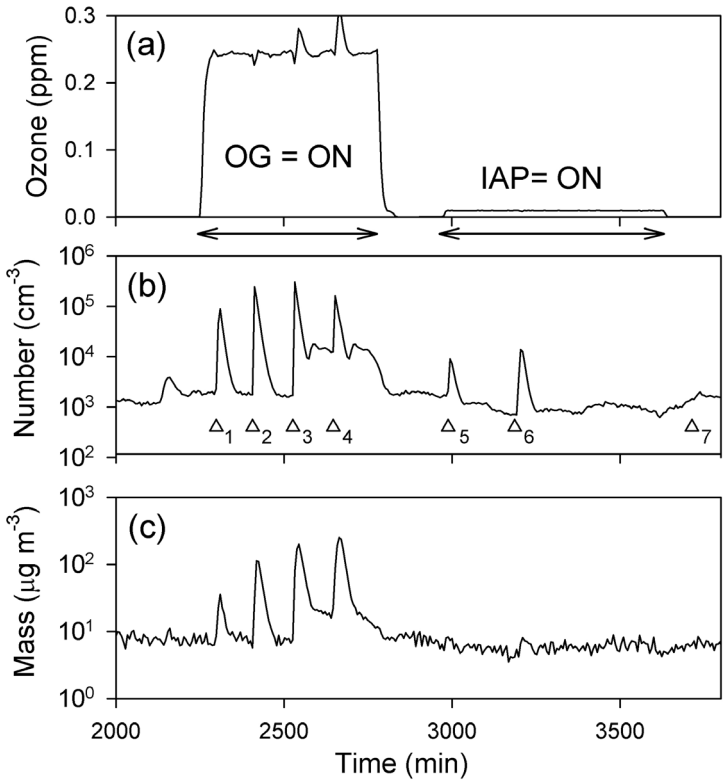

Figure 6.2 Sample measurements of ozone (a) and particle (b) concentrations in a ventilated office. Two plateaus in [O_3] correspond to the OG and IAP operation. Spikes in [O_3] are experimental artifacts (see text). Panels (b) and (c) display the total number and mass concentrations of particles in the 0.01-0.9 μm size range. Triangles represent injections of limonene in the room at a rate of 3 mg min^{-1}; injections 1-7 lasted 5, 10, 15, 20, 5, 15, 15 min, respectively.

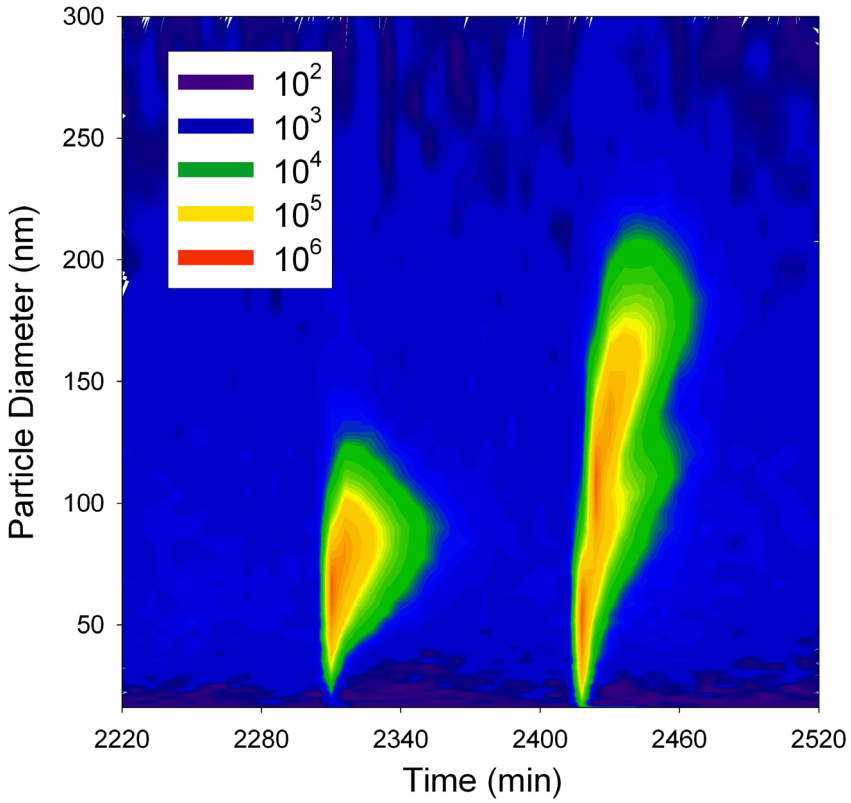

Figurer 6.3: Contour plot of particle bursts caused by addition of limonene to the office room with an operating OG (injections 1-2 in Figure 2). The color contours correspond to the particle size distribution, , in units of dN/dlogD cm^{-3}, logarithmically distributed.

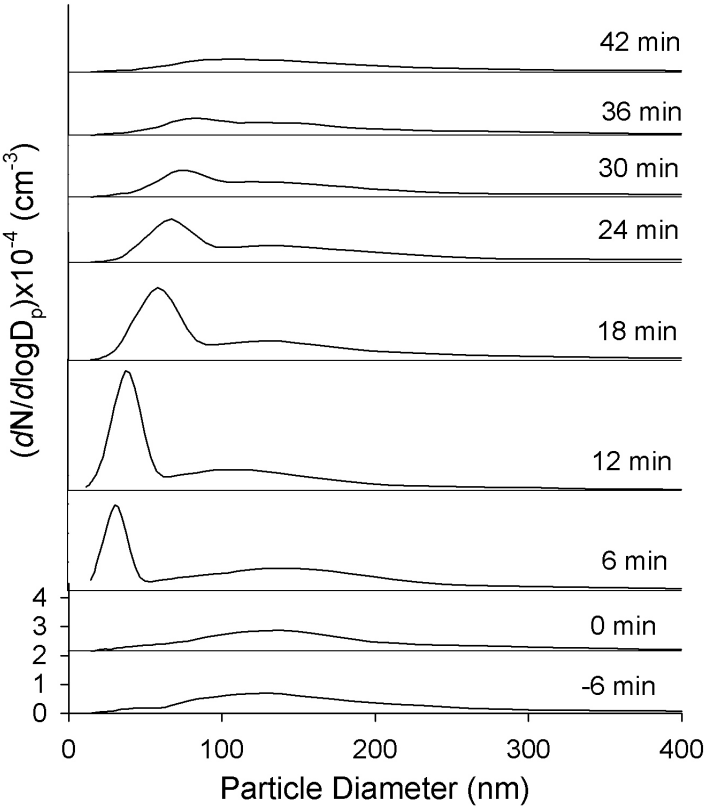

Figure 6.4 Particle size distributions observed after adding limonene to the office room with an operating IAP. Each distribution takes 6 minutes to acquire; limonene is injected in the middle of the "0 min" scan. The distributions are offset for clarity. The vertical scales on all plots are identical; the tick labels are shown for the "-6 min" plot only.

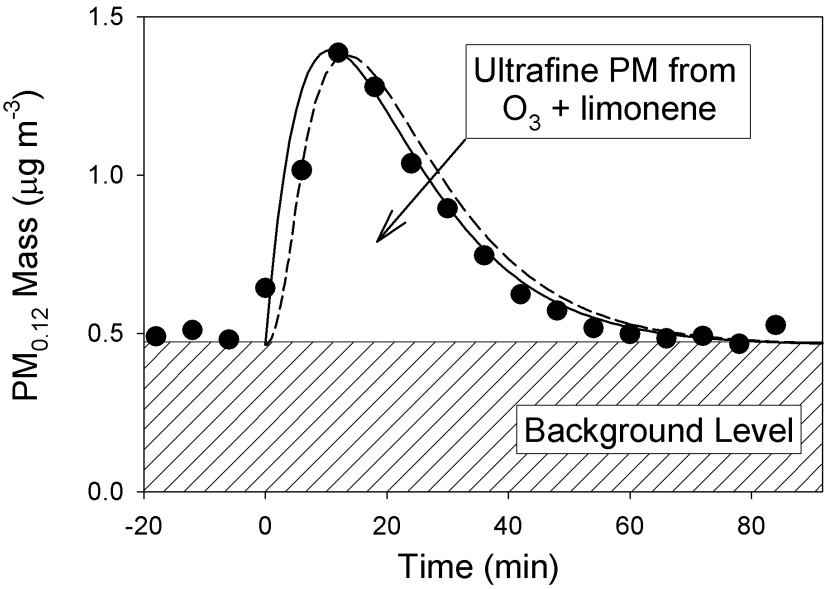

Figure 6.5: Simulations of a representative particle burst event resulting from an addition of 15 mg limonene (for 5 min at t =0) to the office room with operating IAP. Dots: experimental total particle mass concentration for particles with diameters below 0.12 μm ($PM_{0.12}$). Solid line: approximate analytical solution calculated from equation (14). Dashed line: exact numeric simulation of equations (4-6).

References:

1. Sardar, S.B., et al., *Size-Fractionated Measurements of Ambient Ultrafine Particle Chemical Composition in Los Angeles Using the NanoMOUDI.* Environ. Sci. Technol., 2005. 39(4): p. 932-944.
2. Kulmala, M., et al., *Formation and growth rates of ultrafine atmospheric particles: a review of observations.* Journal of Aerosol Science, 2004. 35(2): p. 143-176.
3. Jaenicke, R., *In Chemistry of the polluted and unpolluted Troposphere.* 1982: p. 341-373.
4. Brown, L.M., et al., *Ultrafine particles in the Atmosphere*. 2000, London: Imperial College Press.
5. Preining, O., *The physical nature of very very small particles and its impact on their behavior.* J. Aerosol Sci, 1998. 29: p. 481-495.
6. Zhu, Y., et al., *Study of ultrafine particles near a major highway with heavy-duty diesel traffic.* Atmospheric Environment, 2002. 36(27): p. 4323-4335.
7. Shi, J.P. and R.M. Harrison, *Investigation of Ultrafine Particle Formation during Diesel Exhaust Dilution.* Environ. Sci. Technol., 1999. 33(21): p. 3730-3736.
8. Mysliwiec, M.J. and M.J. Kleeman, *Source Apportionment of Secondary Airborne Particulate Matter in a Polluted Atmosphere.* Environ. Sci. Technol., 2002. 36(24): p. 5376-5384.

9. Kim, S.S., S.; Sioutas,C, Zhu, Y.F.;Hinds,w.c., *Size distribution and diurnalandseasonal trends of ultrafine particles in source and receptor sites of the Los Angeles basin.* J. Air Waste Manage. Assoc., 2002. 52: p. 297-307.

10. Hughes, L.S., Cass, G.R.,Jones,J.,Ames, M. Olmec, L., *Physical and chemical characterization of atmospheric ultrfaine particles in the Los Angeles area.* Envioron. Sci. Technol, 1998. 32: p. 1153-1161.

11. Allen, J.O., et al., *Particle Detection Efficiencies of Aerosol Time of Flight Mass Spectrometers under Ambient Sampling Conditions.* Environmental Science and Technology, 2000. 34(1): p. 211-217.

12. Zhi ning , M.i.D.G.e., K atherine F . M oore , R ebecca S heeley , J ames J . S chauer , C onstantinos Sioutas, *Daily Variation in Chemical Characteristics of Urban Ultrafine Aerosols and Inference of Their Sources.* Enviro. Sci & Technol, 2007. x: p. x.

13. Fang, G.-C., et al., *Characterization of chemical species in PM2.5 and PM10 aerosols in suburban and rural sites of central Taiwan.* The Science of The Total Environment, 1999. 234(1-3): p. 203-212.

14. Chen, M.-L., I.F. Mao, and I.K. Lin, *The PM2.5 and PM10 particles in urban areas of Taiwan.* The Science of The Total Environment, 1999. 226(2-3): p. 227-235.

15. Glen R. Cass, L.A.H.P.B.M.J.K.J.O.A.L.G.S., *The chemical composition of atmospheric ultrafine particles.* Philosophical Transactions of the Royal Society A: Mathematical, Physical and Engineering Sciences, 2000. 358(1775): p. 2581-2592.

16. S atya B . S ardar , P.M.F., A.N.D. Paul R . M ayo , and C.o. Sioutas, *Size-Fractionated Measurements of Ambient Ultrafine Particle Chemical Composition in Los Angeles Using the NanoMOUDI.* Environ. Sci. Technol, 2005. 39: p. 932-944.

17. Seinfeld, J.H.P., J , F., *Organic atmospheric organic particulate matter.* Annual Review of physical Chemistry, 2003. 54: p. 121-140.

18. Hamilton, J.F., ; Webb, P J ; Lewis, A. C., Hopkins, J R; Smith, S; Davy, P., *Partially oxidized organic components in urban aerosol using GCXGC- TOF/MS.* Atmospheric Chemistry and Physics, 2004. 4(5): p. 1279-1290.

19. Turpin, B.J.S.P.A., E, *Measuring and Sumulating Particulate organics in the atmosphere: Problems and prospects.* Atmospheric Environment, 2000. 34(18): p. 2983-3013.

20. Jimenez, J.L., et al., *Ambient aerosol sampling using the Aerodyne Aerosol Mass Spectrometer.* Journal of Geophysical Research, 2003. 108(D7): p. SOS 13/1-SOS 13/13.

21. Boudriesa, H.M.R.C.J.T.J., M.R;Alfarrab, J. Allanc,;K.N. Bowerc;H. Coec;S.C. Pryord;J.L. Jimeneze;J.R. Brookf;S. , *Chemical and physical processes controlling the distribution of aerosols in the Lower Fraser Valley during the 2001 field campaign* Atmospheric Environment, 2004. 38(34): p. 5759-5774.

22. Li, Z., et al., *Sources of fine particle composition in New York city.* Atmospheric Environment, 2004. 38(38): p. 6521-6529.

23. Anttila, T. and V.-M. Kerminen, *Condensational growth of atmospheric nuclei by organic vapours.* Journal of Aerosol Science, 2003. 34(1): p. 41-61.

24. Alves, C., A. Carvalho, and C. Pio, *Mass balance of organic carbon fractions in atmospheric aerosols.* Journal of Geophysical Research, 2002. 107(D21): p. ICC7/1-ICC7/9.

25. Sicre, M.-A.M., J. -C.; Saliot, A. , *n-alkanes, fatty acid esters, and fatty acid salts in size fractionated aerosols collected over the Mediterranean Sea* J Geophysical Research, 1990. 95(D4): p. 3649–3657.

26. Mochida, M.K.K., Nobuhiko Umemoto, Minoru Kobayashi, Sou Matsunaga, Ho-Jin, Lim,Barbara J. Turpin, Timothy S. Bates, and Bernd R. T. Simoneit, *Spatial distributions of oxygenated organic compounds (dicarboxylic acids, fatty acids, and levoglucosan) in marine aerosols over the western Pacific and off the coast of East Asia: Continental outflow of organic aerosols during the ACE-Asia campaign.* J.Geophysical Research, 2003. 108(D23): p. 8638.

27. Chen, Y.-Y. and W.-M. Grace Lee, *Hygroscopic properties of inorganic-salt aerosol with surface-active organic compounds.* Chemosphere, 1999. 38(10): p. 2431-2448.

28. Pope, C.A.D., D. W.; Schwartz, J., Inhalation Toxicol., 1995. 7: p. 1-18.

29. Dockery, D.W., et al., *An association between air pollution and mortality in six U.S. cities.* New England journal of medicine, 1993. 329(24): p. 1753-9.

30. Kreyling, W.G., et al., *Translocation of ultrafine insoluble irridium particles from lung epithelium to extrapulmonary organsis size dependent but very low.* Journal of Toxicology and Environmental Health, Part A, 2002. 65(20): p. 1513-1530.

31. Nemmer, B.N., B; Hoet, P.H.;Vermylen,J; Holyaerts,M F., *Pulmonary inflammation and thrombogenicity caused by diesel particles in hamsters: role of histamine.* Am. J. Respir. Crit. Care Med, 2003. 168(11): p. 1366-1372.

32. Oberdorster, G.G., Robert M.; Ferin, Juraj; Weiss, Bernard *Association of particulate air pollution and acute mortality: Involvement of ultrafine particles?* Inhalation Toxicology, 1995. 7(1): p. 111-124.

33. Seaton, A., *Airborne particles and their effects on health.* Particulate Matter, 1999: p. 9-17.

34. EPA, *Air Quality Criteria for Ozone and Related Photochemical Oxidants (1996). URL:* http://www.epa.gov/iaq/pubs/ozonegen.html. 1996, US Environmental Protection Agency, Office of Research and Development, National Center for Environmental Assessment: Washington, DC.

35. Penner, J.E., Andreae, M.O., Annegarn, H., Barrie, L., Feichter, J., Hegg,D.A.,Jayaraman, A., Leaitch, R., Murphy, D.M., Nganga, J. and Pitari, G.. *Aerosols, their Direct and Indirect Effects.* Third Assessment Report of the Intergovernmental Panel on Climate Change. Cambridge University Press, New York, USA,, 2001: p. 881.

36. Seinfeld, J.H.a.P., S.N., *Atmospheric Chemistry and Physics, From Air Pollution to Climate Change.* 1998: p. 1326.

37. Twomey, S., *Aerosols, clouds and radiation.* Atmospheric Environment, Part A: General Topics, 1991. 25A(11): p. 2435-42.

38. Ellison, G.B., Tuck, A.F. and Vaida, V., *Atmospheric processing of organic aerosols.* J. Geophys. Res., [Atmos.], 1999. 104(D9): p. 11633-11641.

39. Moise, T. and Y. Rudich, *Reactive uptake of ozone by proxies for organic aerosols: Surface versus bulk processes.* J. Geophys. Res., 2000. 105(D11): p. 14667-14676.

40. Thomas, E.R., G.J. Frost, and Y. Rudich, *Reactive uptake of ozone by proxies for organic aerosols: Surface-bound and gas-phase products.* J. Geophys. Res., 2001. 106(D3): p. 3045-3056.

41. Nazaroff, W.W., *Indoor particle dynamics.* Indoor Air, 2004. 14(s7): p. 175-183.

42. Fogh, C.L., et al., *Size specific indoor aerosol deposition measurements and derived I/O concentrations ratios.* Atmospheric Environment, 1997. 31(15): p. 2193-2203.

43. Pasanen, A.L., *A Review: Fungal Exposure Assessment in Indoor Environments.* Indoor Air, 2001. 11(2): p. 87-98.

44. Abt, E., et al., *Relative Contribution of Outdoor and Indoor Particle Sources to Indoor Concentrations.* Environ. Sci. Technol., 2000. 34(17): p. 3579-3587.

45. Jones, N.C., et al., *Indoor/outdoor relationships of particulate matter in domestic homes with roadside, urban and rural locations.* Atmospheric Environment, 2000. 34(16): p. 2603-2612.

46. Riley, W.J., et al., *Indoor Particulate Matter of Outdoor Origin: Importance of Size-Dependent Removal Mechanisms.* Environ. Sci. Technol., 2002. 36(2): p. 200-207.

47. Phillips, T. and C. Jakober, *Evaluation of Ozone Emissions from Portable Indoor "Air Cleaners" that Intentionally Generate Ozone*, in *California ARB Press Release 05-02*. 2006, California Air Resources Board: Sacramento, CA. p. 31.

48. CARB, *Indoor Air Pollution in California: AB1173 Report to the California Legislature*. 2005, California Air Resources Board: Sacramento, CA.

49. Britigan, N., A. Alshawa, and S.A. Nizkorodov, *Quantification of Ozone Levels in Indoor Environments Generated by Ionic and Ozonolysis Air Purifiers.* JAWMA, 2006. 56(5): p. 601-610.

50. Phillips, T.J., et al., *Ozone emissions from a "personal air purifier".* Journal of Exposure Analysis and Environmental Epidemiology, 1999. 9(6): p. 594-601.

51. WHO, *WHO air quality guidelines for Europe (second edition). WHO Regional Publications, European Series, No. 91*. 2000, World Health Organization: Copenhagen. p. 273.

52. Moriske, H.-J., et al., *Concentrations and decay rates of ozone in indoor air in dependence on building and surface materials.* Toxicology Letters, 1998. 96,97: p. 319-323.

53. Grontoft, T. and M.R. Raychaudhuri, *Compilation of tables of surface deposition velocities for O3, NO2 and SO2 to a range of indoor surfaces.* Atmospheric Environment, 2004. 38(4): p. 533-544.

54. Sabersky, R.H., D.A. Sinema, and F.H. Shair, *Concentrations, decay rates, and removal of ozone and their relation to establishing clean indoor air.* Environmental Science and Technology, 1973. 7(4): p. 347-53.

55. Morrison, G.C. and W.W. Nazaroff, *Ozone Interactions with Carpet: Secondary Emissions of Aldehydes.* Environmental Science and Technology, 2002. 36(10): p. 2185-2192.

56. Knudsen, H.N., et al., *Sensory evaluation of emissions from selected building products exposed to ozone.* Indoor Air, 2003. 13(3): p. 223-31.

57. Sarwar, G., et al., *Hydroxyl radicals in indoor environments.* Atmospheric Environment, 2002. 36(24): p. 3973-3988.

58. Weschler, C.J., *Indoor chemistry as a source of particles.* Indoor Environment, 2003: p. 167-189.

59. Weschler, C.J., *Ozone in indoor environments: Concentration and chemistry.* Indoor Air, 2000. 10(4): p. 269-288.

60. Liu, X., et al., *Full-Scale Chamber Investigation and Simulation of Air Freshener Emissions in the Presence of Ozone.* Environmental Science and Technology, 2004. 38(10): p. 2802-2812.

61. Nojgaard, J.K., K.B. Christensen, and P. Wolkoff, *The effect on human eye blink frequency of exposure to limonene oxidation products and methacrolein.* Toxicology Letters, 2005. 156(2): p. 241-251.

62. Wolkoff, P., et al., *Formation of strong airway irritants in terpene/ozone mixtures.* Indoor Air, 2000. 10(2): p. 82-91.

63. John B. Fenn, M.M., Chin Kai Meng, and Shek Fu Wong,Craige M. Whitehouse, *Electrospray ionization-principles and practice.* Mass Spectromety Reviews 1990. 9: p. 37-70.

64. Chen, D.-R., D.Y.H. Pui, and S.L. Kaufman, *Electrospraying of conducting liquids for monodisperse aerosol generaton in the 4 to 1.8 μm diamgeter range.* J. Aerosol Sci., 1995. 26(6): p. 963-977.

65. Bruins, A.P., *Mechanistic aspects of electrospray ionization.* Journal of Chromatography A, 1998. 794: p. 345–357.

66. Kebarle, P., *A brief overview of the present status of the mechanisms involved in electrospray mass spectrometry.* J. Mass Spectrom., 2000. 35: p. 804-817.

67. Kebarle, P. and M. Peschke, *On the mechanisms by which the charged droplets produced by electrospray lead to gas phase ions.* Analytica Chimica Acta, 2000. 406: p. 11-35.

68. Kebarle, P. and L. Tang, *From Ions in Solution to Ions in Gas Phase.* ANALYTICAL CHEMISTRY,, 1993. 65(22): p. 972.

69. Chen, D.-R., D.Y.H. Pui, and S.L. Kaufman, *Electrospraying of conducting liquids for monodisperse aerosol generation in the 4 nm to 1.8 mm diameter range.* Journal of Aerosol Science, 1995. 26(6): p. 963-77.

70. Wallace, W.E., M.A. Arnould, and R. Knochenmuss, *2,5-Dihydroxybenzoic acid: laser desorption/ionisation as a function of elevated temperature.* International Journal of Mass Spectrometry, 2005. 242(1): p. 13-22.

71. D. A. Allwood, et al., *UV Optical Absorption of Matrices Used for Matrix-assisted Laser DesorptiodIonization.* Rapid Communications in Mass Spectroscopy, 1996. 10: p. 1575-1578

72. Cruz, C.N. and S.N. Pandis, *Deliquescence and Hygroscopic Growth of Mixed Inorganic-Organic Atmospheric Aerosol.* Environmental Science and Technology, 2000. 34(20): p. 4313-4319.

73. Biskos, G., et al., *Nanosize Effect on the Deliquescence and the Efflorescence of Sodium Chloride Particles.* Aerosol Science and Technology, 2006. 40(2): p. 97-106.

74. G. Biskos, D.P., L. M. Russell, P. R. Buseck, and S. T. Martin, *Prompt deliquescence and e□orescence of aerosol nanoparticles.* Atmos. Chem. Phys. Discuss, 2006. 6: p. 7051–7073.

75. Fuchs, N.A., *"On the Stationary Charge Distribution on Aerosol Particles in a Bipolar Ionic Atmosphere".* Geophys. Pura Appl., 1963. 56: p. 185.

76. Kerminen, V.-M., *The effects of particle chemical character and atmospheric processes on particle hygroscopic properties.* Journal of Aerosol Science, 1997. 28(1): p. 121-132.

77. McMurry, P.H. and M.R. Stolzenburg, *On the sensitivity of particle size to relative humidity for Los Angeles aerosols.* Atmospheric Environment (1967), 1989. 23(2): p. 497-507.

78. Duce, R.A., et al., *Organic material in the global troposphere.* Reviews of Geophysics and Space Physics, 1983. 21(4): p. 921-52.

79. Gill, P.S., T.E. Graedel, and C.J. Weschler, *Organic films on atmospheric aerosol particles, fog droplets, cloud droplets, raindrops, and snowflakes.* Reviews of Geophysics and Space Physics, 1983. 21(4): p. 903-20.

80. Saxena, P., et al., *Organics alter hygroscopic behavior of atmospheric particles.* Journal of Geophysical Research, 1995. 100(D9): p. 18,755-70.

81. Tang, I.N. and H.R. Munkelwitz, *An investigation of solute nucleation in levitated solution droplets.* Journal of Colloid and Interface Science, 1984. 98(2): p. 430-438.

82. Heim, M., et al., *Filtration Efficiency of Aerosol Particles Below 20 Nanometers.* Aerosol Science and Technology, 2005. 39(8): p. 782-789.

83. Tang, I.N., *Coposition and temperature dependence of the deliquescence properties of hygroscopic aerosols.* Atmospheric Environment, 1993. 27A(4): p. 467-473.

84. Hameri, K., et al., *Theory of Size Dependent Deliquescence of Nanoparticles: Relation to Heterogeneous Nucleation and Comparison with Experiments.* J. Phys. Chem. B, 2001. 105,: p. 7708-7722.

85. Russell, L.M. and Y. Ming, *Deliquescence of small particles.* Journal of Chemical Physics, 2002. 116(1): p. 311-321.

86. Hemminger, B.J.F.-P.a.J.C., *Physical Chemistry of Airborne Sea Salt Particles and Their Components.* J. Phys. Chem. A, 2000. 104: p. 11463-11477.

87. Stokes, R.H. and R.A. Robinson, *Interactions in aqueous nonelectrolyte solutions. I. Solute-solvent equilibriums.* Journal of Physical Chemistry, 1966. 70(7): p. 2126-31.

88. Hanson, H.C.R., M. J. ;Kuloutsou Vakakis; Hameri,K., *NaCl aerosol particles hygroscopicity dependence on mixing with organic compounds.* J. Atmos. Chem, 1998. 31(3): p. 321-346.

89. Chan, M.N.C., C. K., *Mass transfer effects in hygrosocpic measurments of aerosol particles.* Atmos. Chem. Phys., 2005. 5: p. 2703-2712.

90. Sjogren, S., et al., *Hygroscopic growth and water uptake kinetics of two-phase aerosol particles consisting of ammonium sulfate, adipic and humic acid mixtures.* Journal of Aerosol Science, 2007. 38(2): p. 157-171.

91. Chuang, P.Y., *Measurement of the timescale of hygroscopic growth for atmospheric aerosols.* J. geophy Res., 2003. 108(D9).

92. Cubison, M.J., H. Coe, and M. Gysel, *A modified hygroscopic tandem DMA and a data retrieval method based on optimal estimation.* Journal of Aerosol Science, 2005. 36(7): p. 846-865.

93. Xiong, J.Q., et al., *Influence of Organic Films on the Hygroscopicity of Ultrafine Sulfuric Acid Aerosol.* Environmental Science and Technology, 1998. 32(22): p. 3536-3541.

94. Hameri, K.A.L.M.V.T.S., *Hygroscopic growth of ultrafine sodium chloride particles.* j of geophysical research, 2001. 106(D18): p. 749.

95. Derecskei, B., A. Derecskei-Kovacs, and Z.A. Schelly, *Atomic-Level Molecular Modeling of AOT Reverse Micelles. 1. The AOT Molecule in Water and Carbon Tetrachloride.* Langmuir, 1999. 15(6): p. 1981-1992.

96. POCHETTI, C.F.M.G., *Crystal Phases Obtained from Aqueous Solutions of Sodium Dodecyl Sulfate. TheStructure of a Monoclinie Phase of Sodium Dodecyl Sulfate Hemihydrate.* Acta Cryst, 1986. C42: p. 991-995.

97. Investigates, C., *Air cleaners: Behind the hype.* Consumer Reports, 2003. 68(10): p. 26-29.

98. Li, N., et al., *Ultrafine particulate pollutants induce oxidative stress and mitochondrial damage.* Environmental Health Perspectives, 2003. 111(4): p. 455-460.

99. von Klot, S., et al., *Increased asthma medication use in association with ambient fine and ultrafine particles.* European Respiratory Journal, 2002. 20(3): p. 691-702.

100. Pope, C.A., III, et al., *Lung cancer, cardiopulmonary mortality, and long-term exposure to fine particulate air pollution.* J. Amer. Med. Assoc., 2002. 287(9): p. 1132-1141.

101. Delfino, R.J., et al., *Association of asthma symptoms with peak particulate air pollution and effect modification by anti-inflammatory medication use.* Environmental Health Perspectives, 2002. 110(10): p. A607-A617.

102. Brown, S.K., *Assessment of pollutant emissions from dry-process photocopiers.* Indoor Air, 1999. 9(4): p. 259-267.

103. Leovic, K.W., et al., *Measurement of indoor air emissions from dry-process photocopy machines.* Journal of the Air & Waste Management Association, 1996. 46(9): p. 821-829.

104. Finlayson-Pitts, B.J. and J.N. Pitts, *Chemistry of the Upper and Lower Atmosphere: Theory, Experiments, and Applications*. 2000: Academic Press. 1040 pp.

105. Bailey, P.S., *Organic Chemistry, Vol. 39, Pt. 1: Ozonation in Organic Chemistry, Vol. 1: Olefinic Compounds*. 1978: Academic Press. 272 pp.

106. Nazaroff, W.W. and C.J. Weschler, *Cleaning products and air fresheners: exposure to primary and secondary air pollutants.* Atmospheric Environment, 2004. 38(18): p. 2841-2865.

107. Bailey, P.S., *Organic Chemistry, Vol. 39, Pt. 2: Ozonation in Organic Chemistry, Vol. 2: Nonolefinic Compounds*. 1982: Academic Press. 497 pp.

108. Weschler, C.J., *New Directions: Ozone-initiated reaction products indoors may be more harmful than ozone itself.* Atmospheric Environment, 2004. 38(33): p. 5715-5716.

109. Wilkins, C.K., et al., *Upper airway irritation of terpene/ozone oxidation products (TOPS). Dependence on reaction time, relative humidity and initial ozone concentration.* Toxicology Letters, 2003. 143(2): p. 109-114.

110. Kleno, J. and P. Wolkoff, *Changes in eye blink frequency as a measure of trigeminal stimulation by exposure to limonene oxidation products, isoprene oxidation products and nitrate radicals.* International Archives of Occupational and Environmental Health, 2004. 77(4): p. 235-243.

111. Paulson, S.E., M.Y. Chung, and A.S. Hasson, *OH Radical Formation from Gas-Phase Reaction of Ozone with Terminal Alkenes and the Relationship between Structure and Mechanism.* J. Phys. Chem. A, 1999. 103(41): p. 8125-8138.

112. Kroll, J.H., et al., *Mechanism of HOx Formation in the Gas-Phase Ozone-Alkene Reaction. 1. Direct, Pressure-Dependent Measurements of Prompt OH Yields.* Journal of Physical Chemistry A, 2001. 105(9): p. 1554-1560.

113. Rickard, A.R., et al., *OH Yields in the Gas-Phase Reactions of Ozone with Alkenes.* Journal of Physical Chemistry A, 1999. 103(38): p. 7656-7664.

114. Atkinson, R. and J. Arey, *Gas-phase tropospheric chemistry of biogenic volatile organic compounds: a review.* Atmospheric Environment, 2003. 37(Suppl. 2): p. S197-S219.

115. Rohr, A.C., et al., *Generation and quantification of ultrafine particles through terpene/ozone reaction in a chamber setting.* Aerosol Science and Technology, 2003. 37(1): p. 65-78.

116. Wainman, T., et al., *Ozone and limonene in indoor air: a source of submicron particle exposure.* Environmental Health Perspectives, 2000. 108(12): p. 1139-1145.

117. EPA. *Ozone Generators that are Sold as Air Cleaners: An Assessment of Effectiveness and Health Consequences (http://www.epa.gov/iaq/pubs/ozonegen.html)*. 2005 [cited; Available from: http://www.epa.gov/iaq/pubs/ozonegen.html.

118. Boeniger, M.F., *Use of ozone generating devices to improve indoor air quality.* American Industrial Hygiene Association Journal, 1995. 56(6): p. 590-8.

119. CalEPA, *ARB Warns, Danger from Popular "Air Purifying" Machines (ARB Press Release 05-02)*, in *California ARB Press Release 05-02*. 2005, California EPA: Sacramento, CA.

120. Hoeppe, P., et al., *Environmental ozone field study on pulmonary and subjective responses of assumed risk groups.* Environmental Research, 1995. 71(2): p. 109-121.

121. Nielsen, G.D., et al., *Acute airway effects of formaldehyde and ozone in BALB/c mice.* Human & experimental toxicology, 1999. 18(6): p. 400-9.

122. Alexeeff, G.V., et al., *Determination of Acute Reference Exposure Levels for Airborne Toxicants*. 1999, Office of Environmental Health Hazard Assessment (OEHHA). p. C264-C270 (Ozone).

123. Moore, C. and D. Bates, *Smog: Nature's Most Powerful Purifying Agent*, in *Health & Clean Air Newsletter (http://www.healthandcleanair.org/)*. 2002.

124. Bell, M.L., et al., *Ozone and short-term mortality in 95 US urban communities, 1987-2000.* JAMA, the Journal of the American Medical Association, 2004. 292(19): p. 2372-2378.

125. Kleno, J.G., et al., *Determination of ozone removal rates by selected building products using the FLEC emission cell.* Environmental science & technology, 2001. 35(12): p. 2548-53.

126. Lai, C.C., S.H. Yang, and B.J. Finlayson-Pitts, *Interactions of monolayers of unsaturated phosphocholines with ozone at the air-water interface.* Langmuir, 1994. 10(12): p. 4637-44.

127. Moise, T. and Y. Rudich, *Reactive Uptake of Ozone by Aerosol-Associated Unsaturated Fatty Acids: Kinetics, Mechanism, and Products.* Journal of Physical Chemistry A, 2002. 106(27): p. 6469-6476.

128. Dubowski, Y., et al., *Interaction of Gas-Phase Ozone at 296 K with Unsaturated Self-Assembled Monolayers: A New Look at an Old System.* Journal of Physical Chemistry A, 2004. 108(47): p. 10473-10485.

129. Weschler, C.J., A.T. Hodgson, and J.D. Wooley, *Indoor chemistry: ozone, volatile organic compounds, and carpets.* Environmental Science and Technology, 1992. 26(12): p. 2371-7.

130. Morrison, G.C. and W.W. Nazaroff, *The Rate of Ozone Uptake on Carpets: Experimental Studies.* Environmental Science and Technology, 2000. 34(23): p. 4963-4968.

131. CalEPA, *California Adopts New Ozone Standard. Children's Health Focus of New Requirement (ARB Press Release 05-08)*, in *California ARB Press Release 05-08*. 2005, California EPA: Sacramento, CA.

132. *Code of Federal Regulations, Title 21 - Food and Drugs, Subchapter H - Medical Devices, § 801.415 - Maximum acceptable level of ozone.*, in *21 CFR 801.415*. 1976.

133. Mauersberger, K., et al., *Ozone vapor pressure and absorption cross-section measurements: introduction of an ozone standard.* J. Geophys. Res., 1987. 92: p. 8480.

134. Poeschl, U., et al., *Interaction of Ozone and Water Vapor with Spark Discharge Soot Aerosol Particles Coated with Benzo[a]pyrene: O3 and H2O Adsorption, Benzo[a]pyrene Degradation, and Atmospheric Implications.* J. Phys. Chem. A, 2001. 105(16): p. 4029-4041.

135. Cano-Ruiz, J.A., et al., *Removal of reactive gases at indoor surfaces: combining mass transport and surface kinetics.* Atmospheric Environment, Part A: General Topics, 1993. 27A(13): p. 2039-50.

136. Lee, K., et al., *Ozone decay rates in residences.* Journal of the Air & Waste Management Association, 1999. 49(10): p. 1238-1244.

137. SCAQMD. *Historic Ozone Air Quality Trends. URL: http://www.aqmd.gov/smog/o3trend.html*. 2004 May 05, 2004 [cited; Available from: URL: http://www.aqmd.gov/smog/o3trend.html.

138. Pope, C.A., III, *Review: epidemiological basis for particulate air pollution health standards.* Aerosol Science and Technology, 2000. 32(1): p. 4-14.

139. Gauderman, W.J., et al., *Association between air pollution and lung function growth in southern California children: results from a second cohort.* Am. J. Respir. Crit. Care Med., 2000. 166(1): p. 76-84.

140. Von Klot, S., et al., *Ambient air pollution is associated with increased risk of hospital cardiac readmissions of myocardial infarction survivors in five European cities.* Circulation, 2005. 112(20): p. 3073-3079.

141. Schulz, H., et al., *Cardiovascular Effects of Fine and Ultrafine Particles.* Journal of Aerosol Medicine, 2005. 18(1): p. 1-22.

142. Cohen, A.J. and C.A. Pope, 3rd, *Lung cancer and air pollution.* Environmental health perspectives, 1995. 103(Suppl 8): p. 219-24.

143. Krewski, D., et al., *Mortality and Long-Term Exposure to Ambient Air Pollution: Ongoing Analyses Based on the American Cancer Society Cohort.* Journal of Toxicology and Environmental Health, Part A, 2005. 68(13-14): p. 1093-1109.

144. Oberdoerster, G., et al., *Translocation of Inhaled Ultrafine Particles to the Brain.* Inhalation Toxicology, 2004. 16(6-7): p. 437-445.

145. Sarwar, G., et al., *Indoor fine particles: the role of terpene emissions from consumer products.* Journal of the Air & Waste Management Association, 2004. 54(3): p. 367-377.

146. Weschler, C.J. and H.C. Shields, *Indoor ozone/terpene reactions as a source of indoor particles.* Atmospheric Environment, 1999. 33(15): p. 2301-2312.

147. Odum, J.R., et al., *Gas/Particle Partitioning and Secondary Organic Aerosol Yields.* Environmental Science and Technology, 1996. 30(8): p. 2580-2585.

148. Hoffmann, T., et al., *Formation of organic aerosols from the oxidation of biogenic hydrocarbons.* Journal of Atmospheric Chemistry, 1997. 26(2): p. 189-222.

149. Sax, M., et al., *Time Resolved Infrared Spectroscopic Analysis of Aerosol Formed by Photo-Oxidation of 1,3,5-Trimethylbenzene and a-Pinene.* Aerosol Science and Technology, 2005. 39(9): p. 822-830.

150. Koch, S., et al., *Formation of new particles in the gas-phase ozonolysis of monoterpenes.* Atmospheric Environment, 2000. 34(23): p. 4031-4042.

151. Bonn, B., G. Schuster, and G.K. Moortgat, *Influence of Water Vapor on the Process of New Particle Formation during Monoterpene Ozonolysis.* Journal of Physical Chemistry A, 2002. 106(12): p. 2869-2881.

152. Czoschke, N.M., M. Jang, and R.M. Kamens, *Effect of acidic seed on biogenic secondary organic aerosol growth.* Atmospheric Environment, 2003. 37(30): p. 4287-4299.

153. Gao, S., et al., *Low-Molecular-Weight and Oligomeric Components in Secondary Organic Aerosol from the Ozonolysis of Cycloalkenes and a-Pinene.* Journal of Physical Chemistry A, 2004. 108(46): p. 10147-10164.

154. Iinuma, Y., et al., *Aerosol-chamber study of the a-pinene/O3 reaction: influence of particle acidity on aerosol yields and products.* Atmospheric Environment, 2004. 38(5): p. 761-773.

155. Baltensperger, U., et al., *Secondary organic aerosols from anthropogenic and biogenic precursors.* Faraday Discussions, 2005. 130(Atmospheric Chemistry): p. 265-278.

156. Bahreini, R., et al., *Measurements of Secondary Organic Aerosol from Oxidation of Cycloalkenes, Terpenes, and m-Xylene Using an Aerodyne Aerosol Mass Spectrometer.* Environmental Science and Technology, 2005. 39(15): p. 5674-5688.

157. Tolocka, M.P., et al., *Formation of Oligomers in Secondary Organic Aerosol.* Environmental Science and Technology, 2004. 38(5): p. 1428-1434.

158. Presto, A.A., K.E. Huff Hartz, and N.M. Donahue, *Secondary Organic Aerosol Production from Terpene Ozonolysis. 2. Effect of NOx Concentration.* Environmental Science and Technology, 2005. 39(18): p. 7046-7054.

159. Singer, B.C., et al., *Indoor secondary pollutants from cleaning product and air freshener use in the presence of ozone.* Atmospheric Environment, 2006. 40(35): p. 6696-6710.

160. Destaillats, H., et al., *Indoor Secondary Pollutants from Household Product Emissions in the Presence of Ozone: A Bench-Scale Chamber Study.* Environmental Science & Technology, 2006. 40(14): p. 4421-4428.

161. Lai, A.C.K. and W.W. Nazaroff, *Modeling indoor particle deposition from turbulent flow onto smooth surfaces.* Journal of Aerosol Science, 2000. 31(4): p. 463-476.

162. Ward, M., J.A. Siegel, and R.L. Corsi, *The effectiveness of stand alone air cleaners for shelter-in-place.* Indoor air, 2005. 15(2): p. 127-34.

163. Allen, R., et al., *Use of Real-Time Light Scattering Data To Estimate the Contribution of Infiltrated and Indoor-Generated Particles to Indoor Air.* Environmental Science and Technology, 2003. 37(16): p. 3484-3492.

164. Wallace, L., *Indoor particles: a review.* Journal of the Air & Waste Management Association, 1996. 46(2): p. 98-126.

165. Thatcher, T.L., et al., *Effects of room furnishings and air speed on particle deposition rates indoors.* Atmospheric Environment, 2002. 36(11): p. 1811-1819.

166. Grosjean, D., et al., *Atmospheric oxidation of biogenic hydrocarbons: reaction of ozone with b-pinene, D-limonene and trans-caryophyllene.* Environmental Science and Technology, 1993. 27(13): p. 2754-8.

167. Stanier, C.O., A.Y. Khlystov, and S.N. Pandis, *Nucleation Events During the Pittsburgh Air Quality Study: Description and Relation to Key Meteorological, Gas Phase, and Aerosol Parameters.* Aerosol Science and Technology, 2004. 38(Suppl. 1): p. 253-264.

168. Dunn, M.J., et al., *Measurements of Mexico City nanoparticle size distributions: Observations of new particle formation and growth.* Geophysical Research Letters, 2004. 31(10): p. L10102/1-L10102/4.

169. Tolocka, M.P., et al., *Ultrafine nitrate particle events in Baltimore observed by real-time single particle mass spectrometry.* Atmospheric Environment, 2004. 38(20): p. 3215-3223.

170. Kroll, J.H., et al., *Secondary organic aerosol formation from isoprene photooxidation under high-Nox conditions.* Geophysical Research Letters, 2005. 32(18): p. L18808/1-L18808/4.

171. Donahue, N.M., et al., *Critical factors determining the variation in SOA yields from terpene ozonolysis: A combined experimental and computational study.* Faraday Discussions, 2005. 130(Atmospheric Chemistry): p. 295-309.